Physics Reports 1154 (2026) 1–48

Contents lists available at ScienceDirect

Physics Reports

journal homepage: www.elsevier.com/locate/physrep

Review article

On the physical foundations of topological thermoelectricity and its improvement

Daniel Baldomir [a,b,*], Daniel Failde [c]

[a] Departamento de Física Aplicada, Universidade de Santiago de Compostela, Santiago de Compostela, 15782, Spain
[b] Instituto de Materiais iMATUS, Universidade de Santiago de Compostela, Santiago de Compostela, 15782, Spain
[c] Galicia Supercomputing Center (CESGA), Santiago de Compostela, Spain

ARTICLE INFO

Article history:
Received 27 May 2025
Received in revised form 22 October 2025
Accepted 23 October 2025
Available online 31 October 2025
Editor: Fulvio Parmigiani

Keywords:
Thermoelectricity
Topological materials

ABSTRACT

Thermoelectricity has extraordinary scientific and technological interest due to its ability to utilize heat losses through the Seebeck effect and Peltier cooling in circuits. However, the efficiency of thermoelectric materials remains relatively low, making them economically viable in fewer cases than desired. A promising possibility lies in the best thermoelectric materials at room temperature, specifically the well-known tetradymite-type structures, primarily compounds based on Bi_2Te_3. These materials are characterized as topological insulators, allowing for the introduction of new physical perspectives. Therefore, it is reasonable to closely investigate the interplay between topology and thermoelectricity in these systems, with the aim of elucidating the underlying physical mechanisms. We show that, near the surface–bulk interface, the electrodynamics of axions coupled to massless fermions, Thouless pump currents, the chiral anomaly, and topological mass are intimately interconnected in a way that enables the mutual conversion of heat and electrical energy. That gives rise to a thermoelectric effect whose efficiency can be enhanced by integer multiples. We extend this study to heterostructures of topological insulators and topological superconductors. These phases are topologically complementary and may use the proximity effect to share topological quantum numbers. This offers a pathway to enhance topological thermoelectricity.

Contents

* Corresponding author at: Departamento de Física Aplicada, Universidade de Santiago de Compostela, Santiago de Compostela, 15782, Spain.
E-mail address: daniel.baldomir@usc.es (D. Baldomir).

https://doi.org/10.1016/j.physrep.2025.10.004
0370-1573/

1. Introduction

Nowadays, despite the significant technological and scientific interest in thermoelectricity for Peltier refrigeration or Seebeck effect power generation, the dimensionless figure of merit ZT remains around unity for p-semiconductors and even lower for n-semiconductors at room temperature at best; metals perform still worse [1–5]. The dimensionless figure of merit, defined as $ZT = \frac{S^2\sigma}{\kappa_e+\kappa_{ph}}$, quantifies the efficiency of transforming one type of energy into another, where S is the Seebeck coefficient, σ is the electrical conductivity, and $\kappa_e + \kappa_{ph}$ is the sum of electronic and lattice thermal conductivities, respectively. Increasing this efficiency faces two main challenges: first, the design of high-performance thermoelectric materials is inherently complex; second, the semiclassical Boltzmann transport theory remains the standard framework for describing transport, even though the best room-temperature thermoelectrics are topological insulators. These are materials whose functionality relies on global, topological features that go beyond local semiclassical physics [6–11].

Let us examine the fundamental limitations of conventional thermoelectricity. For a free electron gas, the Seebeck coefficient scales as $S \sim C_e/e$ [12,12–19], where C_e is the specific heat and e is the elementary charge. This allows finding the approximate value of $S \sim \left(\frac{k_B}{e}\right)\frac{k_BT}{\xi_F}$ for metals, knowing that only the fraction of electrons k_BT/ξ_F takes part in the electronic transport, where k_B is the Boltzmann constant and ξ_F the Fermi level [6–11]. Notice that as $\xi_F \gg k_BT$ at room temperature, then the Seebeck coefficients of metals are lower than $k_B/e \sim 86\ \mu\text{VK}^{-1}$, the thermopower of the classical electron gas. In contrast, in semiconductors the electrons must be thermally excited across a band gap energy ξ_G, yielding an electrical conductivity $\sigma \sim \sigma_0 exp[-\frac{\xi_G}{2k_BT}]$ [20]. In this regime, the Seebeck coefficient scales as $S \sim (\frac{k_B}{e})(\frac{\xi_G}{k_BT})$. For typical band gaps $\xi_G \sim 10\, k_BT$ at room temperature, this makes the thermoelectricity of the semiconductors more effective than that of the metals.

To be more precise, when the variation of the conductivity with temperature is significant, one should employ the Mott diffusion thermopower formula $S = \frac{\pi^2 k_BT}{3e}[\frac{d}{d\xi}(ln\sigma(\xi))]$ [20]. That allows us to find the numerator of the figure of merit, σS^2, proportional to $\mu(N_V)^{\frac{2}{3}} m_f^{\frac{3}{2}}$, where μ is the carrier mobility, N_V is the degeneracy of the band, and m_f is the effective mass. That gives us the power factor associated with the electronic structure. Under the above conditions, one possible good thermoelectric is the Bi_2Te_3 for which the energy gap $\xi_G = 0.14$ eV, for n or p-types, and presents a thermal transport behavior close to an amorphous crystal [21,22]. All these materials were classified thermoelectrically by Slack, reducing mainly the criteria to their electronic structure using their narrow band and how high the conductivity of carriers is [23–27].

Moving to the denominator of the figure of merit, we find the thermal conductivity $\kappa = \kappa_e + \kappa_{ph}$. Following the Wiedemann-Franz law, we have that $\kappa_e = L\sigma T$, with L the Lorenz number. The phonon contribution is $\kappa_{ph} = \frac{1}{3}C_V v_s l_p$, with C_V the heat capacity at constant volume, v_s the speed of sound in the medium, and l_p the phonon mean free path. In ideal conditions, where the lattice thermal conductivity is zero, we obtain a simple relationship between the Seebeck

coefficient and the figure of merit, $ZT = S^2/L$. For instance, to achieve a figure of merit of 2, considering the Lorenz number of Sommerfeld $L = \frac{\pi^2}{3}\left(\frac{k_B}{e}\right)^2 = 2.44 \times 10^{-8} V^2 K^{-2}$, we have numerically $S^2 = 4.88 \times 10^{-8} V^2 K^{-2}$. Therefore, by taking the above expressions, it would be almost impossible to reach a value higher than $ZT = 3$, given the typical values for the Seebeck coefficient. Broadly speaking, without considering the phonon contribution, the potential difference associated with the Seebeck effect attempts to fix a certain electronic charge at a given temperature gradient, and, on the other hand, this potential creates a greater electronic current proportional to the mentioned charge density. So, if the density of the electric current is high, under an applied external electric field, the same thing happens with the moving electrons, which do not have time to thermalize the sample. In semiconductors, the carriers are separated by an energy gap, which helps the above physical process to occur. This electric separation could be improved, in a very subtle form, when a non-trivial topology is also present, as we shall try to show in this paper. The topological insulators are a paradigmatic example, where the moving electrons are constrained to be in a very narrow surface and their conservation depends on the topology [28].

Some research lines on the thermoelectricity of topological insulators have focused on the characteristics that distinguish these materials: they are metallic on the surface and insulators in the bulk. Thus, the basic idea was to choose materials with a maximal surface/volume ratio, as is the case of nanostructured materials. This is because non-trivial topological transport concentrates at the surface. On the one hand, the electrical conductivity is ballistic and without backscattering with material defects, neglecting the transitions between edge states that counterpropagate [29,30]. On the other hand, the thermal conductivity is almost the same as that of a material with trivial topology except for temperature quantifications, as we will show for massless fermions [31,32]. While this treatment does not really explain how thermoelectricity emerges from a topological context, but rather how it can be described using classical thermoelectricity concepts within the limits outlined above, it provides a useful framework for interpreting experimental results and guiding potential applications. [33–46].

Therefore, it seems necessary to go deeper to understand the topological mechanism that allows the transformation of thermal energy into electrical energy, fighting against the second law of thermodynamics. Historically, the fundamental concepts of topology in materials were introduced after the discovery of the quantum Hall effect [47–52], which allowed new materials to be predicted based on theoretical considerations almost two decades later. One of the most studied is the topological insulator, whose electrodynamics include the pseudoscalar Lorentz invariant $\boldsymbol{E}\cdot\boldsymbol{B}$ besides the usual $E^2-(cB)^2$ scalar in the action. Given that the above pseudoscalar is not invariant under time-reversal symmetry, a new field $\theta(\boldsymbol{r},t)$ has to be introduced to make it time-reversal invariant. This new term in the electromagnetic action, called axion field, has many different interpretations in the literature, going from a Chern–Simons [53] to a sophisticated topological conception through the Atiyah–Singer theorem [54,55], applied to effective coupled massless Dirac electrons. In fact, it appears as a quantum anomaly associated with the breaking of the chiral symmetry that induces the non-conservation of its electronic currents [56–58]. Moreover, there is a kind of complex Thouless pumping [48] between the surface and nearby bulk atoms, where the temperature can play a crucial role in the creation of a topological current of chiral electrons. The Thouless pump works for adiabatic changes that allow determining the Berry curvature and, therefore, the winding numbers associated with the cyclic electronic evolution in the Bloch bands. This will allow treating the thermoelectric parameters as a function of the winding numbers related to the ballistic electrical conductivity and the Seebeck coefficient for determining the power factor from a pure topological scope [31,48,59–63].

The above topological mechanism applies to the Bi_2Te_3, which is the best topological thermoelectric at room temperature and also a topological insulator, as Bi_2Se_3 and Sb_2Te_3, which share the same crystalline rhombohedral structure with space group R-3 m. Considering their topological features, it was found that their figure of merit (in the absence of phonons) would be $ZT = n^2\overline{n}^3\frac{\pi^2}{3\zeta(3)}$, being $\overline{n}$ and n two topological indexes associated with the thermopower and electronic transport [31,64]. This gives an ideal dimensionless figure of merit $ZT = 2.737$, taking the basic topological numbers. Topological indices are integers that can change the thermoelectric values drastically, but their true physical meaning lies behind subtle concepts that we will develop in this review. We have effective massless electrons coupled to an axion electrodynamics that leads to instantons with anomalous tunneling. The energy–momentum of the electromagnetic background, with an average value of zero for self-dual solutions, is in equilibrium with the electronic zero modes close to the surface, in such a form that an increase in the thermal energy implies a change of electronic pumping frequency, due to having electronic localization close to the surface. That is an essential new mechanism for topological thermoelectricity. Furthermore, the proximity effect allows sharing of the topology between topological insulators and topological superconductors in heterostructures, both having their topological behavior mainly on their respective surfaces. That is one of the possibilities of increasing the topological indices presented above in the new figure of merit, considering their complementarity as topological phases [65–67] within the 10-fold classification. In summary, we hope to help understand the physical background of topological materials as well as their aforementioned applications to topological thermoelectricity.

The organization of this paper is as follows: (a) In Section 2, we begin by studying the special electromagnetism that appears as a background of topological materials, mainly on their surface. This modifies Maxwell's equations by including an electric polarization $\boldsymbol{P}$ and a magnetization $\boldsymbol{M}$ originating from the scalar field $\theta(r,t)$, which ensures time-reversal invariance. We analyze the symmetry of dual rotations in electrodynamics and the stability conditions for the self-dual field solutions, ending the section by revisiting the discrete Lorentz symmetries that justify introducing $\theta(r,t)$. (b) In

Section 3, we study the axionic term on the surface of the material by expressing it in terms of potentials, leading to the Chern–Simons term and the anomalous Hall conductivity. We discuss the half-integer Hall conductivity, its resolution through massless fermions, and the complementary dynamical roles of electrons and photons. The Berry phase and the electric polarization defined from electronic bands are also introduced, showing their complementarity with the electromagnetic potential in a principal fiber bundle framework. (c) In Section 4, we show that axial currents are not conserved in an axionic electromagnetic background, a fact fundamental to explaining the Chern–Simons anomalous currents through the Inflow Anomaly. This mechanism connects surface and bulk anomalies, resolving the half-integer Hall effect and relating electric currents to thermal energy by making the domain wall temperature-dependent. (d) In Section 5, we return to the study of the discrete symmetries of the Lorentz group in a quantum context to understand the topological complementarity between topological insulators and superconductors, as well as their classification into ten classes according to time-reversal $\mathcal{T}$, charge-conjugation $\mathcal{C}$, and chiral $\mathcal{S}$ symmetries. (e) Finally, in Section 6, we analyze thermoelectricity from the physical and topological perspectives of these materials. We apply the developed concepts to the topological insulator Bi_2Te_3, obtaining a dimensionless figure of merit close to experimental results, and explore the possibility of increasing efficiency through the inclusion of topological superconductors. At the end of the article, we present the basic and well-known topological models of these materials in an appendix. All of them are based on the electronic part complementary to that of the fields we have developed in the review. The system of units used throughout the paper is SI, except in sections where constants are set equal to one for simplicity and later restored to their full expressions.

There are currently several comprehensive reviews covering some of the topics discussed in this work, including the fundamental physics of topological insulators and superconductors, their experimental realizations, and recent developments in topological materials [68–77]. These works provide an extensive overview of the state of the field and serve as valuable references complementing the theoretical framework developed here.

2. Classical axion electrodynamics

One of the fundamental characteristics of topological materials is that there is a background electromagnetic field, which does not propagate but drastically changes the coupling of the electrons with the fields [78,79]. To preserve the time-reversal symmetry in the electromagnetic action with the two Lorentz invariants associated with the fields, it is necessary to include the new field $\theta(\boldsymbol{r},t)$, whose immediate effect is to change Maxwell's equations. In fact, a new electric polarization $\boldsymbol{P}$ and a magnetization $\boldsymbol{M}$ arise related to the boundary conditions. Obviously, this electrodynamics mixes electricity and magnetism differently than in an ordinary vacuum without the above restrictions. For this purpose, we also analyze the duality rotation symmetry to find self-dual solutions that make the energy–momentum tensor zero and thus determine a stable configuration. We end this section by showing the discrete Lorentz symmetries, which are widely used to classify topological materials, and which we will redefine later within a quantum context.

2.1. Classical axion electromagnetism

The action for the topological materials is [80]

$$\mathcal{S}=\int dx^4\left(\frac{-1}{4\mu_0 c}F_{\alpha\beta}F^{\alpha\beta}-\frac{1}{c}A_\mu J^\mu-\frac{e^2}{32\pi^2\hbar}\theta(r,t)\epsilon_{\mu\nu\alpha\beta}F^{\mu\nu}F^{\alpha\beta}\right) \tag{1}$$

being $\epsilon_{\mu\nu\alpha\beta}$ the Levi-Citiva tensor, with $\epsilon_{0123}=-1$ and $\epsilon^{0123}=+1$, $A^\mu=(\frac{\phi}{c},\boldsymbol{A})$ the 4-potential with ϕ the ordinary electric potential, c the speed of light and $\boldsymbol{A}$ the vector potential. The electromagnetic field is defined by $F^{\alpha\beta}=\partial^\alpha A^\beta-\partial^\beta A^\alpha$ where the derivatives are $\partial^\alpha=(\frac{1}{c}\frac{\partial}{\partial t},-\nabla)$ and $x^\alpha=(ct,\boldsymbol{x})$ the 4-position. $J^\mu=(\rho c,\boldsymbol{J})$ is the 4-current, where ρ is the charge density and $\boldsymbol{J}$ is the current density. The Minkowski metric $\eta_{\alpha\beta}$ is chosen with signature $(1,-1,-1,-1)$ along its principal diagonal. It is essential to note that the first and second terms of the action rise or fall indices with the metric, whereas the third term does so with the Levi-Civita tensor. This distinction indicates that the third term is topological, as it does not depend on the metric.

Making the variation of the potentials, we have the action

$$\mathcal{S}=\int dx^4\left[\partial_\alpha\left(\frac{1}{4\mu_0 c}F^{\alpha\beta}+\frac{e^2}{32\pi^2\hbar}\theta(r,t)\epsilon^{\alpha\beta\mu\nu}F_{\mu\nu}\right)-\frac{1}{c}J^\beta\right]\delta A_\beta, \tag{2}$$

which lead to the equivalent Maxwell's equations

$$\partial_\alpha\left(\frac{1}{4\mu_0 c}F^{\alpha\beta}+\frac{e^2}{32\pi^2\hbar}\theta(r,t)\epsilon^{\alpha\beta\mu\nu}F_{\mu\nu}\right)-\frac{1}{c}J^\beta=0 \tag{3}$$

whose space and time projections give us

$$\nabla\cdot\left(\boldsymbol{E}+2\alpha c\left(\frac{\theta}{2\pi}\right)\boldsymbol{B}\right)=\frac{\rho}{\epsilon_0}, \tag{4}$$

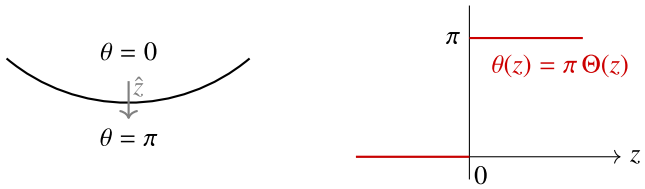

Fig. 1. Schematic illustration of a vacuum–topological insulator interface where the axion field takes values of $\theta = 0$ for the trivial regime and $\theta = \pi$ for the topological insulator. We model the axion field in the boundary as $\theta(z) = \pi\,\Theta(z)$, $\Theta(z)$ is the Heaviside step function.

substituting the Gauss law, and

$$\nabla \times \boldsymbol{B} = \mu_0 \boldsymbol{J} + \frac{1}{c^2}\frac{\partial \boldsymbol{E}}{\partial t} + \frac{2\alpha}{c}\left[\boldsymbol{B}\frac{\partial}{\partial t}\left(\frac{\theta}{2\pi}\right) + \nabla\left(\frac{\theta}{2\pi}\right) \times \boldsymbol{E}\right] \tag{5}$$

instead of the Maxwell-Ampere one, being $\alpha = \frac{e^2}{4\pi\epsilon_0\hbar c}$ the dimensionless fine structure constant. The other two equations, Faraday and the non-existence of isolated magnetic poles, maintain the same form, which justifies the introduction of the potentials.

It is easy to interpret these vector equations by introducing the displacement vector $\boldsymbol{D} = \epsilon_0\boldsymbol{E} + \frac{e^2}{4\pi^2\hbar}\theta\boldsymbol{B}$ and the magnetic induction field $\boldsymbol{B} = \mu_0(\boldsymbol{H} + \frac{e^2}{4\pi^2\hbar}\theta\boldsymbol{E})$, where new electric polarization $\boldsymbol{P} = \frac{e^2}{4\pi^2\hbar}\theta\,\boldsymbol{B}$ and magnetization $\boldsymbol{M} = \frac{e^2}{4\pi^2\hbar}\theta\,\boldsymbol{E}$ arise. These relations clearly show that the axionic field θ couples the electric and magnetic sectors, producing a magnetoelectric response that is a hallmark of topological materials.

We can now look for the bound charge density and the currents induced by the axionic term in a topological insulator. We have that the bound charge density is given by

$$\rho = -\nabla \boldsymbol{P}, \tag{6}$$

and the currents

$$\boldsymbol{J} = \nabla \times \boldsymbol{M} + \frac{\partial}{\partial t}\boldsymbol{P}, \tag{7}$$

which, after a simple calculation, we obtain

$$\rho = -\frac{e^2}{4\pi^2\hbar}\nabla(\theta)\boldsymbol{B} \tag{8}$$

and

$$\boldsymbol{J} = \frac{e^2}{4\pi^2\hbar}\nabla(\theta) \times \boldsymbol{E} + \frac{e^2}{4\pi^2\hbar}\frac{\partial\theta}{\partial t}\boldsymbol{B} \tag{9}$$

using Faraday's law. Its values on the surface, separating the void with $\theta = 0$ from the interior $\theta = \pi$, where we have a Heaviside step function $\Theta(z)$ (see Fig. 1) whose derivative with respect to this coordinate z, associated with the direction orthogonal to the surface, gives us a delta at that point $\delta(z)$. So the charge density on the surface can be obtained at a point z as $\sigma_s(z) = -\frac{e^2}{4\pi^2\hbar}\pi\boldsymbol{B}\delta(z)$ and integrating it gives the total density.

$$\sigma_s = -\int_{-\epsilon}^{+\epsilon} d\boldsymbol{z}\,\frac{e^2}{4\pi\hbar}\boldsymbol{B}\delta(z) \tag{10}$$

with ϵ being a positive or negative infinitesimal of z and gives the charge density on the surface by

$$\sigma_s = -\frac{\theta}{\pi}\alpha\epsilon_0 c\boldsymbol{B}\cdot\hat{\boldsymbol{n}}. \tag{11}$$

Similarly, we could obtain the current density using the same physical–geometric assumptions and neglecting the time variations of θ

$$J_s = \frac{\alpha\theta}{c\mu_0\pi}\hat{\boldsymbol{n}} \times \boldsymbol{E} \tag{12}$$

Therefore, while the Lorentz equation remains unaffected by the modifications introduced in axionic electromagnetism and therefore does not influence the dynamics of charge motion, the associated charge densities undergo substantial changes [81–85].

2.2. Duality rotations

The electromagnetic field $F^{\mu\nu}$ is an antisymmetric second-order tensor that in Minkowski space satisfies the condition

$$**F^{\mu\nu} = -F^{\mu\nu}, \tag{13}$$

where the operator $*$ is defined with the Levi-Civita tensor that gives the dual of the electromagnetic field when applied to it.

Actually, the duality operator $*$ must be properly defined on the algebra of exterior differential forms where the electromagnetic field is a 2-form. In that algebra $*$ corresponds to the Hodge operator and has the property that if applied twice on a p-form we have $*\cdot* = *^2 = (-1^{p(n-p)+s})I$, where p is the order, n is the dimension of space, I is the identity operator, and s is the difference between the positive and negative signs in the Minkowski metric. For the electromagnetic field, we have $p = 2$, $n = 4$, and for the chosen metric $s = 1$ [31,86]. Then

$$** F^{\mu\nu} = (-1)^{2(4-2)+1}F^{\mu\nu} = -F^{\mu\nu} \tag{14}$$

Note that changing the dimensionality or the number of minus signs would change the square of this operator. In the Euclidean case $s = 0$ and $**F^{\mu\nu} = +1F^{\mu\nu}$ and ± 1 for the eigenvalues of the dual operator $*$.

Therefore, in the Minkowski metric, the eigenvalues of this operator are $\pm i$. A fundamental observation is that the space–time dimension must be pair for the above equality between fields and their duals; i.e., they don' t exist in odd space–time dimensions, as it happens with the quantum chiral anomalies, and for odd rank tensors as J_μ and A_μ. This can be generalized to obtain rotations in the complex plane

$$\overline{F}^{\mu\nu} = e^{-i\varphi}F^{\mu\nu}; *\overline{F}^{\mu\nu} = e^{i\varphi} * F^{\mu\nu}, \tag{15}$$

which we can rewrite in three dimensions (Fig. 2)

$$E \to \overline{E} = E\cos\varphi + Bc\sin\varphi \tag{16}$$

$$Bc \to \overline{B}c = -E\sin\varphi + Bc\cos\varphi \tag{17}$$

with the scalar Lorentz invariant being angle–dependent

$$(\overline{E}^2 - \overline{B}^2c^2) = (E^2 - B^2c^2)\cos 2\varphi + 2EBc\sin 2\varphi, \tag{18}$$

while the density of energy

$$\overline{E}^2 + \overline{B}^2c^2 = E^2 + B^2c^2 \tag{19}$$

remains unchanged. So these transformations, which are also independent of the metric, do not follow the Lorentz group, while energetically, they remain invariant under the group of rotations $SO(2)$. In fact, this invariance can be extended to the energy–momentum tensor because the Poynting vector $\boldsymbol{N} = \boldsymbol{E} \times \boldsymbol{H}$ and the stress tensor $T_{ij} = \epsilon_0 E_i E_j + \mu_0 H_i H_j - \frac{1}{2}(\epsilon_0 E^2 + \mu_0 H^2)$ make it. So, these transformations leave the equation of motion for charged particles invariant, even though their action does not. Therefore, they have nothing to do with the transformations between electricity and magnetism associated with the movement with respect to an observer. Its most common name in the literature is dual rotations [87–89]. Experimental realizations exploiting this symmetry have been reported in Ref. [90]. That suggests that the axionic action is a dual transformation of the Maxwell action, where $\tan\varphi = \frac{e^2}{32\pi^2\hbar}\theta(r,t)$. In general, this is not true, among other things, because it would mean that the dual rotations angle φ would depend on the coordinates locally, which is false. However, if we take φ for a material with constant θ, then such difficulty would be overcome, and the mixture of electricity and magnetism would take place in a different form than the usual one in Maxwell's electrodynamics. One example is the topological insulator, where $\theta = \pi$ [91]. Physically, it corresponds to a mixture of electricity and magnetism depending on the value of this angle φ. For $\varphi = \pi(2n \pm 1)$, with n an integer value, we recover the usual relationship between electric and magnetic fields. For $\varphi = \pi(2n \pm \frac{1}{2})$, the electric and magnetic fields are interchanged. The other values have both electricity and magnetism depending on the value of the angle φ [92].

It is easy to see that a self-dual or anti-self-dual solution in Minkowski's space–time, $\overline{F}_{\mu\nu} = \pm i * \overline{F}_{\mu\nu}$ gives a null value to the tensor energy–momentum

$$T_{\mu\nu} = \frac{1}{\mu_0}[F^\varphi_\mu F_{\varphi\nu} + \frac{1}{4}\eta_{\mu\nu}F_{\alpha\beta}F^{\alpha\beta}], \tag{20}$$

where $\eta_{\mu\nu}$ is the Minkowski metric, which can be rewritten as $\frac{1}{2\mu_0}[F^\varphi_\mu F_{\varphi\nu} + *F^\varphi_\mu * F_{\varphi\nu}]$, for obtaining

$$T_{\mu\nu} = \frac{1}{2\mu_0}(F^\varphi_\mu + i * F^\varphi_\mu)(F_{\varphi\nu} - i * F_{\varphi\nu}) = 0, \tag{21}$$

which is zero for such solutions. Notice that the self-dual and anti-self-dual solutions lead to $E = \pm cB$, which is a minimum of the action and Maxwell equations.

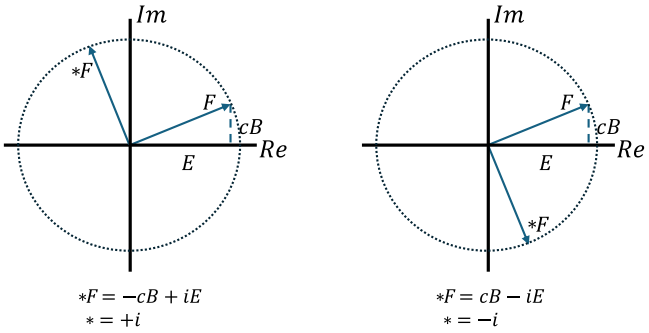

Fig. 2. Dual rotations for the electromagnetic field in a complex representation induced by the eigenvalues of the dual operator.

We note that the axionic term is not included in the energy–momentum tensor because it does not depend on the spacetime metric. In our calculation, we employ the Hilbert formulation for its calculation

$$T^{\mu\nu} = -\frac{2}{\sqrt{-\eta}}\frac{\delta \mathcal{S}}{\delta \eta_{\mu\nu}}, \tag{22}$$

where η is the determinant of the metric. This leads to the same expression for regular Maxwell electromagnetism with only one additional term $\frac{e^2}{32\pi^2\hbar}\theta(r,t)\epsilon_{\mu\nu\alpha\beta}F^{\mu\nu}F^{\alpha\beta}$, if we note that the axionic term does not depend on the metric. Note that to apply this Hilbert formalism, it is necessary to introduce $\sqrt{-\eta}$ into the action integral in Eq. (1).

$$\partial_\mu T^{\mu\nu} = \frac{e^2}{32\pi^2\hbar}\partial^\nu\theta(r,t)\epsilon_{\mu\nu\alpha\beta}F^{\mu\nu}F^{\alpha\beta} \tag{23}$$

This expression reveals a nontrivial coupling between the electromagnetic field and the axionic field θ, which breaks the conservation of the energy–momentum tensor, which prevents its conservation. When θ is constant, this extra term vanishes, and $T^{\mu\nu}$ reduces to the usual electromagnetic energy–momentum tensor [93,94].

For the Euclidean metric, where the time coordinate is Wick-rotated as $x_0 = ict$, the metric tensor has all negative signs along its main diagonal. Under this transformation, the self-dual solutions discussed above become real quantities rather than complex ones, and the electromagnetic duality rotations characteristic of Minkowski spacetime no longer apply. These solutions were first studied in the context of the non-Abelian Yang–Mills equations, where they were called instantons. In fact, in such non-Abelian theories, the action is finite and proportional to integer values. For self-dual configurations, these integers can be interpreted as topological numbers associated with distinct homotopy classes [95]. In Euclidean space, these quantities are real and correspond to instanton numbers that describe tunneling processes between different vacuum states. It is worth noting that topological insulators also host degenerate electronic states protected by Kramers' theorem, a feature we will revisit in the context of thermoelectric materials.

Thus, these solutions provide an electromagnetic background that does not require external energy input to sustain itself. This property is particularly relevant to axion electrodynamics, where lattice vibrations can assist in the Thouless pumping process. Although we might be tempted to regard these configurations as ordinary instantons, we must exercise caution: when rewriting Minkowski spacetime in Euclidean form, we are restricted to electrodynamics with an Abelian gauge group $U(1)$ (or equivalently $SO(2)$ for the dual field transformations mentioned earlier), and in this case, the action is not finite as in the non-Abelian scenario. This makes their interpretation as particle-like entities difficult, although their behavior remains similar in that they describe tunneling between distinct states.

Note that this background has significant physical implications, as it defines a geometrical context different from that of the usual vacuum. For instance, in electrodynamics the derivatives D_μ must be defined covariantly for the group $U(1)$ as $D_\mu = \partial_\mu - i\frac{e}{\hbar}A_\mu$. This leads to $[D_\mu, D_\nu] = -i\frac{e}{\hbar}F_{\mu\nu}$, which may also contain nontrivial topological solutions since its homotopy group $\pi_1(U(1)) \cong \mathbb{Z}$ can be nonzero [96], where $\mathbb{Z}$ denotes the set of integers. Furthermore, this will allow us to establish a direct relationship between the vector potential $\boldsymbol{A}$ and the Berry connection, as will be discussed later.

2.3. Discrete symmetries

The term $F_{\mu\nu} * F^{\mu\nu}$ does not have the discrete Lorentz symmetries associated with time $\mathcal{T}$, and parity $\mathcal{P}$ symmetries, because it contains the Levi-Civita tensor, and this is a difficulty that needs to be addressed in many topological materials. Classically, it is easy to show the discrete symmetries on the equation of motion of an electric charge e, i.e., the Lorentz equation $\frac{d}{dt}\boldsymbol{p} = e(\boldsymbol{E} + \boldsymbol{v}\times\boldsymbol{B})$. For the time-reversal $\mathcal{T} : t \mapsto -t$, we see that $\boldsymbol{B}(\boldsymbol{r},t) = -\boldsymbol{B}(\boldsymbol{r},-t)$. The magnetic field changes its sign while the electric field $\boldsymbol{E}(\boldsymbol{r},t) = \boldsymbol{E}(\boldsymbol{r},-t)$ remains invariant. For the spatial inversion $\mathcal{P} : \boldsymbol{r} \mapsto -\boldsymbol{r}$, the opposite occurs, and for charge conjugation $\mathcal{C} : e \mapsto -e$, both change sign. Therefore, the $\mathcal{CPT}$ theorem associated

with the Lorentz group $SO(3,1)$ is satisfied, which forces the composition of these three operator transformations to be invariant.

Finally, we should note that, in order to obtain a self-dual solution for the electromagnetic background such as the one described above, where $\boldsymbol{E}(\boldsymbol{r},t) = \pm c\,\boldsymbol{B}(\boldsymbol{r},t)$, it is necessary to exercise caution when applying discrete symmetries to them, since the electric field and the magnetic follows different discrete symmetries. In particular, this introduces an additional constraint that must be satisfied when attempting to combine, for instance, a superconductor and a topological insulator to achieve the desired proximity effect. It is also important to recall that dual rotations leave the equations of motion invariant and can therefore serve as a general test for verifying the discrete symmetries discussed above in the framework of electrodynamics.

The difficulty arising from the term $F_{\mu\nu} * F_{\mu\nu}$, which is not invariant under time-reversal $\mathcal{T}$ or spatial inversion $\mathcal{P}$, is resolved by coupling it to a dimensionless pseudoscalar field $\theta(\boldsymbol{r},t)$ that satisfies $\mathcal{T}\theta(\boldsymbol{r},t) = -\theta(\boldsymbol{r},t)$ and $\mathcal{P}\theta(\boldsymbol{r},t) = -\theta(\boldsymbol{r},t)$. There are, however, two exceptional cases. When $\theta = \pi$, the field is invariant because of its 2π periodicity, making π and $-\pi$ physically equivalent. For $\theta = 0$, the axionic term vanishes, and consequently, the electromagnetic theory remains fully invariant under both $\mathcal{T}$ and $\mathcal{P}$ symmetries. The condition $\theta = \pi$ corresponds to topological insulators, whereas $\theta = 0$ characterizes topologically trivial materials [97].

3. Quantum axion electrodynamics

In the quantum formalism of path integrals, the action appears directly within a phase, so it is not surprising that θ does. Furthermore, θ is part of a term that is a surface integral and, therefore, must act on the surface of a finite material. The curious thing is that if you want to make this action $\mathcal{S}$ time-reversal symmetric, then it looks like the electrical conductivity notices it through the Chern–Simons formalism in anomalous form. We will see in this section that the chiral currents of the electrons on the bands will be necessary to recover the proper electronic conductivity obtained by the Chern–Simons fields. Furthermore, we develop the Berry phase formalism showing the complementarity of the band electrons behavior with electromagnetic fields background in topological materials [98–103].

3.1. The $\theta(\boldsymbol{r},t)$ field as an angle with periodicity 2π

The axionic term of the action

$$\mathcal{S}_\theta = \frac{e^2}{32\pi^2\hbar}\int_{T^4} dx^4\theta(r,t)\epsilon_{\mu\nu\alpha\beta}F^{\mu\nu}F^{\alpha\beta}, \tag{24}$$

which is added to the usual of Classical Electrodynamics, is also known as the one corresponding to the axial anomaly of Quantum Field Theory, and was introduced for the first time to explain the decay time of a neutral pion to two photons $\pi^0 \to \gamma\gamma$. That is, a term that breaks the classic axial symmetry by being quantized and very well contrasted experimentally [104–108].

If the electric and magnetic fields are confined to the Brillouin zone as a torus $T^4 = T^2 \times T^2$ in 4-dimensional space–time. The total electromagnetic flux in this 4-dimensional torus is given by

$$\Phi_{T^4} = \int_{T^4} dx^4 \boldsymbol{E}\boldsymbol{B} = \int_{T^2} dx_0 dx_1 E \int_{T^2} dx_2 dx_3 B = v_F \Phi_B^2. \tag{25}$$

Keeping in mind that the electric field is the space–time component of the electromagnetic field, and the magnetic field is the pure spatial component. For example, $F_{01} = \frac{-E_1}{c}$ and $F_{23} = B_1$. In the exterior algebra of differential forms, these projections appear specific and ready to be used in an integral like this one for the 2-form of the electromagnetic field[86]. This suggests that these fluxes must be quantized if we imagine the electric and magnetic fields not time-varying within the torus, acting as an Aharonov–Bohm effect on the electrons, where both fluxes give $\Phi_B = \frac{\Phi_E}{v_F} = n\frac{h}{e}$. The fields hence take the values $\boldsymbol{E} = n\frac{hv_F}{ea^2}\hat{x}$ and $\boldsymbol{B} = n\frac{h}{ea^2}\hat{x}$ where a is the lattice constant, n is an integer, h is Planck's constant, and v_F is the Fermi velocity that replaces the light velocity c in this effective relativistic formalism in a solid. So, we have

$$\mathcal{S}_\theta = \theta\frac{e^2}{4\pi^2\hbar}\Phi_B^2 = n^2\hbar\theta. \tag{26}$$

The partition function becomes $\exp[i\frac{S_\theta}{\hbar}] = \exp[in^2\theta]$ once the given value is substituted for the fields. Therefore, θ must take periodic values of $2\pi m$ radians with m an integer number, although we will see that its relationship with topology is deeper in the following sections. So, the aim of these calculations is only to help us have a picture of how the new mixed electromagnetic fields can survive in the material, creating polarizations, although they cannot propagate.

Let us summarize the basic physical and geometric concepts underlying this subsection. The first important observation is that this axion term produces a quantized action that can be interpreted as parallel electric and magnetic fluxes confined within a T^2 torus. The second is that it modifies the internal structure of the material by introducing electric polarizations and magnetizations of topological origin. This tells us that these fields are very special and that their effective velocity does not have to be the c of vacuum. Their real role is to exchange energy with the electronic medium in the topological region of the material. A critical point is the dimensional change between the volume and the surface, where the θ field

undergoes a drastic change, in addition to the electromagnetic field. We will see how the Chern–Simons mechanism induces a topological mass on the photons of odd-dimensional space. In the case we will develop in the next subsection, the volume has even dimensions, $3+1$, and the surface has odd dimensions, $2+1$. This is also another sign that photons at the surface must move at a speed lower than c and the electrons associated with the gapless bands have speed v_F. But we will also see how massless electrons with speed v_F must match the currents associated with these fields, so we associate them with an effective Fermi velocity [109–114].

The defined electric and magnetic fields are actually separate and do not interact for the axion term, as a magnet and an electrically charged body might. That is, they are static fields that are assumed to be confined in separate tori, such that T^4 appears as the product of two other $T^2 \times T^2$ fields in the Brillouin zone if we consider them as two fields associated with different coordinates. One torus corresponds to two spatial (magnetic) coordinates, while the other corresponds to space–time (electrical) coordinates [115–117]

3.2. Anomalous electronic transport

The other important feature of this non-local term of the action is that it leads to a Chern–Simons on the surface. Speaking with more accurate mathematical language, we know that the torus is a compact manifold whose boundary is zero, which belongs to the class of closed manifolds. So, when we refer to the surface, we mean the boundary that cannot be extended trivially by the Brillouin zones, which are closed [96,118]. Coming back to the axion term

$$\begin{aligned}\mathcal{S}_\theta &= \frac{e^2}{32\pi^2\hbar}\int_\Omega dx^4\theta(\boldsymbol{r},t)\epsilon_{\mu\nu\alpha\beta}F^{\mu\nu}F^{\alpha\beta}\\ &= \frac{e^2\theta}{4\pi^2\hbar}\int_\Omega dx^4\epsilon_{\mu\nu\alpha\beta}\partial^\mu(\epsilon_{\mu\nu\alpha\beta}A^\nu\partial^\alpha A^\beta)\\ &= \frac{e^2\theta}{4\pi^2\hbar}\int_{\partial\Omega} dx^3\epsilon_{\nu\alpha\beta}A^\nu\partial^\alpha A^\beta\end{aligned} \tag{27}$$

using Stocke's theorem, Ω is the 4-volume of integration and $\partial\Omega$ its geometric border. Note that this cannot be the compact manifold Brillouin Zone associated with a torus T^4 because the above border would be zero. We note that on the surface of the topological insulator, θ goes from $\theta = 0$ (in vacuum) to $\theta = \pi$ (in the material), so we can consider it to follow a Heaviside step function on the surface, i.e. $\theta(\boldsymbol{r},t) = \theta\Theta(x^\mu)$, where $\Theta(x^\mu)$ is the Heaviside's function with value 0 or 1. On the other hand, this function varies only with respect to the direction orthogonal to the surface, and its derivative gives $\frac{\partial}{\partial x_\mu}\Theta(x_\mu) = \delta(x_\mu)$, where x^μ is the direction orthogonal to the surface. This allows us to obtain it as a constant of the integral for that coordinate and, therefore, double the value of the surface integral. The density of currents derived from this action, taking θ constant, is

$$J_i(x) = \frac{\delta\mathcal{S}_\theta}{\delta A^i(x)} = \theta\frac{e^2}{4\pi^2\hbar}\epsilon_{i\nu\alpha}\partial^\nu A^\alpha, \tag{28}$$

and considering the space projections, we have

$$J_i = \theta\frac{e^2}{2\pi h}\epsilon_{0ij}E^j \tag{29}$$

or using Ohm's law

$$J_i = \sigma_{ij}E^j, \tag{30}$$

being σ_{ij} the conductivity tensor, whose elements are out of the principal diagonal

$$\sigma_{ij} = \theta\frac{1}{2\pi}\frac{e^2}{h} = \frac{e^2}{2h}, \tag{31}$$

that we can take it as the fundamental state of conductivity with $n = 0$. Note that all these calculations were performed using the correspondence bulk-boundary in Stokes theorem, hence the above conductivity is on the surface, when $\theta = \pi$ is assumed to be constant as it should be for a non-trivial topological insulator. Thus, the resulting Hall conductivity is given by [119]

$$\sigma_{ij} = \left(n + \frac{1}{2}\right)\frac{e^2}{h} \tag{32}$$

Obviously, this result alone is not faithful because we know that the conductivity scales with the integer numbers $\mathbb{Z}$ associated with Chern numbers,which must always be integer numbers. We will see that this anomalous outcome can be cured and is due to the coupling between the Chern–Simons field and massless fermions, which reveals an essential property for thermoelectricity within these topological materials [120]. In nontrivial topological insulators, we will see that the surface hosts electronic states that carry precisely half of the quantum of conductance. It is remarkable that massless Dirac electrons, when coupled to the electromagnetic field, give rise to such topological currents, as we explore in more

detail below. Although this mechanism is quite complex, it is very well proven experimentally in the field of fundamental particles for pion decay [121]. It is known as a chiral anomaly because the symmetry of classical electrodynamics is violated when introducing quantum corrections. In condensed matter, this effect has been observed experimentally for the Wey semimetals Na_3Bi, $GdPtBi$, $ZrTe_5$, Cd_3As_2, and $TaAs$ [122]. An easier way to interpret and overcome this difficulty is found in magnetic topological materials, which we will examine in more detail in this section [123,124].

3.3. Axion detection in topological insulators

The idea behind the field associated with θ dates from the 70s [125], and was deeply developed by Weinberg and Wilczek [126,127] to explain the non-breaking of the *CP* symmetry in the strong nuclear interaction, just as it happens with the weak interaction. The most paradigmatic example is the neutron, which must have an electric dipole moment according to the Standard Model of fundamental particles, the value of which was even calculated quite accurately, and yet, after many very precise experiments, it refused to appear. The existence of the neutron electric dipole moment would explain the *CP* symmetry violation (equivalent to *T* violation) for the strong interaction, and thus, this helps the axion existence. These days, it has regained considerable attention because it is perhaps the leading candidate to explain dark matter in galactic haloes, although, in fundamental particle physics, there is still no fully convincing explanation. In topological insulators and Weyl semimetals, this axion field appears as electronic excitations forming quasiparticles that play a similar role to those axion particles. Thus, we can establish a wave equation for a scalar field whose action could be confirmed experimentally [91,128]. In the case of topological insulators, their surface is metallic and could be thought of as an ideal system to apply the Casimir methodology and see the influence of this axionic field [129].

Let us examine the contribution of this effect to the topological insulators and the new pressure that appears when its size diminishes. The density of energy of these topological axion electromagnetic fields $\xi_\theta = \frac{1}{2}(\boldsymbol{E_\theta D_\theta} + \boldsymbol{H_\theta B_\theta})$ is given by $\xi_\theta = \frac{\pi\hbar v_F}{\alpha_s a^4}$, neglecting the contribution of the electric polarization P and magnetization M, due to the small magnitude of the factor $\frac{e^2}{4\pi^2\hbar}$ [130,131]. α_s is the fine structure constant in the solid [132]. Notice that if the surfaces are far from each other $d = Na$, this effect would be negligible with P and M defined by the dipolar moments in the bulk. Thus, the density energy of the fields in each unit cell would be $\xi_\theta = \frac{\pi\hbar v_F}{\alpha_s a^4}$, and we can obtain [130]

$$P = -\frac{\pi^2\hbar v_F}{60d^4}, \tag{33}$$

which is the pressure due to the Casimir effect for the axion field $\theta(\boldsymbol{r}, t)$ in the topological insulators. In the same form, it is possible to extend it to non-zero temperatures

$$P = -\frac{\pi^2\hbar v_F}{60d^4} + \frac{2\pi k_B T}{d^3} exp\left(-\frac{2\pi\hbar v_F}{k_B T d}\right) - \frac{(k_B T)^4}{2\pi^2(\hbar v_F)^3}\zeta(4). \tag{34}$$

In the low temperature/distance limit, we can write the force or pressure exerted on the surfaces as $P = P_0\left(1 + \frac{1}{3}(\frac{T}{T^*})^4\right)$. This follows the same dependence as the Casimir force but redefines its main variables $P_0 = -\frac{\pi^2\hbar v_F}{60d^4}$, and the effective temperature $T^* = \hbar v_F/(k_B d)$ [130–135]. Although this effect is weak compared to the ordinary Casimir effect, it is significant, and it could be enhanced under certain experimental conditions. It could even be found whether the axions transform into photons or phonons using the Primakoff effect, as is considered in some experiments related to dark matter in astrophysics [136].

3.4. Berry's phase and topological electronic transport

In a solid with a periodic potential, the Bloch theorem shows that each eigenstate of the Hamiltonian $\mathcal{H}$ is labeled by a pair of quantum numbers: the band-index n and the wave number k associated with the momentum $p = \hbar k$. This justifies the importance of the band representation for the electronic structure. Thus, in the Brillouin zone (BZ), the states $|\psi_{nk}\rangle = e^{i\boldsymbol{kr}}|u_{nk}\rangle$ of the stationary Schrödinger equation $\mathcal{H}\psi_{nk}(\boldsymbol{r}) = \xi_{nk}\psi_{nk}$, are defined in such a form that the periodicity is given in $|u_{nk}(\boldsymbol{r} + \boldsymbol{R})\rangle = |u_{nk}(\boldsymbol{r})\rangle$ and the eigenvalues $\xi_{nk} = \xi_{nk+k'}$ with spatial period $\boldsymbol{R}$, belonging to the Bravais lattice. So, it is defined the Bloch Hamiltonian $\mathcal{H}(\boldsymbol{k}) = e^{i\boldsymbol{kr}}\mathcal{H}e^{-i\boldsymbol{kr}}$, where the eigenvalues ξ_{nk} and eigenstates $|u_{nk}(\boldsymbol{r})\rangle$ define unequivocally the electronic bands.

For an adiabatic evolution of the system, it arises a new phase associated with the states, which cannot be gauged and, therefore, it is real and measurable, known as Berry' s phase [137,138]

$$\gamma_n = -i\int_0^t dt\langle\psi_{nk}|\frac{\partial}{\partial t}|\psi_{nk}\rangle. \tag{35}$$

Geometrically, the integrand of the previous phase plays the role of a connection, named the Berry connection, just like the electromagnetic potential does. Its expression is $a_n = -i\langle\psi_{nk}|\frac{\partial}{\partial t}|\psi_{nk}\rangle$ [137,139]. Like the electromagnetic potential, it is also gauge-dependent, while the curvature

$$\Omega^n_{k_i k_j} = i\left[\langle\frac{\partial u}{\partial k_i}||\frac{\partial u}{\partial k_j}\rangle - \langle\frac{\partial u}{\partial k_j}||\frac{\partial u}{\partial k_i}\rangle\right] \tag{36}$$

is not. This allows us to define the first Chern number as a topological invariant

$$C_n = -\frac{1}{2\pi}\int_M d^2k\,\Omega^n_{k_ik_j} \tag{37}$$

with integer numbers, where n refers to the n-band. Then, for the n-band on the torus T^2 associated to the BZ, we have

$$C_n = -\frac{1}{2\pi}\int_{T^2} d^2k\,\Omega^n_{k_xk_y}, \tag{38}$$

and the electric conductivity is defined by

$$\sigma_{xy} = -\sum_n \frac{e^2}{2\hbar}\int_{T^2} dk^2\,\Omega^n_{k_xk_y} \tag{39}$$

where n sums over the bands below the Fermi energy. This result is the famous TKNN invariant and shows that the Integer Quantum Hall Effect (IQHE) has a topological origin [48]. Furthermore, this quantization of the Hall currents is linked to the emergence of gapless edge states on the sample boundaries [140], and it is called a quantum anomalous Hall insulator (QAHI) when the Chern number is non-zero. Haldane extended the Su–Schrieffer–Heeger (SSH) model to a hexagonal graphene lattice for obtaining a QAHI without needing a magnetic field in the background state [49,141]. The trick is that there are two inequivalent points, A and B, which, after using the periodicity with the Bloch theorem, show a pseudospin that breaks time-reversal symmetry as the magnetic field does in the above Chern–Simons currents [49]. This model was also generalized by Kane–Mele thanks to introducing spin–orbit terms in the Hamiltonian, where each spin has an independent TKNN integer $n_\uparrow$, $n_\downarrow$. Observing that the $\mathcal{T}$ symmetry requires $n_\uparrow + n_\downarrow = 0$, while their difference $n_\uparrow - n_\downarrow$ is nonzero and defines a quantized spin Hall (QSH) conductivity. Topologically, this leads to the introduction of a new topological invariant Z_2 [142]. Independently, Bernevig and Zhang also found another model in which the spin–orbit played a fundamental role by using the spin instead of the magnetic field [51]. This Berry formalism, using simple toy models, was very successful, even in predicting new topological materials. However, the electromagnetic non-trivial topological behavior of these materials was almost omitted. By the way, the Berry phase cannot give any information about bosons, it only does for fermions [80]. We will develop these models in Appendix A to understand them more thoroughly.

Finally, we finish this section by introducing the electrical polarization as a function of Berry' s phase as it is defined today. Taking the Fourier transform of the Bloch states, we have the local relationship between states

$$|W_n(\boldsymbol{R})\rangle = \frac{e}{2\pi}\oint dk e^{-i\boldsymbol{k}(\boldsymbol{R}-\boldsymbol{r})}|u_n(k)\rangle \tag{40}$$

in momentum space, which are known as Wannier states. They do not need to be eigenstates, but they allow us to calculate the electric polarization P in two dimensions by

$$\begin{aligned}\boldsymbol{P} &= e\langle W_n(\boldsymbol{R})|\boldsymbol{R}-\boldsymbol{r}|W_n(\boldsymbol{R})\rangle \\ &= i\frac{e}{2\pi}\oint_{BZ}\langle u_n(k)|\nabla_k|u_n(k)\rangle \\ &= \frac{e}{2\pi}\gamma_n,\end{aligned} \tag{41}$$

where the last integral corresponds to Berry' s phase. Note that the integral employed, in a non-contracting loop (non-trivial 1-cycles) in the Brillouin zone (i.e., a torus), makes this connection gauge-independent and applies only to a Hilbert subspace expanded by the Bloch eigenstates $|u(\boldsymbol{r})\rangle$ and not those of $|\psi\rangle = \exp\{i\boldsymbol{kr}\}|u(\boldsymbol{r})\rangle$. These particularities define the Zak phase [139] for electrical polarization rather than the more general Berry phase. That is the way that electrical polarization is currently defined. Geometrically, the Berry phase and the electric polarization correspond to holonomies in the principal fiber bundle modeling the topological materials, as we show shortly in the next section [95,96].

3.5. General Berry's phase and Chern–Simons geometrical background

Formally, although the Berry phase and the electromagnetic potential are very different physical objects, they can be understood as connections of the principal fiber bundle (PFB) whose fibers result in the Abelian group $\mathcal{U}(1)$ and the torus T^4 being the basis. In the topologically non-trivial case, it would not be possible to find a global section of the entire fiber bundle $T^4 \times \mathcal{U}(1)$ [95,96,118]. We have taken the toroid relation $T^4 = T^2 \times T^2$ for a physical interpretation of the electromagnetic fields in it (see Fig. 3). The connections allow us to relate the point of the fibers in two different points of the base by parallel transport. Although it is too abstract and not necessary in many respects for following the purpose of this paper, let us roughly give an idea of how to determine the general topology when we have the product of a manifold $SU(N)$ (fiber) times the space–times manifold M (base) defining a principal fiber bundle $P = SU(N) \times M$ locally, provided with a projection π carrying elements of P on the base, $\pi : P \to M$. Since the whole fiber bundle can have twists between

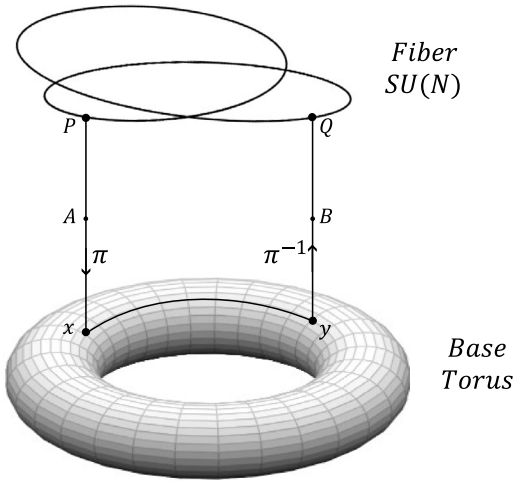

Fig. 3. Möbius band on a torus $\pi : S^1 \to S^1 \times S^1$. There are two possibilities of circles crossing (non-trivial) and without crossing (trivial). This can represent the connection of the magnetic potential $\boldsymbol{A}$ with the Berry connection $\boldsymbol{a}$.

the fiber and the base, as it happens in the non-trivial topology, then it is necessary to define the characteristic classes and the Chern Character using the invariance of the curvature Ω

$$ch\Omega = m + \left(\frac{i}{2\pi}\right)\mathrm{tr}\Omega + \frac{1}{2!}\left(\frac{i}{2\pi}\right)^2 tr\Omega^2 + \cdots, \tag{42}$$

which corresponds to a series expansion as a function of curvature, and m is a matrix associated with the m-representation chosen for the fiber. The integral of each term, called the Chern character, depending on the curvature, gives an integer number which defines the Chern numbers. The general formula is $C_{n+1} = \frac{1}{(n+1)!}\int_M d^{n+1}k(\frac{i\Omega(k)}{2\pi})^{n+1}$, where M is the BZ when the curvature $\Omega(k)$ is defined with Berry's phase. The importance is that each of these integrals corresponds to an integer number. In case of taking the Berry curvature, the Chern number integral is defined in the BZ. Physically in the last section, we have found the electric conductivity of the topological insulators associated with this C_1 and we will see that the C_2 is related to the instanton solutions. In our case, the fiber $U(1)$ is too simple, but we can enlarge the symmetry group to $SU(2)$ if we take into account the degeneracy of the states on the torus T^4, and this formalism could be very useful. For example, we can prove how electromagnetism and the Berry phase formalism are related in a simple form. In our case, the only difference is the choice of Berry connection a_n or the electromagnetic potential A_μ as connections for making the parallel translations, but the topology of the PFB is the same. We assume that the electromagnetic potential $A_\mu(x)$ is defined at every spacetime point where the quantum states $|\psi_n\rangle$ are uniquely specified, once a gauge condition is fixed for both. Moreover, both the electromagnetic potential and the quantum states are inherently gauge-dependent and transform as elements of the $U(1)$ gauge group. Making a parallel translation (physical adiabatic condition) on a given section, having the covariant derivative $D_\mu = \partial_\mu - i\frac{e}{\hbar}A_\mu$ acting on the states $|\psi_n\rangle$; i.e., $D_\mu|\psi_n\rangle = 0$. If we multiply by the left the last equation by $\langle\psi_n|$, we have

$$\frac{e}{\hbar}A_\mu = -i\langle\psi_n|\partial_\mu|\psi_n\rangle = a_\mu \tag{43}$$

where the electromagnetic potential is equivalent to the Berry connection once the gauge is fixed, given that there is an inner magnetic field, as it happens with the axionic one. This identification is valid under the assumption that the only parameters entering the Berry phase are the spacetime coordinates via the quantum states, and that the system is described by non-degenerate states in the standard Hilbert space. Note that this can be directly associated with the quantization of the magnetic flux as $B = \partial_i A_j - \partial_j A_i = \frac{\hbar}{e}\Omega_{ij}$ and, hence, its surface integral is given by the Chern number [64,143].

The Wilson loops are gauge-invariant operators under this parallel transport around closed loops. In the case of the Chern–Simons, we have the action

$$\mathcal{S}_{cs} = \frac{\kappa}{4\pi}\oint dx^3\epsilon^{\mu\nu\alpha}A_\mu\partial_\nu A_\alpha \tag{44}$$

being κ a dimensionless integer called level. Taking the general connections A_i, we have the invariant object using the circular integral

$$\omega_i = \oint_{\gamma_i} dx^i A_i \tag{45}$$

being γ_i non-contractible curves on the torus. Thus, we have $\omega_i \to \omega_i + 2\pi n$, where n is a winding number. To avoid this difficulty and define properly a gauge-invariant object, we introduce the Wilson loops

$$W_j = exp\left(i\frac{e}{\hbar}\oint_{\gamma_i} dx^i A_i\right) = exp(i\omega_i) \tag{46}$$

which are complex numbers of unitary modulus. The canonical commutation relations of these connections are

$$[A_1(x_1), A_2(x_2)] = \frac{i}{\kappa}\delta^2(x_1 - x_2) \tag{47}$$

or $[\omega_1, \omega_2] = \frac{2\pi i}{\kappa}$. Their product is $e^{i\omega_i}e^{i\omega_j} = e^{\frac{[\omega_i,\omega_j]}{2}}e^{(\omega_i+\omega_j)}$ or $W_iW_j = e^{i\frac{2\pi}{\kappa}}W_jW_i$ which cannot be implemented in a single vacuum state. Hence, the ground state must be degenerate. The smallest representation is

$$W_1|n\rangle = e^{\frac{2\pi ni}{\kappa}}|n\rangle \tag{48}$$

and

$$W_2|n\rangle = |n+1\rangle \tag{49}$$

Wilson loops are the principal physical observables of Chern–Simons theories, which in principle have the problem of not being gauge invariant because they explicitly depend on the potential. However, their expectation values depend on how the braiding between them is established. However, topological invariants are associated with the topological theory of knots[144–147].

3.6. Magnetic topological materials

The integer quantum Hall effect (IQHE) occurs in two-dimensional electron systems and was historically the first manifestation of topology in condensed matter physics. This was theoretically established by Thouless, Kohmoto, Nightingale, and den Nijs (TKNN) [148], who showed that the quantized Hall conductance is governed by integer-valued Chern numbers derived from the Berry curvature of the electronic bands. Shortly thereafter, the fractional quantum Hall effect (FQHE) was discovered; however, its origin lies primarily in strong electron–electron correlations rather than band topology, and it is therefore not classified as a topological band insulator. In parallel, the Hall effect also arises in magnetic materials such as ferromagnets, even in the absence of an external magnetic field. This phenomenon, known as the anomalous Hall effect (AHE), naturally raises the question of whether a quantized version exists. Indeed, the quantum anomalous Hall effect (QAHE) was later predicted theoretically for graphene's honeycomb lattice [49]. However, pristine graphene exhibits extremely weak intrinsic spin–orbit coupling, making experimental realization impractical. The QAHE was subsequently modeled in two-dimensional ferromagnetic systems with sufficiently strong spin–orbit coupling or complete carrier localization at the Fermi level. Its experimental observation only became possible after the successful realization of ferromagnetic topological insulators based on these theoretical proposals. This stands as a remarkable example in condensed matter physics where theory decisively preceded and guided experiment. Without such theoretical insight, these materials would likely never have been engineered [53,68,149,150].

Magnetic Topological Insulators (MTIs) naturally build upon the previously derived expression for the anomalous quantized Hall conductivity [151]. In the ground state, this expression contains a non-integer contribution, which, by itself, cannot serve as a topological invariant. This situation parallels the case of the Chern–Simons conductivity in systems where time-reversal symmetry is explicitly broken. Nevertheless, such materials always host surface states whose intrinsic Hall conductivity is quantized as $\sigma = \frac{e^2}{2h}$, a direct consequence of time-reversal symmetry breaking induced by the magnetic order. To resolve the apparent ambiguity of half-integer topological numbers, one considers the combined contribution of all surface channels: their total conductivity is either $\sigma = \frac{e^2}{h}$ (indicating nontrivial topology) or vanishes entirely (signaling a trivial phase). The sign of the half-quantized contribution is determined by the discrete symmetries of the surface lattice [152].

To clarify the topological origin of the half-quantized Hall response, we consider the minimal low-energy model for a gapped Dirac surface state (see Fig. 4). The effective Hamiltonian in two dimensions reads

$$H(\mathbf{k}) = d_1(\mathbf{k})\,\sigma_x + d_2(\mathbf{k})\,\sigma_y + d_3\,\sigma_z, \tag{50}$$

where the vector $\mathbf{d}(\mathbf{k}) = (\hbar v_F k_x,\ \hbar v_F k_y,\ m)$ encodes the momentum dependence and the mass term. Here, $\hbar$ is the reduced Planck constant, v_F the Fermi velocity, m a real parameter that opens a gap at the Dirac point. For simplicity, we set $\hbar = v_F = 1$ during the calculation and restore physical units at the end. The energy eigenvalues are

$$\varepsilon_{\pm}(\mathbf{k}) = \pm|\mathbf{d}(\mathbf{k})| = \pm\sqrt{k^2 + m^2}, \tag{51}$$

with $k = |\mathbf{k}|$. The normalized eigenstates are

$$|u_{\pm}(\mathbf{k})\rangle = \frac{1}{\sqrt{2|\mathbf{d}|(|\mathbf{d}| - d_3)}}\begin{pmatrix} d_3 \pm |\mathbf{d}| \\ d_1 - id_2 \end{pmatrix}. \tag{52}$$

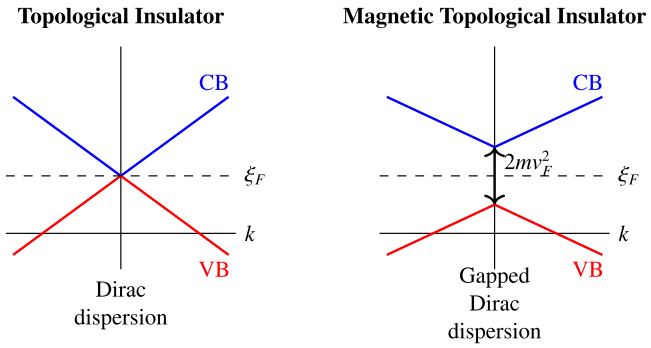

Fig. 4. Comparison of surface band structures in (left) a time-reversal-invariant 3D topological insulator (TI) and (right) a magnetic topological insulator (MTI). In the TI, the surface states form a gapless Dirac cone protected by $\mathcal{T}$ symmetry. In the MTI, magnetic order breaks $\mathcal{T}$, opening a gap of magnitude $2mv_F^2$ at the Dirac point. The dashed line denotes the Fermi level ξ_F, and CB and VB the conduction and valence bands, respectively.

From this, the Berry connection is defined as $a_\alpha(\mathbf{k}) = i\langle u_-|\partial_{k_\alpha} u_-\rangle$. A straightforward calculation yields

$$a_x = -\frac{k_y}{2\sqrt{k^2+m^2}\left(\sqrt{k^2+m^2}+m\right)}, \qquad a_y = \frac{k_x}{2\sqrt{k^2+m^2}\left(\sqrt{k^2+m^2}+m\right)}. \tag{53}$$

The Berry curvature follows as $\Omega_{xy} = \partial_{k_x} a_y - \partial_{k_y} a_x$, which simplifies to

$$\Omega_{xy}(\mathbf{k}) = \frac{m}{2\left(k^2+m^2\right)^{3/2}}. \tag{54}$$

Integrating over the entire 2D Brillouin zone, the Chern number associated with the gapped surface band is

$$C = \frac{1}{2\pi}\int_{\mathbb{R}^2} \Omega_{xy}(\mathbf{k})\, d^2k = \frac{1}{2\pi}\int_0^{2\pi} d\theta \int_0^{\infty} \frac{m\, k\, dk}{2\left(k^2+m^2\right)^{3/2}} = \frac{1}{2}\,\mathrm{sign}(m).$$

Restoring physical units, the Hall conductivity of a single gapped surface is therefore

$$\sigma_{xy} = \frac{e^2}{h}\, C = \frac{e^2}{2h}\,\mathrm{sign}(m), \tag{55}$$

in agreement with the result derived in Section 3.2 from axion electrodynamics. The origin of the gap parameter m in magnetic topological insulators lies in the breaking of time-reversal symmetry (TRS). For spin-1/2 electrons, the antiunitary time-reversal operator is $T = i\sigma_y K$, where K denotes complex conjugation. Acting on the Hamiltonian, one finds

$$TH(\mathbf{k})T^{-1} = H(-\mathbf{k}) = -\hbar v_F k_x \sigma_x - \hbar v_F k_y \sigma_y + m\sigma_z. \tag{56}$$

TRS requires $TH(\mathbf{k})T^{-1} = H(-\mathbf{k})$, which is only satisfied if $m = 0$. Thus, a non-zero m explicitly breaks TRS. In magnetic materials, this mass term arises from the exchange coupling between the spin of itinerant surface electrons s_z and localized magnetic moments S_z, assuming the magnetization is oriented perpendicular to the surface (along z). This interaction takes the form

$$H_{\mathrm{ex}} = -J\,\mathbf{s}\cdot\mathbf{S} \quad \Rightarrow \quad m\sigma_z = -n_s J s_z S_z, \tag{57}$$

where J is the exchange constant, and n_s the density of localized spins. The sign and magnitude of m are thus controlled by the direction and strength of the magnetic order. Consequently, while conventional topological insulators preserve TRS and host gapless Dirac cones, magnetic topological insulators break TRS and exhibit gapped surface states with a half-quantized Hall conductance. In a thin film geometry with uniform perpendicular magnetization, the top and bottom surfaces contribute with the same sign, yielding a total Chern number $C = 1$ (nontrivial) or $C = 0$ (trivial) depending on the relative alignment of the surface gaps, enabling the quantum anomalous Hall effect without external magnetic fields.

Magnetic topological materials represent one of the most promising platforms for technological applications in topological quantum matter, as they can be externally controlled by a magnetic field. Key experimental techniques—such as angle-resolved photoemission spectroscopy (ARPES) and scanning tunneling microscopy/spectroscopy (STM/STS) have enabled direct visualization of the gapped Dirac surface states and their spin-momentum locking. Complementary probes, including the magneto-optic Kerr and Faraday effects, provide evidence of the topological magnetoelectric response associated with axion electrodynamics. Two primary mechanisms are known to induce magnetic order and open a gap in the surface Dirac cone: (i) the carrier-mediated Ruderman–Kittel–Kasuya–Yosida (RKKY) interaction, as realized in Mn-doped Bi_2Te_3 [153], and (ii) the local-moment Van Vleck mechanism mediated by valence electrons, observed in

Cr-doped Bi_2Te_3 [154]. These systems typically exhibit weak ferromagnetic or antiferromagnetic ordering below low Curie (T_C) or Néel (T_N) temperatures, respectively, while largely preserving the underlying crystal symmetries essential for topological protection. Despite the challenges in material synthesis and the sensitivity required for experimental characterization, significant progress has been made in recent years. Comprehensive reviews on the theory, growth, and transport properties of magnetic topological insulators are available in Refs. [80,155–157].

4. Chiral anomaly and axion electrodynamics

The axion term, $\frac{e^2}{32\pi^2\hbar}\theta(r,t)\epsilon_{\mu\nu\alpha\beta}F^{\mu\nu}F^{\alpha\beta}$, has a well-established physical–mathematical meaning within field theory. As mentioned before, its origin began with the decay of the neutral pion π^0 into two photons, that is, $\pi^0 \longrightarrow \gamma\gamma$. Using the partially conserved axial current model (PCAC), this gives a decay rate value three orders of magnitude less than the observed one. This difficulty was overcome by taking into account the aforementioned axial term. In addition, we show how the axion term is topologically quantized, allowing the non-conservation of the chiral currents and justifying the fractional anomalous Chern–Simons currents. Both are glued and related to the temperature as the first step to topological thermoelectricity. The units used in this section are still SI units, but given the number of constants present, they are omitted from the calculations, although they appear at the end in the expressions of interest.

4.1. Chiral anomaly and axion electrodynamics

Classically, the gauge transformation of the potentials $A_\mu \longrightarrow A_\mu + \partial_\mu \Lambda(x)$ and states $\psi(x) \longrightarrow \psi(x)e^{i\Lambda(x)}$ are glued using a $U(1)$ symmetry for obtaining a Noether current given by $J^\mu = \overline{\psi}\gamma^\mu\psi$, with associated action

$$S = \int dx^4 i\overline{\psi}\gamma^\mu(\partial_\mu - ieA_\mu)\psi, \tag{58}$$

where γ^μ are the Dirac matrices and $\overline{\psi} = \psi^\dagger\gamma^0$. This current J^μ is known as a vector current. In the same form, it can also be defined an axial current such as $J_a^\mu = \overline{\psi}\gamma^\mu\gamma^5\psi$ associated with the axial symmetry $\psi \longrightarrow e^{i\Lambda\gamma^5}\psi$ which appears as a classical Noether current taken in this way, but this symmetry is broken when the theory is quantized and, therefore, produce an axial or chiral quantum anomaly [158,159].

Let us define very shortly the basic tools employed in the quantum formalism. In the Weyl basis, the Dirac matrices 4×4 appear as

$$\gamma^0 = \begin{pmatrix} 0 & 1 \\ 1 & 0 \end{pmatrix}, \qquad \gamma^i = \begin{pmatrix} 0 & \sigma^i \\ -\sigma^i & 0 \end{pmatrix} \tag{59}$$

with $\gamma^5 = -i\gamma^0\gamma^1\gamma^2\gamma^3 = \begin{pmatrix} 1 & 0 \\ 0 & -1 \end{pmatrix}$, the Minkowski's metric with signature $(+---)$ and σ^i the Pauli's matrices. In the case of the massless Dirac fields, the states can be separated as

$$\psi = \left(\frac{1+\gamma^5}{2}\right)\psi + \left(\frac{1-\gamma^5}{2}\right)\psi = \psi_L + \psi_R, \tag{60}$$

being $P_\pm = \frac{1}{2}(1 \pm \gamma^5)$ projectors at right or left polarizations. The covariant derivatives $D_\mu = \partial_\mu - ieA_\mu$ or $D = \gamma^\mu(\partial_\mu - ieA_\mu)P_+$, $D^\dagger = \gamma^\mu(\partial_\mu - ieA_\mu)P_-$. So, we have two independent polarizations for $P_\pm\psi_\pm = \psi_\pm$ and $\gamma^5\psi_\pm = \pm\psi_\pm$, where the Hilbert space is divided in two subspaces $\mathcal{H} = \mathcal{H}_+ \oplus \mathcal{H}_-$ in this four dimensional space–time. Provided with these definitions, it is straightforward to obtain one of the applications of the Atiyah–Singer index theorem for the elliptic Dirac operators in an Euclidean space–time

$$index(\gamma^\mu D_\mu) = n_+ - n_- \tag{61}$$

where n_+ are the zero modes of D and n_- the ones of $D^\dagger$. Notice that $i\gamma^\mu D_\mu\psi_n = \xi_n\psi_n$ and ξ_n must be real because $i\gamma^\mu D_\mu$ is an Hermitian operator. On the other hand, $\gamma^5\psi_n$ is also an eigenfunction in such a form that ψ_n and $\gamma^5\psi_n$ have to be orthogonal, because these states cannot have the same eigenvalue ξ_n simultaneously. Only in the case of a zero mode, i.e., when $\xi_n = 0$, does one not encounter this issue.

On the other hand, using the Fujikawa formalism [105], we can analyze the measure of the integrals for fermions coupled to the electromagnetic field within a Grassmann algebra

$$\int \mathfrak{D}\psi\mathfrak{D}\overline{\psi} \tag{62}$$

where $\mathfrak{D}$ denotes the differential in the spinor Hilbert space. Physically, this provides a way to formalize Pauli's exclusion principle for the integral. Choosing a fixed electromagnetic field, we have for the Dirac operator $i\gamma^\mu D_\mu\phi_n = \xi_n\phi_n$

where ϕ_n are 4-component eigenspinors. Thus, we can write the general spinors $\psi, \overline{\psi}$ in a Grassmann formalism by $\psi(x) = \sum_n a_n \phi_n(x)$, $\overline{\psi}(x) = \sum_n \overline{b_n}\,\overline{\phi_n}(x)$. This allows us to express the fermionic integral measure in a simple form as

$$\prod_n \int d\overline{b_n} da_n, \tag{63}$$

where a_n and $\overline{b_n}$ are Grassmann numbers whose integrals are straightforward: $\int da = 0$ and $\int a\, da = 1$, with the same properties for $\overline{b_n}$. The chiral spinors can be expanded using a first-order approximation $\overline{\psi}' = \overline{\psi} + i\epsilon\overline{\psi}\gamma^5$ and $\psi' = \psi + i\epsilon\psi\gamma^5$, where ϵ is the ordinary infinitesimal. Hence, the Jacobian of the new integral may be calculated, and the surprising result is that it appears a new term

$$\int \mathfrak{D}\psi\mathfrak{D}\overline{\psi} exp\left(-i\frac{e^2}{16\pi^2}\int \epsilon^{\mu\nu\alpha\beta}F_{\mu\nu}F_{\alpha\beta}dx^4\right) \tag{64}$$

and therefore the axial current $J_a^\mu = i\overline{\psi}\gamma^\mu\gamma^5\psi$ is not conserved. It follows that

$$\partial_\mu J_a^\mu = \frac{e^2}{16\pi^2}\epsilon^{\mu\nu\alpha\beta}F_{\mu\nu}F_{\alpha\beta} \tag{65}$$

confirming the chiral anomaly. Finally, we can write the Atiyah–Singer theorem [160] as

$$index(\gamma^\mu D_\mu) = \frac{e^2}{16\pi^2}\epsilon^{\mu\nu\alpha\beta}F_{\mu\nu}F_{\alpha\beta} = n_+ - n_-. \tag{66}$$

This justifies in a much deeper form how the axion electrodynamic term is quantized and related to the zero modes of the Weyl equation. Thus, the topology associated with the pseudoscalar Lorentz invariant term of the action in the quantum formalism is quite subtle, because it is related to the measure of the integral of the fermion action and the coupling of the massless electrons with the axionic electromagnetic background.

4.2. Classical $\theta(\boldsymbol{r}, t)$ field meaning versus quantum field theory

Following the Fujikawa formalism developed above, it is easy to see that there is an immediate interpretation of the θ field as one phase of a global gauge transformation. In fact, it would be associated with the chiral massless electrons coupled to the electromagnetism of the axion. Taking $\psi_+ \longrightarrow e^{i\Lambda}\psi_+$ and $\psi_- \longrightarrow e^{-i\Lambda}\psi_-$, and infinitesimal transformations given by $\delta\psi_+ = i\epsilon\psi_+$, $\delta\psi_- = i\epsilon\psi_-$, the fermionic measure is transformed as

$$\int \mathfrak{D}\psi\mathfrak{D}\overline{\psi} \longrightarrow \int \mathfrak{D}\psi\mathfrak{D}\overline{\psi} exp\left(-i\frac{e^2\Lambda}{16\pi^2}\int \epsilon^{\mu\nu\alpha\beta}F_{\mu\nu}F_{\alpha\beta}dx^4\right). \tag{67}$$

Therefore, we have obtained the same expression introduced in the first section, if we consider $\theta = 2\Lambda$ or a phase shift $\theta \rightarrow \theta - 2\Lambda$. This means that θ can be gauged because it only changes the phase of one state of an isolated fermion. Note that this does not invalidate the existence of the $\theta(\boldsymbol{r}, t)$ field that we have introduced in the first section because in that case it is defined for many fermions with local phases. Axionic electromagnetism requires a local change of Wannier states to obtain the electric polarization $\boldsymbol{P}$ and the magnetization $\boldsymbol{M}$ [161–164].

4.3. Anomaly inflow and local currents

The mass of electrons in topological insulators can be thought of as evolving from having non-zero mass in the volume to having mass equal to zero at their edge. We will see how to explain the semi-integer value of the electrical conductivity obtained in the previous section for the Chern–Simons theory, which is unrealistic due to the presence of half-integer Chern numbers. We assume that the coordinate spanning from the interior of the material to the surface is z, with the plane $z = 0$ precisely marking the region where the electrons have zero mass and containing the point $\bar{z}$. Taking the mass of the electrons as

$$m(z) = m_0 tanh(z) \tag{68}$$

with $\lim_{z\to+\infty} m(z) = +m_0$ and $\lim_{z\to-\infty} m(z) = -m_0$ (see Fig. 5). Note that z varies as a function of temperature, $z(T)$, meaning that the electrons attached to the bulk atoms must be considered when accounting for the dimensional transformation of the electron mass. So, if we have these electrons coupled to the electromagnetic background field, its action would be

$$\mathcal{S} = \int dx^4[i\overline{\psi}\mathfrak{D}\psi - m(z)\overline{\psi}\psi] \tag{69}$$

and the Dirac equation

$$i\partial_0\psi_- + i\sigma^i\partial_i\psi_- = m\psi_+, i\partial_0\psi_+ + i\sigma^i\partial_i\psi_+ = m\psi_-. \tag{70}$$

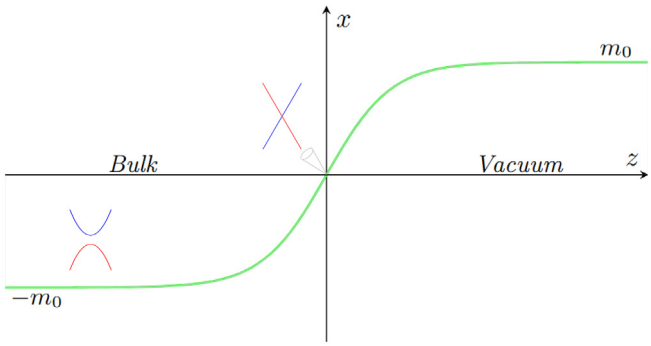

Fig. 5. Hyperbolic tangent for the electronic mass close to the surface. Condition leading to only one type of two-dimensional Dirac spinors (surface) that can be directly related to Chern–Simons electric charge currents.

There is always a solution independent of the value of the energy

$$\psi_+ = i\sigma^3\psi_- = exp\left[-\int_0^{z'} dz' m(z')\right]\phi(x^i), \tag{71}$$

where ϕ is the eigenspinor in vacuum, ψ is localized around $z = 0$, where the mass should be zero and $i = 0, 1, 2$. This is known as a Fermi zero mode. So, we have $\partial_0\phi + \sigma^1\partial_1 + \sigma^2\partial_2\phi = 0$, which turns out to be the $(2+1)-D$ Dirac equation for a massless fermion. Besides that, we must notice that the other solution $\psi_- = i\sigma^3\psi_+$ is not normalizable, and therefore we have only half of the possible electrons given by $\psi_+ = i\sigma^3\psi_-$. This implies that only this limited number of electrons contribute to electronic transport, as they are localized in the plane $z = 0$, just as we observed in Section *I*, where the electromagnetic Chern–Simons term was studied. Therefore, if we add or subtract the Chern–Simons currents found in a previous section from those in this one, we obtain the fully integer-quantized conductivity, as expected, following the TKNN theorem. At low energies, we have a single massless chiral fermion ϕ_+ localized at the domain wall, carrying charge $+1$ under an electromagnetic field with an internal $U(1)$ symmetry [165,166]. The first observation to make is that the domain wall is placed where the dimensionality of the material changes from odd to even or vice versa. The second is that the duality rotation for the electromagnetic field and the chiral symmetries are only well-defined in even-dimensional space. Third, the electric conductivity must employ the Chern–Simons axion electromagnetism and chiral Weyl fermions to be properly defined.

This tells us that these electronic currents are localized and have lower degrees of freedom than usual in non-topological materials. This means that thermodynamic quantities such as entropy must also be smaller and be able to be considered locally, as we will see later. This suggests a cyclic transformation of a set of many electrons in a given microcanonical configuration since we will calculate more explicitly, taking into account the density of states and their occupancy to obtain the figure of merit [166–168].

4.4. Temperature and anomalies

In the case of massless fermions, we have a Lagrangian for the Weyl spinor representation

$$\mathcal{L} = \overline{\psi}(x)i\gamma^\mu(\partial_\mu + ieA_\mu)\psi(x). \tag{72}$$

That is, in addition to being invariant under the local gauge transformation $\psi(x) \longrightarrow \psi'(x) = e^{i\Lambda(x)}\psi(x)$, $\psi(x) \longrightarrow \psi'(x) = e^{i\Lambda\gamma_5}\psi(x)$, it is also invariant for the transformation of the metric $g_{\mu\nu} \longrightarrow g'_{\mu\nu} = \Lambda(x)g_{\mu\nu}$, and coordinates $x^\mu \longrightarrow x'^\mu = \Lambda(x)x^\mu$ [169–172]. Thus, representing the Euclidean spacetime within the complex numbers with $ds^2 = dzd\bar{z}$, where $z = x_0 + ix_1$ for $(1+1)$-dimensions, and $\bar{z}$ is the conjugate complex. Performing an infinitesimal transformation $z \longrightarrow z + \epsilon(z)$, with $\epsilon(z) = \sum_{n=-\infty}^{\infty}\epsilon_n z^n$, being $f(z+\epsilon(z)) = [1 + \sum_{n=-\infty}^{\infty}\epsilon_n z^{n+1}\partial_z]f(z)$ analytic, a Virasoro algebra is obtained for the operators $L_n = -z^{n+1}\partial_z$, with external product $[L_n, L_m] = (n-m)L_{n+m}$. This conformal symmetry is broken when turning into the quantum formulation, where time is given by $t = \frac{\hbar}{k_B T}$, leading to the emergence of anomalies. Classically, the covariant derivative of the energy–momentum tensor vanishes, as does its trace, i.e., $D_\mu T^{\mu\nu} = 0$ and $T^\mu_\mu = 0$. However, at the quantum level, the trace of the energy–momentum tensor does not vanish but instead appears as

$$T^\mu_\mu = -\frac{c}{24\pi}\mathcal{R}, \tag{73}$$

where $\mathcal{R}$ is the scalar Ricci tensor associated with the metric and c is the central charge, with the other central charge $\bar{c} = 0$. We have chosen the units of the Newton constant and velocity of light to be one. Calculating the T_{00} component

of the energy–momentum tensor, we have that the 1-dimensional density of energy would be $\xi(x) = \frac{\pi c}{12 v_F \hbar \beta^2}$, and as $\xi(x) = p(x) v_F$, we also have the density of momentum as $p(x) = \frac{\pi c}{12 \hbar \beta^2}$, with $\beta^{-1} = k_B T$. Thus, considering that the thermal current is proportional to the momentum, we have the thermal Hall conductivity in one dimension, given by [32,173–175]

$$K_H = \frac{\partial p(x)}{\partial T} = \frac{\pi k_B^2 T}{6\hbar} c. \tag{74}$$

We see that this thermal conductivity depends directly on the central charge c, which has a difficult physical interpretation. Notice that this conductivity was defined in the continuous lattice as the theory of defects does [176] in crystal and, therefore, this thermal conductivity might be associated with the lattice κ_{ph}. The value of the central charge c for fermions in a torus is smaller than one, $c = 0.5$, but the one for bosons is more complex to be determined theoretically [177].

Although this formalism is quite different from what we are developing, it is crucial to observe how temperature can be related to the geometry of the material and the action of Dirac electrons coupled to the electromagnetic field.

5. Inner symmetries, dimensionality, and topology

Topological materials are assumed to have a relativistic linear dispersion law, with $\xi = p v_F = \hbar k v_F$, where the Fermi velocity v_F replaces the speed of light c in this effective space–time. This simple identification leads to the fact that these bands carry zero mass electrons and that they might have non-trivial topology. Moreover, this effective system has its symmetries associated with the Lorentz group $SO(1,3)$ or with the Poincaré group if we add the translations. But what characterizes the topology of Hermitian Hamiltonians are their discrete time-reversal, charge-conjugation, and chiral symmetries, as has been known since the beginning of the last century.

One way to see that these are linear bands, $\xi = \hbar k v_F$, following the relativistic formalism for a rest mass particle, despite working with such low energies, is with the Landau levels, which are measured with scanning tunneling spectroscopy techniques [178,179]. A paradigmatic case is graphene, which has a Fermi velocity $v_F = \frac{3a|t|}{2\hbar} \equiv 10^6\, ms^{-1}$, which is independent of k, where a and t are the lattice constant and the hopping energy, respectively. For graphene monolayers under a magnetic field up to 12T, it is possible to see that the Landau levels follow the quantization based on the relativistic formalism

$$\xi = \pm v_F \sqrt{2\hbar e B n}\,, \tag{75}$$

where n are natural numbers labeling the states. Positive values correspond to massless electrons, while negative values correspond to massless holes. So it seems quite natural to analyze the discrete symmetries of the Lorentz group and see how they topologically classify materials into just ten classes.

5.1. Unitary symmetries in topological materials

Electrons are assumed within a tight-binding model and with a Hermitian Hamiltonian with associated unitary symmetries. That is, $U\mathcal{H}U^{-1} = \mathcal{H}$, where $U^{-1} = U^{\dagger}$. Therefore, we can always find a basis in which $\mathcal{H}$ and U are diagonal block matrices because they commute $[\mathcal{H}, U] = 0$. This block has a common eigenvalue $\xi(k)$ that could correspond to a degenerate state $|\psi_i\rangle$. This is a key point, as it enables the use of non-Abelian unitary symmetries in these quantum topological systems. For example, consider an insulator with m occupied bands below the Fermi level, $\xi_i(k) < \xi_F$, and n unoccupied bands with $\xi_i(k) > \xi_F$. Performing an adiabatic transformation from the Hamiltonian $\mathcal{H}(k)$, which keeps the gap energy unchanged, we can see that the unitary transformations define a differential manifold M such that it appears as a coset space

$$M = \frac{U(n+m)}{U(n)U(m)}, \tag{76}$$

where the matrices associated with $U(n+m)$ of $(n+m)\times(n+m)$ elements define a map from the Brillouin zone torus (transformed into an equivalent "sphere" after physical–mathematical manipulations, see [31]) to M, whose homotopy group can be determined. For example, under the conditions mentioned above, $\pi_d(M) = 0$ for odd dimensions $d = 1, 3, 5$, which corresponds to trivial topology, where all elements can be continuously reduced to a single one. On the other hand, $\pi_d(M) = \mathbb{Z}$ for even dimensions $d = 2, 4$, where there exists an integer class of independent elements. In the latter case, there are several states for each integer $\mathbb{Z}$ that cannot be continuously deformed with each other [96,180,181]. This idea will be generalized in the 10-fold Way formalism. Note that these symmetries belong to the Hamiltonian, not the Lagrangian, and therefore are not directly associated with Noether currents.

5.2. Inner discrete symmetries

Discrete symmetries were defined using the Lorentz equation of classical electrodynamics, but this is not sufficient for quantum systems. A system is time-reversal symmetric if the operator $\hat{\mathcal{T}}$ commutes with the Hamiltonian $[\hat{\mathcal{H}}, \hat{\mathcal{T}}] = 0$. That means that the time-reversal symmetry induces a degeneracy of states because, for the Schrödinger equation $\mathcal{H}|\psi\rangle = \xi|\psi\rangle$, we also have $\hat{\mathcal{H}}\hat{\mathcal{T}}|\psi\rangle = \xi\hat{\mathcal{T}}|\psi\rangle$.

For bosons $\hat{\mathcal{T}}|\psi\rangle = +|\psi\rangle$ always, but for fermions $\hat{\mathcal{T}}|\psi\rangle \neq |\psi\rangle$. This property is the basis of the Kramers degeneracy [182–184]. In the time-dependent Schrödinger equation $i\hbar\frac{\partial}{\partial t}|\psi(t)\rangle = \hat{\mathcal{H}}|\psi(t)\rangle$, while $|\psi(-t)\rangle$ is not a solution if the time-reversal symmetry must be followed, due to the first order derivative in t. For solving this basic quantum feature, we notice that $\hat{\mathcal{T}}i\hbar\hat{\mathcal{T}}^{-1} = -i\hbar$, which means that the time-reversal symmetry induces a complex conjugation operator $\hat{K}$, where $\hat{K}^2 = 1$, obviously.

In general, we can write $\hat{\mathcal{T}} = \hat{U}_{\mathcal{T}}\hat{K}$, being the time-reversal operator $\hat{\mathcal{T}}$ equal to the product of one unitary operator $\hat{U}_{\mathcal{T}}$ by the complex conjugation operator $\hat{K}$. So, when it acts on an operator $\hat{O}$, we have $\hat{\mathcal{T}}\hat{O}\hat{\mathcal{T}}^{-1} = \hat{U}_{\mathcal{T}}\hat{K}\hat{O}\hat{K}\hat{U}_{\mathcal{T}}^{\dagger} = \hat{U}_{\mathcal{T}}O^*\hat{U}_{\mathcal{T}}^{\dagger}$. By joining both conditions, the time operator becomes antiunitary instead of unitary. A possible representation is given by $U_{\mathcal{T}} = exp(-i\pi\frac{S_y}{\hbar})$, being S_y the spin in the y-direction and the square of $\hat{\mathcal{T}}$ gives $\hat{\mathcal{T}}^2 = e^{(-2i\pi\frac{S_y}{\hbar})}$. Therefore, for bosons $\hat{\mathcal{T}}^2 = 1$, and for half-integer spin fermions we have $\hat{\mathcal{T}}^2 = -1$ and $\hat{\mathcal{T}} = -i\sigma_y K$. Thus $\hat{\mathcal{T}}$ is an antiunitary operator under these conditions.

The parity operator $\hat{\mathcal{P}}$, which changes the sign of the spatial coordinate, is Hermitian, i.e., $\hat{\mathcal{P}} = \hat{\mathcal{P}}^{\dagger}$, and is its own inverse, i.e., $\hat{\mathcal{P}}^{\dagger} = \hat{\mathcal{P}}^{-1}$. It is the least important discrete symmetry because it can be replaced by a unitary operator. To clarify, we can think of it as a rotation by π degrees.

In the same form, we have used the non-relativistic Schrödinger equation for the time-reversal symmetry. In the case of charge conjugation $\hat{\mathcal{C}}$, it is necessary to work with the Dirac relativistic equation $i\gamma^{\mu}\partial_{\mu}\psi = m\psi$. Doing the generic transformation $\psi' = U_{\mathcal{C}}\psi$, we have the condition $U_{\mathcal{C}}\gamma'^{\mu}U_{\mathcal{C}} = \gamma^{\mu}$, where the γ'^{μ} and γ^{μ} are the Dirac gamma matrices in different basis, but with the same commutation rules. Thus, we can find, as in the time-reversal symmetry, that $\hat{\mathcal{C}}\hat{\mathcal{H}}\hat{\mathcal{C}}^{-1} = \hat{\mathcal{H}}$ and $\hat{\mathcal{C}} = U_{\mathcal{C}}\hat{K}$, with $\hat{\mathcal{C}}^2 = \pm 1$, which gives two possibilities $\hat{\mathcal{C}} = +1$ and $\hat{\mathcal{C}} = -1$. Furthermore, a third operator needs to be introduced to account for the composition of the charge conjugation and time reversal symmetries that define $\hat{S} = \hat{\mathcal{T}}\hat{\mathcal{C}}$, known as the chiral operator. It is also antiunitary because in the Fock space $\hat{S}i\hat{S}^{-1} = -i$ and commutes with the Hamiltonian defined on a Fock space (second quantization), $\hat{S}\mathcal{H}\hat{S}^{-1} = \mathcal{H}$. For the single-particle first quantization Hilbert space, it is unitary because the composition of the time-reversal and charge conjugation operators is unitary, as $\hat{K}^2 = 1$ [185]. This operator has only two possible values: 0 and 1.

Let us apply these concepts to a model, where these three discrete symmetries are easy to calculate, such as it happens with the two-band Su–Schrieffer–Heeger (SSH) model, see Appendix A. We assume that we have a chain of two types of atoms, A and B. The Bloch Hamiltonian is given by

$$H(k) = \begin{pmatrix} 0 & t_i + e^{ik}t_o \\ t_i + e^{-ik}t_o & 0 \end{pmatrix} = \sum_i d_i(k)\sigma^i, \tag{77}$$

where

$$d_x(k) = t_i + t_o\cos(ka), \quad d_y(k) = t_o\sin(ka), \quad d_z(k) = 0. \tag{78}$$

The eigenvectors of this Hamiltonian are given by

$$|\pm u(k)\rangle = \frac{1}{\sqrt{2}}\begin{pmatrix} \pm e^{-i\phi(k)} \\ 1 \end{pmatrix}. \tag{79}$$

It is straightforward to compute the Berry connection

$$a(k) = i\langle u(k)|\partial_k|u(k)\rangle = \frac{d\phi_k}{dk}i\langle u(k)|\partial_{\phi_k}|u(k)\rangle = \frac{1}{2}\frac{d\phi_k}{dk}. \tag{80}$$

This results in a winding number

$$w = \frac{1}{\pi}\int_{-\pi}^{\pi} dk\frac{1}{2}\frac{d\phi_k}{dk}, \tag{81}$$

which takes the value $w = 1$ for the non-trivial phase and $w = 0$ for the trivial phase. Physically, this corresponds to the conditions $t_i > t_o$ and $t_o > t_i$, respectively.

Time-reversal symmetry $\mathcal{T}$ is evident in this model since $\hat{\mathcal{T}} = \hat{K}$, where $\hat{K}$ is the complex conjugation operator. Thus,

$$\hat{\mathcal{T}}H(k)\hat{\mathcal{T}}^{-1} = H(-k). \tag{82}$$

Chiral symmetry $\mathcal{S}$ in this spinless model is unitary, and we have

$$\sigma_z H(k)\sigma_z = -H(k), \tag{83}$$

due to the condition $d_z = 0$. This implies the existence of an antiunitary symmetry

$$\{H(k), \sigma_z\} = H(k)\sigma_z + \sigma_z H(k) = 0. \tag{84}$$

This imposes a constraint such that

$$\sigma_z|\xi_k\rangle = |-\xi_k\rangle, \tag{85}$$

where $|\xi_k\rangle$ is an eigenstate with eigenvalue ξ. Notably,

$$H(k)\sigma_z|\xi\rangle = -\sigma_z H(k)|\xi\rangle, \tag{86}$$

which means that setting a potential difference between atoms A and B, allowing for t_i hopping, is difficult. This condition is not realistic, hence, this symmetry is not strictly physical either. However, it is commonly accepted that this discrete symmetry characterizes the SSH model in the 10-fold way classification. In this framework, chiral symmetry is the only symmetry that persists under perturbations, placing the SSH model in the AIII Cartan class. We will analyze this aspect more deeply in the next subsection.

Charge conjugation symmetry $\mathcal{C}$ can be expressed as a combination of the previous two symmetries

$$\hat{\mathcal{C}} = \sigma_z\hat{\mathcal{T}} = \sigma_z\hat{K}, \tag{87}$$

which implies the following action on the Hamiltonian

$$\hat{\mathcal{C}}H(k)\hat{\mathcal{C}}^{-1} = -H(-k). \tag{88}$$

This induces the constraints:

$$d_x(k) = d_x(-k), \quad d_y(k) = -d_y(-k), \quad d_z(k) = -d_z(-k) \tag{89}$$

for a two-band model.

In summary, $\hat{\mathcal{T}}$, $\hat{\mathcal{C}}$ and $\hat{\mathcal{S}}$ are antiunitary operators in the Fock space, while $\hat{\mathcal{P}}$ is unitary. These are the main ingredients that must be used for the topological classification of the Hermitian Hamiltonians employed in the topological materials.

5.3. The 10-fold way

Historically, in 1926, Cartan [186] was able to classify Riemannian symmetric spaces by taking into account the invariance of their curvature tensor under parallel transport, in only 10 classes. This is a Riemannian, or pseudo-Riemannian, manifold provided with inversion discrete symmetries at every point. This can be studied with the concept of holonomy that he introduced also in the same year, and which allows one to employ the geometric concepts of connection and curvature in an algebraic form for fiber bundles [95,187]. Actually, what we are trying to find is a classification of fermion Hamiltonians (Hermitian matrices) based on their topological features in a simple and finite way. The basic concept is the symmetry-protected topological phase, that we can define for two local gapped Hamiltonians H_a and H_b with symmetry group G and unique ground states $|\psi_a\rangle$ and $|\psi_b\rangle$, if and only if, there exists a set of Hamiltonians H_α such that $\alpha \in [0, 1]$, with $H_a = H_0$ and $H_b = H_1$; i.e., both Hamiltonians can be continuously joined. Considering Wigner's theorem, any transformation of the ray space of quantum states can be represented by a unitary or antiunitary transformation of the Hilbert space, unique up to a phase factor. This allows us to find irreducible representations of the symmetry group G associated with the Hamiltonian H, to obtain the usual irreducible Hilbert spaces

$$\mathcal{H} = \oplus_\alpha \mathcal{H}_\alpha \tag{90}$$

which leads to an irreducible Hamiltonian without unitary symmetries; i.e., $[U, \mathcal{H}] \neq 0$ with $UU^* = e^{i\alpha}\mathbb{I}$ by Schur' s Lemma, being $\mathbb{I}$ the identity matrix. They are the "irreducible blocks" of all Hamiltonians associated with the irreducible representations of the group G without the unitary ones.

One direct application is a Lorentzian manifold where the antiunitary operators $\hat{\mathcal{T}}$ and $\hat{\mathcal{C}}$ in addition to his composition $\hat{S} = \hat{\mathcal{T}}\hat{\mathcal{C}}$, known as chiral symmetry operator, are defined associated to its discrete symmetries. The parity $\hat{\mathcal{P}}$ does not appear because it is equivalent to a unitary operator, which only changes the base of the space, but not the topology. In 1997, Atland and Zimbauer recovered this classification to classify topological materials as the 10-fold Way [67,188–190]. The 10 times comes because $\hat{\mathcal{T}}^2$ and $\hat{\mathcal{C}}^2$ have three possible values, ± 1 and 0 when it does not exist, while $\hat{S}$ only has the values 0 or $+1$. Thus, we have $(3 \times 3 - 1) + 2 = 10$ different possibilities if we suppress the case that $\hat{\mathcal{T}} = \hat{\mathcal{C}} = 0$, i.e, without any symmetry. This allows us to find a table for the topological phases, see the Cartan table (Table 1).

Recalling that topological insulators use time reversal $\mathcal{T}$ to define their non-trivial topological structure and that topological superconductors do so with charge conjugation $\mathcal{C}$, a more detailed look at how these concepts are introduced can be seen in the appendices. For example, the Chern insulator in class A, the time-reversal topological insulator in *AII*, and the p-wave superconductor in Cartan class *D*. The SSH model is simple to analyze in terms of its symmetries and, therefore, holds special importance for us. It can be thought of as an embryonic topological insulator and also has a direct relationship with the Kitaev chain for superconductors. So we are going to analyze it in a bit of detail, following what we already said in the previous subsection. If we classify the SSH model within the *AIII* class, then we assume that the

Table 1
Cartan table with two complex classes, *A*, *AIII*, and the remaining eight real classes, allowing the topological classification of fermionic Hamiltonians for topological insulators and topological superconductors.

Class	$\mathcal{T}$	$\mathcal{C}$	$\mathcal{S}$	0d	1d	2d	3d	4d	5d	6d	7d
A	0	0	0	$\mathbb{Z}$	0	$\mathbb{Z}$	0	$\mathbb{Z}$	0	$\mathbb{Z}$	0
AIII	0	0	1	0	$\mathbb{Z}$	0	$\mathbb{Z}$	0	$\mathbb{Z}$	0	$\mathbb{Z}$
AI	+1	0	0	$\mathbb{Z}$	0	0	0	$2\mathbb{Z}$	0	$\mathbb{Z}_2$	$\mathbb{Z}_2$
BDI	+1	+1	1	$\mathbb{Z}_2$	$\mathbb{Z}$	0	0	0	$2\mathbb{Z}$	0	$\mathbb{Z}_2$
D	0	+1	0	$\mathbb{Z}_2$	$\mathbb{Z}_2$	$\mathbb{Z}$	0	0	0	$2\mathbb{Z}$	0
DIII	−1	+1	1	0	$\mathbb{Z}_2$	$\mathbb{Z}_2$	$\mathbb{Z}$	0	0	0	$2\mathbb{Z}$
AII	−1	0	0	$2\mathbb{Z}$	0	$\mathbb{Z}_2$	$\mathbb{Z}_2$	$\mathbb{Z}$	0	0	0
CII	−1	−1	1	0	$2\mathbb{Z}$	0	$\mathbb{Z}_2$	$\mathbb{Z}_2$	$\mathbb{Z}$	0	0
C	0	−1	0	0	0	$2\mathbb{Z}$	0	$\mathbb{Z}_2$	$\mathbb{Z}_2$	$\mathbb{Z}$	0
CI	+1	−1	1	0	0	0	$2\mathbb{Z}$	0	$\mathbb{Z}_2$	$\mathbb{Z}_2$	$\mathbb{Z}$

$\mathcal{S}$ symmetry is still fulfilled and the other two, $\mathcal{T}$ and $\mathcal{C}$, disappear. In the table, it can be seen that we have $\mathbb{Z}$ infinite gapped phases. It could also be in the *BDI* class if we assume that the three discrete symmetries are well protected against perturbations. However, we have seen that the chiral symmetry was enough to have the topological phase well-defined. As in *AIII*, it could also be in the *D* class that only uses the $\mathcal{C}$ charge symmetry as the only protected symmetry in this case. This is the most interesting one for us because it is common to the Kitaev chain that we will use in our example. We could do the same with the Kitaev model for topological superconductivity, which also falls into the topological class *D*. Unfortunately, the generalization to higher-dimensional Hamiltonians of topological insulators and real superconductors is not such a simple task.

All topological insulators and superconductors known nowadays are classified in terms of their symmetries (unitary *U*, orthogonal *O*, symplectic *Sp*) and spatial dimension. These classes are related if we change the dimensionality of the Hamiltonian cyclically using what is called the Bott periodicity [191], being the homotopies of the unitary group 2-periodic, $\pi_k(U) = \pi_{k+2}(U)$ ($A \rightarrow AIII \rightarrow A$), while the orthogonal and symplectic groups are 8-periodic($AI \rightarrow BDI \rightarrow D \rightarrow DIII \rightarrow AII \rightarrow CII \rightarrow C \rightarrow CI \rightarrow AI$), i.e., $\pi_k(O) = \pi_{k+8}(O)$ and $\pi_k(Sp) = \pi_{k+8}(Sp)$. *O* represents the orthogonal group (it keeps the metric invariant), and *Sp* is the symplectic group (the same as the unitary *U* if we replace the complex field numbers $\mathbb{C}$ by the quaternionic $\mathcal{H}$). In general, these Lie groups are considered by the cosets G/H to every symmetry class with the spatial dimension d and associated boundary $d-1$ for calculating the homotopy groups. So, there are two kinds of non-trivial topological insulators and superconductors if their boundaries meet the conditions, either $\pi_{d-1}(G/H) = \mathbb{Z}_2$ or $\pi_{d-1}(G/H) = \mathbb{Z}$ depending on if $d = 2n+1$ is odd or $d = 2n+2$ is even. Thus, the combination of topological insulators and superconductors belonging to different dimensionality opens the possibility of new topological structures. In any spatial dimension d, there are only five classes of topological insulators or superconductors distinguished by the $\mathbb{Z}$ (integers), $2\mathbb{Z}$ (even integers), or $\mathbb{Z}_2$ (cyclic group of order 2) for their associated topological invariant.

We can consider again the insulator of the previous Section 5.1 within this more general context. We choose a simplified Hamiltonian $Q(\boldsymbol{k})$ with m eigenvalues $\xi_m = 1$ and n with $\xi_n = -1$, associated respectively with the upper and lower bands with respect to the Fermi level, to study the topological properties. In this case, we do not have any discrete symmetry and thus we are in the Cartan class *A*. Therefore, it could be written as

$$Q(\boldsymbol{k}) = \mathcal{U}(\boldsymbol{k}) R \mathcal{U}(\boldsymbol{k})^{\dagger}, \tag{91}$$

where $\mathcal{U}(\boldsymbol{k})$ belongs to the unitary group $U(m+n)$, and R is the matrix

$$R = \begin{pmatrix} \mathbb{I}_m & 0 \\ 0 & -\mathbb{I}_n \end{pmatrix}, \tag{92}$$

where $\mathbb{I}_m$ and $\mathbb{I}_n$ are identity matrices, $m \times m$ and is $n \times n$ respectively. When $\mathcal{U}(\boldsymbol{k})$ can be written in the gauge form

$$\mathcal{U}(\boldsymbol{k}) = \begin{pmatrix} U_1(\boldsymbol{k}) & 0 \\ 0 & U_2(\boldsymbol{k}) \end{pmatrix} \tag{93}$$

$Q(\boldsymbol{k})$ is equivalent to R. Therefore, if we consider the function $Q(\boldsymbol{k}) : BZ \longrightarrow U(m+n)/U(m) \times U(n)$, which corresponds to a physical configuration at zero temperature, where there is a phase shift between the m states and the n occupied states below the Fermi level. Then, the homotopy group, in dimension d, $\pi_d(U(m+n)/U(m) \times U(n))$ will give us the type of topology of this material. A general classification by the group symmetries could be seen in [185].

Let us finish this section by highlighting that today, there are materials that go beyond the previously presented homotopy groups, such as higher-order topological insulators. The fundamental idea is that, in addition to time-reversal symmetry and charge conjugation, crystalline discrete symmetries are included. Thus, in the boundary of the bulk (bulk-edge correspondence), it is possible to predict gapless hinge states. However, homology or cohomology groups, which can help define homotopy groups, clearly establish that the boundary of the boundary is always zero or trivial topologically. So,

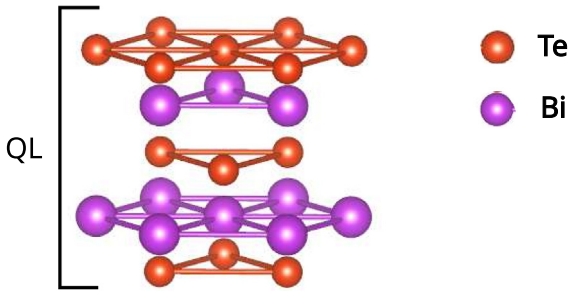

Fig. 6. Quintuple layers, Te-Bi-Te-Bi-Te, where Bi-Te has polar covalent bonds, while the quintuple Te-Te is a fairly weak Van der Waals bond.

the background topology of these compounds is certainly complex and not yet fully proven. That prevents us from going into this interesting topic in this review, given its mathematical and physical complexity despite its possible usefulness for thermoelectricity [185,192–195].

6. Topological thermoelectricity

We introduce topological insulators and topological superconductors, trying to apply the fundamental physics previously exposed [44,49–51,68,69,156,196–203]. A topological expression applied to the best thermoelectric at room temperature, Bi_2Te_3, is presented, which gives a numerical result very close to the experimental one for its figure of merit when minimizing lattice thermal contributions. In addition, the possibility of the proximity effect between superconductors and topological insulators to improve thermoelectricity is studied.

6.1. Bismuth telluride crystal and electronic structure

Almost all solid-state devices used as Peltier coolers are based on Bi_2Te_3 through microstructure engineering or nanostructuring [204]. That is the best thermoelectric at room temperature [205–213]. In recent years, a detailed structural study of Bi_2Te_3 has been carried out, both for being a good thermoelectric and for its condition as a topological insulator [214]. Let us briefly describe its main features. The coordination of Bi and Te is octahedral, being a rock salt with a compact hexagonal structure of the Te layers. They are in a set of quintuple layers, Te-Bi-Te-Bi-Te (Fig. 6), where Bi-Te has polar covalent bonds, while the quintuple Te-Te is a fairly weak Van der Waals bond. This arrangement justifies a significant anisotropy in the electrical conductivity, which is smaller for the Van der Waals planes, $\frac{1}{6}$ for the n-type and $\frac{1}{3}$ for the p-type. In the same way, the thermal conductivity in these planes is low, half that in the other planes. The Seebeck coefficient is nearly isotropic, and therefore, the figure of merit strongly depends on the orientation of the electric currents [215,216]. Furthermore, the electronic structure is quite rich if we consider the role played by the spin–orbit interaction [217]. Fundamentally, it can be seen as the interaction of the p-valence states of the Bi and Te atoms within the quintuple layer (QL), because *sp* hybridizations are negligible due to their relatively long separation. The interaction of the Te atoms is not important in van der Waals quintuple layers. It has 0.14 eV for the indirect gap measured by absorption and optical transmittance. Its formation strongly depends on the spin–orbit interaction since it does not have the same value for the Bi atoms as for the Te ones. Its application at the Γ point of the Brillouin zone decreases the energy of the Bi6*p* with respect to the states of the valence band Te5*p*, causing the inversion of bands. However, the strong band interaction of these electrons avoids the crossing that opens a new gap slightly displaced from the Γ point [218–221].

The importance of the crystalline structure of this compound with such a large anisotropy for electrical conductivity explains a singular behavior of the thermoelectricity of Bi_2Te_3 as a thermoelectric. As we know, the figure of merit is always higher for n-type than for p-type semiconductors because the mobility is much higher for electrons than for holes. However, for the Bi_2Te_3, the opposite occurs. The figure of merit ZT of the holes has a higher value than that of the electrons. The reason lies in the anisotropy of the electrons, which is much greater than that of the holes in this material. The highest value found experimentally was 2.4 for its dimensionless figure of merit ZT for p-type using alternating layers in a superlattice with Sb_2Te_3 [155,222–225].

6.2. Topological mass

We have analyzed the anomaly inflow and interpreted the change in mass of the electrons when approaching the surface. The Chern–Simons used corresponds to the electromagnetic field and, therefore, has an inner symmetry $U(1)$. That prevents defining instanton solutions if a non-Abelian symmetry group of higher rank is not considered. For this reason, we take into account that there are degenerate states induced by Kramers' theorem, as we have shown previously using Wilson's loop algebra. This allows us to define a non-Abelian Berry connection to perform the parallel transport of the electrons and overcome this situation. Furthermore, we will choose a five-dimensional spacetime so that the

Chern–Simons places us in ordinary four-dimensional Euclidean spacetime, following mainly [31,53]. In particular, we will analyze instantons as finite solutions of the classical fields associated with the basic Hamiltonian of topological insulators. We will see how there is a natural extension of the duality rotations we have previously studied for axion electrodynamics. This could directly translate into more realistic dimensions, but the more we reduce the dimensionality, the less general the formalism to be applied will seem.

The non-Abelian Berry connection can be generalized as

$$a_j^{\alpha\beta}(k) = i\langle\alpha, k|\partial_{k_j}|k, \beta\rangle, \tag{94}$$

where the corresponding curvature is given by

$$f_{ij}^{\alpha\beta} = \partial_i a_j - \partial_j a_i + i[a_i, a_j]^{\alpha\beta}. \tag{95}$$

From this, we can compute the second Chern number, which is expressed as

$$C_2 = \frac{1}{8\pi^2}\int_{BZ} d^4k\,\epsilon^{ijmn}\frac{1}{4}\,\mathrm{tr}(f_{ij}f_{mn}), \tag{96}$$

where the Levi-Civita tensor indices $i, j, m, n = 1, 2, 3, 4$ correspond to spacetime indices, while α, β refer to the occupied bands. Thus, for the 4×4 Hamiltonian describing the 3D topological insulator, we have

$$\mathcal{H} = \sum_k \psi_k^\dagger d_a(k)\Gamma^a\psi_k, \tag{97}$$

where

$$d_a(k) = (mv_F^2 + t\sum_i \cos k_i, \sin k_x, \sin k_y, \sin k_z, \sin k_w), \tag{98}$$

which represents the map from the Brillouin zone (BZ) torus to the sphere. Here, Γ^a are the Clifford matrices satisfying the anticommutation relation $\{\Gamma^\mu, \Gamma^\nu\} = 2g^{\mu\nu}\mathbb{I}_5$. This Hamiltonian is the most general form for topological insulators, following the classification presented in [51,53]. It is a generalization of the tight binding model introduced by Haldane, with 16 real parameters that can be expanded in the bases given by the direct products *spin* $\otimes$ *orbital*, $\{\sigma_i, \mathbb{I}\} \otimes \{\mathbb{I}, \tau_i\}$, where σ_i are the Pauli matrices, τ_i the ones associated to the orbitals and $\mathbb{I}$ the 2×2 unitary matrix [80].

The non-Abelian term of the axion action can be written as the integrand of the second Chern

$$\epsilon_{ijkl}Tr(f^{ij}f^{kl}) = 4\partial^i[\epsilon_{ijkl}Tr(a_j a_k a_l - \frac{2i}{3}a_j a_k a_l)], \tag{99}$$

which can be interpreted within a pure gauge Yang–Mills formalism where its solutions transform by $a_\mu = T^i a_\mu^i$ and $f_{\alpha\beta} = T^i f_{\alpha\beta}^i$, being the T^i's the generators of the inner symmetry group, which in this case is $SU(2)$. For $U \in SU(2)$ being position dependent, we have the gauge transformations for the potentials $a_i \to a_i^U = U^{-1}a_i U + U^{-1}\partial_i U$ and the fields $f_{ij} \to f_{ij}^U = U^{-1}f_{ij}U$. It is immediate to observe that the non-Abelian fields are not gauge invariant, unlike what happens with the Abelian ones, which tells us that the curvature depends on the group representation in this case, but not on the associated topological numbers. At infinity, $f_{ij} \to 0$ and the gauge potential is $a_i \to iU^\dagger\partial_i U$. Thus, we have the term

$$\epsilon_{ijkl}Tr(a^i a^k a^l - \frac{2i}{3}a^i a^k a^l) = \frac{1}{3}Tr(U^\dagger\partial^i UU^\dagger\partial^k UU^\dagger\partial^l U) \tag{100}$$

and the second Chern–Simons is transformed as

$$\begin{aligned} W(a^U) \to W(a) &- \frac{\mu}{8\pi^2}\int dk^3[\epsilon_{ijm}\partial_i Tr(\partial_j UU^{-1}a_m) + \\ &+ \frac{\mu}{24\pi^2}\int dk^3[\epsilon_{ijm}Tr(U^{-1}\partial^i UU^{-1}\partial^j UU^{-1}\partial^m U) \end{aligned} \tag{101}$$

where $W(a) = -\frac{\mu}{8\pi^2}\int dk^3\epsilon^{ijm}Tr(a_i\partial_j a_m - \frac{2i}{3}a_i a_j a_m)$ and μ a winding number. We see that this Chern–Simons term is not gauge invariant, $W(a) \to W(a) + \frac{\mu}{12\pi}24\pi^2 w(U) = W(U) + 2\pi\, w(U)$, but the path integral $e^{i\frac{W(a)}{\hbar}}$ is the quantity which must be invariant and therefore μ must be an integer [226]. Returning to the non-abelian Chern–Simons gauge-invariant formulation, we can define the action

$$\mathcal{S} = \frac{1}{16\pi^2}\int dk^4 f_{\mu\nu}f^{\mu\nu} \tag{102}$$

that in the case of having a self-dual solution $*f_{\mu\nu} = f_{\mu\nu}$, we can rewrite it as

$$\mathcal{S} = \frac{1}{16\pi^2}\int dk^4 *f_{\mu\nu}f^{\mu\nu}, \tag{103}$$

which is quantized in integer numbers. But it also leads to a minimum finite action, following Bogomolny [227], because

$$\frac{1}{2}tr(*f_{\mu\nu} \pm f_{\mu\nu})^2 = tr(f_{\mu\nu}f^{\mu\nu}) \pm tr(*f_{\mu\nu} * f_{\mu\nu}) \tag{104}$$

taking into account the equality $*f_{\mu\nu} * f_{\mu\nu} = f_{\mu\nu}f_{\mu\nu}$ in Euclidean space. Since the left-hand side of the equation is positive, we can write the inequality

$$\int dk^4 \,\mathrm{tr}(f_{\mu\nu}f^{\mu\nu}) \geq \left| \int dk^4 \,\mathrm{tr}(*f_{\mu\nu}f^{\mu\nu}) \right|, \tag{105}$$

which allows us to conclude that the action S has a minimum value

$$\mathcal{S} \geq \frac{1}{8\pi^2}|\mu|, \tag{106}$$

where μ is the winding number, which is essential for defining the instantaneous as topological objects. Therefore, these localized self-dual solutions (instantons) yield a finite action in Euclidean space–time that is quantized in integer units. Physically, they allow tunneling events between topologically distinct vacuum states. Our interest lies in exploring whether such configurations can propagate from the bulk to the surface or vice versa. One of the key features of instantons is that they tunnel among all vacua, but since they are now coupled to massless fermions, they cannot do so. They are concentrated in the atoms near the surface, as we have mentioned before. This is crucial because the minima of the energy–momentum tensor, within the domain of the wall, are concentrated at these zero modes.

Beyond recognizing that a non-Abelian representation may give rise to topological sectors labeled by the integers μ, it is essential to emphasize the fundamental role of the bulk–surface correspondence. This correspondence is mediated by the Chern–Simons form, which intrinsically relates an even-dimensional manifold to its odd-dimensional boundary. In our case, the bulk corresponds to a $(3+1)$-dimensional spacetime, while the surface is $(2+1)$-dimensional. It follows that the term accompanying the Chern–Simons form has the physical dimensions of mass. This implies the emergence of a finite energy gap for the confined electromagnetic modes at the surface. These modes propagate with an effective velocity smaller than c, typically associated with the Fermi velocity v_F of the electronic system. This interpretation naturally connects the electromagnetic response to the underlying electronic structure of topological materials. [228,229]. This is one more reason why we have chosen their speed to be the Fermi speed. Furthermore, this contribution is of purely topological origin, as it emerges from a term where the duality operator, rather than the metric tensor, is responsible for raising or lowering indices. This quantity is referred to as the *topological mass*, and we shall develop it on its general formulation below, following the framework outlined in [53].

Returning to the higher-dimensional Hamiltonian involved in the bulk-boundary correspondence using the instanton solutions for thermoelectricity, the second Chern associated with this Hamiltonian is [53]

$$C_2 = \frac{3}{8\pi^2}\epsilon^{abcde}\int dk^4 \hat{d}_a \frac{\partial \hat{d}_b}{\partial k_x}\frac{\partial \hat{d}_c}{\partial k_y}\frac{\partial \hat{d}_d}{\partial k_z}\frac{\partial \hat{d}_e}{\partial k_w}, \tag{107}$$

which in this case corresponds to the winding number resulting from the map $\hat{d}_a = \frac{d_a}{|d_a|}$ of a four-dimensional torus T^4 to a sphere S^4. The particle Hamiltonian $h(k) = d_a(k)\Gamma^a$ has eigenvalues $\xi(k) = \pm[\sum_{k,\mu} d_a^2]^{\frac{1}{2}}$. The system is gapped at half-filling when this value is different than zero in the Brillouin zone. C_2 can only change if $\sum_{k,\mu} d_a^2(k,m) = 0$, which leads to the mass m associated with the spinors Γ's five critical values given by this condition. Leading to

$$C_2 = \begin{cases} 0, m \notin (-4p, 4p) \\ +1, m \in (-4p, -2p) \\ -3, m \in (-2p, 0) \\ +3, m \in (0, 2p) \\ -1, m \in (2p, 4p) \end{cases} \tag{108}$$

where $p = 2\frac{k_B T}{v_F^2}$ is a mass parameter that gives a relationship between the main energies involved in this atomic layer close to the surface. The temperature and mass of the fermion particles are considered to play a fundamental external role. Note that this characterization of the topology is independent of that usually described in the models of materials, see appendices, and yet plays a basic role in electrical–thermal transport.

6.3. Instantons and tunneling probability with massless fermions

The equations for the non-Abelian field $f_{\mu\nu}$, known as Yang–Mills equations, $\partial_\mu f^{\mu\nu} = 0$, turn out to be the same for the dual field $*f^{\mu\nu}$ that satisfies the Bianchi identity, i.e., $\partial_\mu f^{\mu\nu} = \partial_\mu *f^{\mu\nu} = 0$. Therefore, the self-dual solutions $*f^{\mu\nu} = \pm f^{\mu\nu}$ are the only real ones different from zero in the Euclidean spacetime since they minimize the action on a given topological sector. Remember that the eigenvalues of the dual operator, acting on the fields, are ± 1 in this space and $\pm i$ in Minkowski's spacetime, as we studied in the dual rotations section. The solution for $+f^{\mu\nu}$ is the instanton, and the corresponding to $-f^{\mu\nu}$ is the anti-instanton. Both solutions are topological since we already saw how the duality operator does not need

the metric to raise or lower indices. Furthermore, we already introduced in the previous section how the second Chern number characterizes them. In quantum field theory, they are used to calculate the probability that a particle jumps from one state to another by tunneling. On the other hand, within this Euclidean space associated with the instanton solutions, in Statistical Mechanics the partition function is defined in a quite similar form by $Z(\beta) = tre^{-\beta H}$, relating the time with the temperature by $\tau = \hbar\beta = \hbar/k_B T$ [230,231]. In fact, we should think of time periodically $\tau = \tau_0 + \hbar\beta$, passing in cycles S^1 associated with the electronic pumping of the topological currents that we are going to see. This could be studied in a Floquet context [59] , but here we see how the instantons help to link electromagnetism with temperature and to quantify both physical magnitudes. We will specify these fundamental ideas later for the calculation of the Seebeck coefficient.

In a semi-classical approximation, the ground state of the system is the sum of all the fundamental states $|n\rangle$, given by $|\theta\rangle = \sum_n e^{in\theta}$ [226]. However, in the case of having massless fermions, as is our case, this simple picture is no longer valid. For the amplitude of probability for tunneling between two fermion states $|n\rangle$, we have

$$\begin{aligned}&\langle\psi_n||\psi_{n+\alpha}\rangle = \\ &= N\int \mathfrak{D}A\mathfrak{D}\psi\mathfrak{D}\overline{\psi}exp\left(-\int dx^4\mathcal{L} + i\int dx^4\overline{\psi}\gamma^\mu D_\mu\psi\right) = \\ &= N\int \mathfrak{D}Adet(i\gamma^\mu D_\mu)exp\left(-\int dx^4\mathcal{L}\right)\end{aligned} \tag{109}$$

being α a winding number, N a normalization factor, and $\mathcal{L}$ the Lagrangian density associated with the $f_{\mu\nu}$ fields. However, since fermions have a zero mode in every configuration with $det(\gamma^\mu D_\mu) = 0$, the prior tunneling probability between the two ground states is zero when massless fermions are present. The only possibility to avoid this would be to locate the state where the mass was zero and eliminate it from the global calculation. This concentrates the instantons around the zero-mass electrons near the surface.

If we consider this result for the states where the bulk-surface transition occurs, we see that the electrons will not be able to pass from one state to another by tunneling due to the instantons. We can assume that both states are bound and that, therefore, the electrons are not free as if they were purely metallic. This characteristic allows them to directly receive thermal energy just like the atoms to which they are bound. It also justifies that they are assigned quasi-localized states, which are essential for the Thouless pumping effect.

6.4. Lattice oscillations and topological currents

Looking at the lattice, we know that the axion electrodynamics creates an electric polarization $\boldsymbol{P}$ that produces a V_t potential that separates the bulk atoms from the edge ones. Furthermore, the dilatation or contraction due to the temperature changes the periodicity of the atoms on the surface to those on the interior, so a Thouless potential [48,232,233] could be imagined as

$$V_t = V_b \sin^2\left(\frac{\pi x}{R_b} + \frac{\pi}{2}\right) + V_e \sin^2\left(\frac{\pi x}{R_e} - \frac{\phi}{2}\right), \tag{110}$$

where R_b, and R_e are the spatial periods in the bulk and the edge lattice layers, respectively, and ϕ is the phase, modulus 2π, whose variation gives a periodically modulated potential. This phase measures the relative spatial atomic positions of these layers. Let us note how important the cut made of the set of quintuple layers defining the surface of the topological insulator, $Te - Bi - Te - Bi - Te$, can be for the efficiency of thermoelectricity. They also depend on the temperature and varying the phase adiabatically, we produce Thouless pump cycles with period $\tau = \frac{2\pi}{\omega}$. So, although a particle located in the Bloch state $|u_n(k,\phi)\rangle$ associated with the Hamiltonian $H(k,\phi(t))$ remains in the same state under an adiabatic regime, without changing its eigenvalues. However, a new Berry phase will emerge proportional to $\partial_t\phi$. Choosing as parameters the moment $\hbar k$ and the phase ϕ, we have the curvature $\Omega^n_{k,\phi} = i[\langle\partial_k u_n||\partial_\phi u_n\rangle - \langle\partial_\phi u_n||\partial_k u_n\rangle]$ of the n-band occupied during the pumping [48,59,234–240]. This leads to a topological electric current

$$J_T = Ne\Omega^n_{k,\phi}\partial_t\phi, \tag{111}$$

where N is the number of electrons per volume in this region where Thouless pumping is possible (Fig. 7). The first Chern number associated with each cycle in the Bloch band n is defined by

$$\overline{n} = \frac{1}{2\pi}\int_{BZ} dk\int_{-\pi}^{\pi} d\phi\Omega_n(k,\phi). \tag{112}$$

Therefore, integrating over one full cycle the phase ϕ we obtain a current proportional to an integer number of electrons. Notice that the displacement on x is necessary due to the non-commutativity between the momentum $\hbar k$ and the position x.

Another way to see this is through the Wannier states

$$|W_{nR}\rangle = \frac{V_{cell}}{2\pi}\int_{BZ} e^{ikR}|\psi_{nk}\rangle, \tag{113}$$

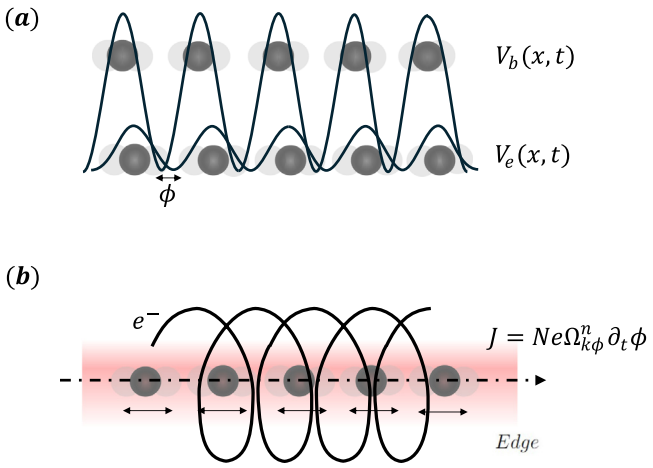

Fig. 7. **(a)** Representation of the Thouless potential as a function of the phase variation ϕ over time due to temperature changes. **(b)** Topological current associated with the Thouless pumping.

which allows the Wannier charge center to be defined as the diagonal element [241], $\overline{r_n} = \langle W_{n0}|\hat{r}|W_{n0}\rangle$, which is equivalent to

$$\bar{r}_n = \frac{V_{\text{cell}}}{2\pi}\int_{\text{BZ}} i\langle u_{nk}|\hat{r}|u_{nk}\rangle\, d^3k, \tag{114}$$

where V_{cell} is the cell volume, and u_{nk} is the periodic part of the Bloch state $\psi_{nk}(r) = e^{ikr}u_{nk}$. Therefore, the Zak phase is directly related to the position of the charges and this position depends on the thermal vibrations of the lattice. Note that these electrons are not like the free metal because, as we have shown in detail, they belong to the bulk-surface by the Inflow effect. The Inflow anomaly transforms the Dirac spinors of the bulk into half of them at the surface, the same as the Chern–Simons does for those involved in conductivity. This allows them to be added together to obtain the usual integer conductivity, but this subtle behavior means that this electronic transport is directly related to the bulk atoms of the lattice and therefore to their thermal vibrations. This is a key observation for understanding the possibility of topological thermoelectricity because it allows us to almost directly transform heat into electric currents.

6.5. Topological Seebeck coefficient

As we have shown, the topological insulators have an electric polarization $\boldsymbol{P}$ in their surface directly related to Berry's phase

$$\triangle P = \frac{e}{2\pi}\int_0^{\tau} dt \int_{-\frac{\pi}{a}}^{\frac{\pi}{a}} dk \sum_{n\in occu} f_n(k), \tag{115}$$

being $f_n(k) = i[\frac{\partial}{\partial k}\langle\psi_{nk}(t)|\frac{\partial}{\partial t}|\psi_{nk}(t)\rangle - \frac{\partial}{\partial t}\langle\psi_{nk}(t)|\frac{\partial}{\partial k}|\psi_{nk}(t)\rangle]$ and a the lattice constant. Under a gauge transformation of the electromagnetic potentials $A_\mu \rightarrow A_\mu + \partial_\mu\Lambda(x^\mu)$, the electron wave function transforms simultaneously by $\psi \rightarrow \psi\, exp(ie\frac{\Lambda}{\hbar})$. This exponential function needs to be single-valued, however, the function $\Lambda(x,t)$ does not. Thus, we can write $\Lambda(x,t) = \frac{2\pi\mu\hbar\tau}{e\hbar\beta} = \mu\frac{2\pi\tau}{e\beta}$, μ is the winding number associated with the Chern–Simons, that in the non-Abelian case has five quantized branches given by the Riemann–Hurwitz formula [31], $\beta = \frac{1}{k_BT}$, and τ is the period of the Thouless pumped charge between the surface and its closest bulk layer. This allows finding an electric potential directly related to the temperature within this Euclidean spacetime and Matsubara frequencies [242] by

$$V \rightarrow V + \mu\frac{2\pi}{e}k_BT, \tag{116}$$

which means that we have transformed the electric potential into another that includes a new thermal term $\mu\frac{2\pi}{e\beta}$. This turns out to be a fundamental result associated with the Inflow anomaly of electrons in the wall condition of the temperature domain, where Chern–Simons photons are produced by thermal vibrations of the lattice and Thouless electrons fuse. This property also strongly depends on having the instantons coupled to massless fermions, since in this case, they lose the property of tunneling all vacuum states and only concentrate their energy in the fermion zero modes near the surface. Therefore, there are several conditions to carry out this transformation of temperature into

electricity that must be followed, and that we have been studying throughout this work. Thus, we can calculate the Seebeck coefficient [31]

$$S = \mu \frac{2\pi}{e} k_B + \frac{2\pi}{e} \frac{\partial \mu}{\partial T} k_B T \tag{117}$$

choosing a gauge condition $V = -\mu \frac{2\pi}{e} k_B T$. The relevant point is that the topological branches allow finding a new term in the Seebeck coefficient, which can increase it depending on the temperature. On the other hand, due to the small space considered near the surface, electron–hole Schwinger pairs are created, as long as the electric field E is large enough. Calculating the critical electric field E_C following the Heisenberg–Euler formula (24), we observe that the limit to obtain a large number of real electron–hole pairs is

$$E_C = \frac{m v_F^2}{e\hbar} \simeq 0.15 eV/nm \tag{118}$$

where we have considered that the energy gap is 0.21 eV and the Fermi velocity $v_F \simeq 6 \times 10^5$ m/s. This provides a critical electric field almost 10 orders of magnitude lower than the critical electric field of QED and with an equivalent temperature of $\zeta = 1.74 \times 10^{-6}$ K/nm , these values being accessible in the topological materials.

6.6. Dimensionless figure of merit ZT

Now let us calculate the contribution to the figure of merit in the TIs in 2+1-dimensions, where the nontrivial topology is determined by the first Chern number $\overline{n}$ and n is a winding number of the states. Assuming an adiabatic evolution of the states under a thermal flux, we can define the Seebeck coefficient through the entropy as $S = \frac{k_B}{e}(ln|\frac{\psi_b}{\psi_t}| + in\vartheta)$, where ψ_b and ψ_t are the final and initial states, and ϑ is the angle between them. The winding number could be taken $n = 1$ for the topological insulator alone. However, we will see that this value can increase if we also add the superconducting phase. In fact, we are representing the entropy of one Riemann surface associated with the Hilbert space expanded for these states in (2+1)-dimensions. Notice that although the von Neumann entropy would be zero considering pure states, this is not true considering that these states are entangled due to their global topological properties. Taking the previous formula, we see that $ln|\frac{\psi_b}{\psi_t}| = 0$, closing the cycle, and the Seebeck coefficient turns out to be

$$S = \frac{k_B}{e} in\vartheta = \frac{k_B}{e} n \int_C \langle \psi(r)|\nabla|\psi(r)\rangle dr = \frac{k_B}{e} \pi n \overline{n}, \tag{119}$$

being θ the angle directly associated with the Berry phase on the closed curve C in the BZ, and $\overline{n}$ the first Chern number. To determine the electronic contribution to the figure of merit, it remains only to calculate the electrical and thermal conductivity associated with each counter-propagating mode. The first is given by $\sigma_e = \overline{n}\frac{e^2}{\hbar}$, which is half the quantum conductance times the first Chern number [52,243]. To obtain the electronic thermal conductivity, we consider the $2D$ density of states in the semimetallic region

$$D(\xi) = \frac{1}{(2\pi)^2} \int \delta(\xi - \hbar v_F k) 2\pi k dk = \frac{1}{2\pi\hbar^2 v_F^2} \xi, \tag{120}$$

which leads to an electronic thermal conductivity

$$\kappa_e = \frac{\partial}{\partial T} \int d\xi D(\xi) \xi f(\xi) v_F l = \frac{3\zeta(3)}{h} k_B^2 T \tag{121}$$

considering that the conduction takes place at the edge and a temperature-dependent mean free path l. $\zeta(3)$ is the Riemann zeta function of dimension three (Apery's constant), and $f(\xi)$ is the Fermi–Dirac distribution function. This assumption is taken considering a gas of electrons on the surface, which allows us to avoid the details of entering the special form of the bands.

Therefore, despite using so different expressions than Boltzmann's ones, which are outside of the topological physical behavior, we obtain a Wiedemann-Franz law, given by the ratio κ_e/σ_e, similar to its conventional value. That does not stand for the Seebeck coefficient, whose topological expression gives a significant value of $\sim$ 270 μV/K ($n = \bar{n} = 1$). Finally, the electronic contribution to the figure of merit figure $ZT = \sigma_e S^2/\kappa_e$ for the topological insulators turns out to be

$$ZT = n^2 \overline{n}^3 \frac{\pi^2}{3\zeta(3)}. \tag{122}$$

The numerical value for $\overline{n} = n = 1$ is $ZT = 2.73$, which closely approximates the maximum experimental value discovered in Bi_2Te_3/Sb_2Te3 superlattices, a configuration that minimizes lattice thermal contributions. It is worth noting that this expression could be refined by establishing a deeper connection between electronic thermal conductivity and topological invariants. A detailed exposition of various thermal Hall effects can be found in Ref. [244], where a relationship between thermal conductivities and Berry curvature is addressed. In this reference, a value of $\kappa_e \approx \frac{\pi k_B^2}{12\hbar} T\ \overline{n}$ is achievable under

several assumptions. Additionally, to complete the figure of merit, it is essential to consider the role of phonons. The thermal conductivity of phonons in terms of the central charge could be expressed as $\kappa_{ph} = \frac{\pi k_B^2 T}{6\hbar} c$, which is equal to the previous electronic part when considering $c = 1/2$. This underscores the singular role of phonons in this topological context, leading to an effective figure of merit of $ZT = 3$ for the most basic topological numbers.

6.7. Weyl semimetals and thermoelectricity

Weyl semimetals are materials whose electrons behave like Weyl fermions. That is, particles with zero rest mass that satisfy the Dirac equation. Interestingly, such particles have not been found experimentally as fundamental particles in high-energy physics, although they have been extensively studied within the framework of quantum field theory. However, their condensed-matter analogs were experimentally discovered in 2015 in these semimetals, following earlier theoretical predictions [245–249].

The fundamental idea is to achieve a crossing of the conduction and valence bands at the Fermi level, occurring at points known as Weyl nodes. According to the geometry of their scattering cones in momentum space, they are divided into Type-I and Type-II. The dispersion law of these semimetals, close to the Fermi level, is $\xi(\boldsymbol{k}) = \hbar \boldsymbol{w} \cdot \boldsymbol{k} \pm v_F \hbar k$, where $\boldsymbol{w}$ is a velocity associated with the inclination of the Weyl cone. If it is less than the Fermi velocity, then the semimetal is classified as Type-I, and Type-II otherwise. This can be realized by starting from an insulator in which either time-reversal symmetry ($\mathcal{T}$) or inversion symmetry ($\mathcal{P}$) is broken. The symmetry breaking generates a topological phase transition that closes the bulk band gap, thereby driving the system from an insulating to a semimetallic state. As discussed, this process admits a topological interpretation: the Berry curvature becomes singular at the band-touching points, and Weyl nodes can thus be viewed as monopoles of Berry curvature in momentum space.

The topological charge of a Weyl node is defined by the quantized integral of the Berry curvature over a closed surface enclosing the node. This integral yields the Chern number, whose sign is determined by the node's chirality. Weyl nodes always appear in pairs of opposite chirality, and on the material's surface, they give rise to unique electronic states known as Fermi arcs, which connect nodes of opposite chirality in momentum space. The Berry curvature acts as an effective internal magnetic field in reciprocal space. These materials realize key aspects of axionic electrodynamics and the chiral anomaly from quantum field theory, although with important modifications dictated by the specific crystalline symmetries of each compound. A notable example is that Weyl semimetals breaking time-reversal symmetry ($\mathcal{T}$), such as Mn_3Sn [250], $Co_3Sn_2S_2$ [251], and $YbMnBi_2$ [252], exhibit a magnetoelectric response. In contrast, those that break spatial inversion symmetry ($\mathcal{P}$), such as TaAs [247–249] and NbAs [253], do not display magnetoelectricity. This diversity of symmetry-breaking patterns makes it extremely challenging to construct a general theoretical model, as we did with topological insulators [254].

Weyl semimetals are inherently more complex than topological insulators, which makes the development of a simple analytical model for their thermoelectric figure of merit particularly challenging. From conventional transport formalism, near a Weyl point, the energy dispersion is linear, $\xi(k) = \pm \hbar v_F k$ (extreme Type-I). In three dimensions, the density of states is obtained as

$$D(\xi) = \frac{g}{(2\pi)^3} \int d^3k \, \delta\big(\xi - \xi(k)\big) = \frac{g\,\xi^2}{2\pi^2(\hbar v_F)^3},$$

where g is a degeneracy factor that accounts for the number of Weyl nodes and their chirality in the Brillouin zone.

In the low-temperature limit, the Seebeck coefficient can be estimated using Mott's formula [255,256]:

$$S = -\frac{\pi^2 k_B^2 T}{3e} \left.\frac{d \ln \sigma(\xi)}{d\xi}\right|_{\xi=\xi_F} \propto -\frac{\pi^2 k_B^2 T}{3e\xi_F},$$

which typically yields a value about one order of magnitude smaller than the Seebeck coefficients of high-performance thermoelectric materials [257–260]. It is true that the degeneracy factor g can be large, enhancing the density of states. For instance, in TaAs $g = 24$; similarly, in NbAs, TaP, and NbP the same $g = 24$ applies, and in $MoTe_2$ as well [261–264]. However, this increase in g does not enhance the Seebeck coefficient; on the contrary, a larger g raises the Fermi level, which further suppresses S.

The interplay between symmetry and electronic topology seems to govern the thermoelectric behavior of Weyl semimetals. For example, when time-reversal symmetry ($\mathcal{T}$) is broken or when tilting of the Weyl cones introduces Berry curvature effects, unconventional thermoelectric responses such as the magneto-Seebeck and magnetic-field–antisymmetric Seebeck effects appear [256,265]. In these cases, S becomes strongly field-dependent yet remains moderate in absolute value. Overall, although the intrinsic Seebeck response of Weyl semimetals is smaller than that of high-performance thermoelectric materials, their tunable Berry curvature and magneto-thermoelectric effects make them attractive for novel thermoelectric applications.

6.8. Thermoelectricity in superconducting phase

The first research carried out on this topic was due to Meissner in 1927, denying its existence, as Ginzburg wrote in his Nobel Lecture [266,267] in 2003. When a temperature gradient ∇T is applied to a superconductor in addition to an electric field $\boldsymbol{E}$, a current $\boldsymbol{J}_n$, carried by the unpaired electrons or holes, arise at finite temperatures in any superconductor

$$\boldsymbol{J}_n = \sigma(\boldsymbol{E} - \frac{\nabla\mu}{e} - S\nabla T) \tag{123}$$

where σ, μ, S are the electric conductivity, chemical potential, and Seebeck coefficient, respectively. In the superconducting phase, i.e., when the temperatures are below the critical one T_c, the whole current in the bulk must be zero due to the Meissner effect. So, $\boldsymbol{J} = \boldsymbol{J}_n + \boldsymbol{J}_s = 0$, where $\boldsymbol{J}_s = n_s e v_s$ are the superconductor currents, being n_s the superconducting electron density and v_s their average density considering the simple London model.

In the stationary case, we have that

$$\boldsymbol{E} - \frac{\nabla\mu}{e} = 0 \tag{124}$$

and therefore the J_n currents appear as

$$J_n = -J_s = -\sigma S\nabla T, \tag{125}$$

which tells us that the superconductors have thermoelectricity, as long as we have a temperature gradient for the fermion currents (electrons or holes). More in detail, if we consider the condensate wave function of superconductor phase, $\psi_s(\boldsymbol{r}) = \sqrt{\frac{n_s}{2}} exp(i\phi(\boldsymbol{r}))$, where $\phi(\boldsymbol{r})$ is a macroscopic phase and n_s the concentration of the electrons, the superconductivity currents can be written as $J_s = \frac{n_s e\hbar}{2m}\nabla\phi(\boldsymbol{r})$, which gives a measurable phase difference

$$\Delta\phi = \frac{2m\sigma S}{n_s e\hbar}\Delta T \tag{126}$$

This is true in the case of topological materials due to the Thouless electronic pumping, which creates a very special electronic conduction where the entropy of the bulk and surface states is not the same. Note that this phenomenon would be enhanced when the surface was formed by two different chemical potentials on the surface, such as a topological insulator–superconductor.

6.9. Experimental topological superconductivity

Topological superconductivity is still a subject that needs development to be applied technologically. In any case, we have seen how it complements topological insulators within the classification of topological materials. Thus, although its application to topological thermoelectricity is in an embryonic state, we complete this section by trying to express the state of the art on this topic nowadays and how it could affect topological thermoelectricity.

Experimental topological superconductors began with topological insulators using the proximity effect [268–270]. Of special interest are the states that develop at the interface between a TI and an s-wave superconductor (SC), where the proximity effect generates a quasi-two-dimensional quantum state similar to a spinless $p_x + ip_y$ superconductor but without breaking time-reversal symmetry [268,271,272]. There is another way to achieve superconductivity using topological insulators by changing the number of carriers by metal doping, for example, Bi_2Se_3 doped with Cu, Sr, or Nb [273–276]. Finally, the superconductivity of a great number of topological insulators is due to the change of crystal structure under pressure [277–279]. Since this drastically increases the electrical conductivity over the thermal without changing the electron density too much and, therefore, also the Seebeck coefficient, the figure of merit should increase. This point is encouraging, although there are serious problems with its application. The critical temperature of superconductivity is very low, of the order of 4 K in most of them, and that precludes the maximum technological use for such topological thermoelectricity in general. Still, its effect should be important for the ultracold Peltier effect, at least.

6.10. Basic theoretical topological superconductivity

Topological insulators and topological superconductors can be thought of in parallel if we consider that the band gap of the topological insulator maps to the band gap of the topological superconductor, which should close in a function space under certain physical conditions. This general perspective establishes an analogy between the Hamiltonians of insulators and superconductors and their respective topological solutions. We will begin with the topological superconductor, using a Hamiltonian similar to the Su–Schrieffer–Heeger (SSH) model for a chain. While these represent very different physical phases in a material, such an analogy could be useful for understanding their topological behavior. This idea has been more broadly explored in the literature [214,280], and mathematically, it is very appealing.

The Hamiltonian of a crystalline lattice in second quantization for a superconductor can be represented as

$$\mathcal{H} = h_0 - \sum_{i=1}^{N} U c_{i\downarrow}^{\dagger} c_{i\uparrow}^{\dagger} c_{i\uparrow} c_{i\downarrow}, \tag{127}$$

where the term h_0 accounts for the electronic one-body behavior, with

$$h_0 = \sum_{i=1}^{N} (\xi_i - \mu) c_{i\downarrow}^{\dagger} c_{i\uparrow}^{\dagger}, \tag{128}$$

while the last term represents the two-body interaction under the U potential. Here, $c_{i\downarrow}^{\dagger}$ is the creation operator for an electron with spin down at site i, and $c_{i\downarrow}$ is the annihilation operator for the spin-down electron at site i. The other two operators correspond to different spin orientations. In the case of a superconductor, we aim to have an attractive electronic interaction to form electron pairs with opposite spins, i.e., boson singlets for s-wave superconductors. For p-wave superconductors, the triplet pairing would need to be considered, and so on.

To achieve this, we introduce a mean-field approximation, considering only the first linear term in the Hamiltonian, yielding

$$\mathcal{H}' = h_0 + \sum_{i=1}^{N} \left(\Delta_i c_{i\downarrow}^{\dagger} c_{i\uparrow}^{\dagger} + h.c. + \frac{|\Delta_i|^2}{U} \right), \tag{129}$$

where the pairing potential is defined as $\Delta_i = -U\langle c_{i\uparrow} c_{i\downarrow} \rangle$. Therefore, the number of particles is not conserved, although its parity is, since the change occurs in pairs of particles.

This is the BCS mean-field Hamiltonian that can be diagonalized using the Bogoliubov transformations through the operators

$$\psi_{i\sigma}^{\dagger} = \sum_{j=1}^{N} (u_{ji} c_{i\sigma}^{\dagger} + v_{ji} c_{j,-\sigma}) \tag{130}$$

where $\sigma \in [\downarrow, \uparrow]$ denotes the spin-$\frac{1}{2}$ state, being u_{ji} and v_{ji} complex numbers, whose square modulus is associated with the probability of the non-occupation or occupation state $(k\uparrow, -k\downarrow)$ respectively, with $|u_{ji}|^2 + |v_{ji}|^2 = 1$. This allows us to obtain the effective Bogoliubov–de Gennes equation working on the amplitudes

$$\mathcal{H}_{BdG} \begin{pmatrix} u_i \\ v_i \end{pmatrix} = \xi_i \begin{pmatrix} u_i \\ v_i \end{pmatrix}, \tag{131}$$

where the $\mathcal{H}_{BdG}$ is given by

$$\mathcal{H}_{BdG} = \begin{pmatrix} h_0 & -i\Delta(p_x - ip_y) \\ i\Delta^*(p_x + ip_y) & -h_0 \end{pmatrix}, \tag{132}$$

being $h_0 = \frac{p_x^2 + p_y^2}{2m} - \mu$, and μ the chemical potential. Thus, the quasiparticle spectrum is obtained by

$$\xi(p_x, p_y) = \pm\sqrt{h_0^2 + |\Delta|^2 p^2} \tag{133}$$

which is particle–hole symmetric and, therefore, the i index of the quasiparticles only runs over the N positive eigenvalues ξ_i of the excited states $\sum_{i\sigma} \xi_i \psi_{i\sigma}^{\dagger} \psi_{i\sigma}$. After some approaches, it is obtained the gap equation

$$1 \simeq \frac{U_0}{2} D(\xi_F) \int_{\xi_F}^{\xi_F + \hbar\omega_c} d\epsilon \frac{1}{\xi - \epsilon} = \frac{U_0}{2} D(\xi_F) ln \left(\frac{\xi - 2\xi_F - 2\hbar\omega_F}{\xi - 2\xi_F} \right), \tag{134}$$

where $D(\xi_F)$ is the density of states per spin at the Fermi level, U_0 a constant attractive potential, $\hbar\omega_D$ the Debye energy for the shell thickness on the Fermi sphere, ξ the energy associated with the paired state, and $\hbar\omega_c$ the cut-off energy to have it smaller than the Debye one. When $\Delta = 0$, the superconductivity phase disappears because there are no bosonic Cooper pairs [281–283].

To analyze the topological behavior of superconductivity, we can choose a one-dimensional string of spinless particles, a toy model, as Kitaev's one [284–287]. In this case, the Hamiltonian can be reduced to

$$\mathcal{H} = \sum_{i}^{N} -t(c_i^{\dagger} c_{i+1} + h.c.) + \Delta(c_i c_{i+1} + h.c) - \mu c_i^{\dagger} c_i. \tag{135}$$

Performing a Fourier transform, we have the Hamiltonian

$$\mathcal{H} = \sum_{k} \left(c_k^{\dagger} c_{-k} \right) h(k) \begin{pmatrix} c_k \\ c_{-k}^{\dagger} \end{pmatrix}, \tag{136}$$

where

$$h(k) = \vec{\mathrm{d}} \cdot \vec{\sigma} = \begin{pmatrix} -2t\cos k - \mu & \Delta \sin k \\ \Delta \sin k & 2t\cos k + \mu \end{pmatrix}, \tag{137}$$

with $d_x(k) = \Delta \sin k$, $d_y(k) = 0$, $d_z(k) = -2t\cos k - \mu$, and $\xi(k) = \pm|\vec{\mathrm{d}}|$. By performing a transformation of a closed loop, we obtain the eigenvectors

$$|k_+\rangle = \begin{pmatrix} \cos\frac{\vartheta}{2} \\ e^{i\phi}\sin\frac{\vartheta}{2} \end{pmatrix}, \quad |k_-\rangle = \begin{pmatrix} -\sin\frac{\vartheta}{2} \\ e^{i\phi}\cos\frac{\vartheta}{2} \end{pmatrix}.$$

The Berry connection is then computed as

$$a(-k) = i\langle k_-|\frac{d}{dk}|k_-\rangle = -\frac{1}{2}\frac{d\phi}{dk},$$

assuming $d_z = 0$. Therefore, the Berry phase in the Brillouin zone is

$$\gamma_- = \frac{1}{\pi}\int a(-k)\,dk = -\gamma_+, \tag{138}$$

which results in either 1 or 0, depending on whether or not it surrounds the singularity. This is given by

$$\overline{\gamma}_- = \oint \langle k_-|\nabla \vec{\mathrm{d}}\,|k_-\rangle d\boldsymbol{l} = \int_S \frac{1}{2}\frac{\vec{\mathrm{d}}}{d^3} d\boldsymbol{S}.$$

Thus, a topological transition is associated with this singularity. In the case of the Kitaev chain, it has $\Delta = t > 0$, $\mu = 0$ for the non-trivial topological phase, and $\Delta = t = 0$, $\mu \neq 0$ for the trivial topological regime [70,288]. We should note that this result is formally similar to the SSH model, differing only in the physical interpretation. We will develop this further in the appendix.

If we observe that the superconducting quasi-particles appear as an electron–hole superposition, as we saw above, and are therefore neutral, we have a perfect physical example for a Majorana representation of the solutions of Weyl's equation. Thus, we can define the creation and annihilation operators in terms of Majorana modes as $c^\dagger = \frac{1}{2}(\gamma_1 + i\gamma_2)$ and $c = \frac{1}{2}(\gamma_1 - i\gamma_2)$, where $\gamma_1 = \gamma_1^\dagger$ and $\gamma_2 = \gamma_2^\dagger$ are real quantities or representations of the Majorana spinors. γ_1 and γ_{2N} do not appear, and the energy that differentiates a filled state from an empty one is $2t$. This definition allows us to obtain isolated Majoranas in the extreme terms of the chain, which have zero energy, i.e., they are Majorana zero modes. The bands associated with them come from $\xi(k) = \pm\sqrt{(2tcosk + \mu)^2 + 4\Delta^2 sin^2 k}$. The bulk gap closes at $\mu = \pm 2t$, where the positive and negative energy bands meet at $\xi = 0$ for $k = \pi$ ($\mu = 2t$) or $k = 0$ ($\mu = -2t$). We can see the analogy that exists with the topological insulators that we have used previously, although the bands we are talking about are completely different in both phases [51,289–291].

Finally, we can find the zero-modes close to $k \approx 0$ where the Hamiltonian is

$$h(k) = \begin{pmatrix} -2t - \mu + O(k^2) & \Delta ak \\ \Delta ak & 2t + \mu - O(k^2) \end{pmatrix} \tag{139}$$

which is Dirac's Hamiltonian for fermions of mass $m = 2t + \mu$ and velocity $v = a\Delta$, being a the lattice constant. Introducing a domain wall where the mass of the fermion changes sign at $z = 0$, i.e., $m(z) = m_0 \tanh(z)$ when $\to \pm\infty$, we will find a similar situation of the localized zero-mode Dirac fermion on this domain wall. Thus, we have

$$\begin{pmatrix} m(z) & -iv\partial_z \\ iv\partial_z & -m(z) \end{pmatrix}\begin{pmatrix} \psi_\uparrow \\ \psi_\downarrow \end{pmatrix} = \begin{pmatrix} 0 \\ 0 \end{pmatrix} \tag{140}$$

whose solution is given by

$$\begin{pmatrix} \psi_\uparrow \\ \psi_\downarrow \end{pmatrix} = \begin{pmatrix} 1 \\ -i \end{pmatrix} exp\left[\pm\frac{1}{v}\int_0^z dz' m(z')\right] \tag{141}$$

where only one of the solutions is normalized and localized in the plane $z = 0$. Noticing that the matrix $\begin{pmatrix} 1 \\ -i \end{pmatrix}$ belongs to both spinor up and down, we may make the combination of operators $c - ic^\dagger = (c - ic^\dagger)^\dagger$ which is immediate to see that it is a Majorana. Therefore, we have a Majorana in the zero mode at $z = 0$. This means a parallel topological behavior to the topological insulators, so we can hope that both phases coincide on the surface of the topological material. That tells us that there is a possibility that the electrons involved in the Thouless pumping can surround more topological singularities, increasing the value of the winding [292] and thus do it also with the figure of merit of thermoelectricity. In the simplest case, in which we had both phases, topological superconductor and insulator, then $n = 2$, and therefore, the figure of merit would be four times higher.

At present, this is an extraordinarily active area of research, as reflected in the numerous recent advances reported in the literature [141,293–300]. In addition, several comprehensive review articles provide an excellent overview of the field, offering insight into the conceptual and experimental challenges associated with the physical interpretation of the results [301–305].

7. Discussion

Throughout this review, we have analyzed the physical and mathematical conditions, as well as the theoretical tools, that could enable thermoelectricity with efficiencies far exceeding current values. At present, an analytical expression for the figure of merit of the most efficient room-temperature thermoelectric material, namely Bi_2Te_3, has been reported in the literature [31]. This expression yields values that are remarkably close to experimental measurements when realistic material parameters are considered. However, the central challenge is to generalize this formulation to achieve much higher efficiencies. This line of reasoning suggests that multiple topological phases could be combined within the same material, with the most promising configuration being a topological insulator–superconductor structure. Beyond the formidable experimental challenges associated with the synthesis of such materials and the measurement of subtle physical quantities, it is essential to understand the underlying mechanisms governing their behavior. This calls for a detailed examination of the interfacial physics in topological insulators and superconductors, both of which exhibit the transport concentrated at the surface. Clearly, the correspondence between bulk and boundary is crucial for understanding their physical properties, particularly in relation to thermoelectricity. These considerations have motivated our in-depth study of axionic electrodynamics, encompassing both its classical and quantum aspects. From this analysis, it becomes apparent that the Hall conductivity in topological materials arises from two distinct sources: chiral electronic currents confined to the surface and Chern–Simons photons from the bulk. These are accompanied by persistent polarization $\boldsymbol{P}$ and magnetization $\boldsymbol{M}$ fields surrounding them. Furthermore, thermal energy acts on bulk electrons, inducing a Thouless pump that drives them toward the surface within a highly specific electromagnetic framework. For this process to occur efficiently, however, certain rather subtle conditions induced by their topological invariants, which produce robust electron transport, must be satisfied.

In Topological Insulators, Maxwell electromagnetism is extended by introducing a pseudo-scalar Lorentz invariant into the action, $\epsilon^{\mu\nu\alpha\beta}F_{\mu\nu}F_{\alpha\beta}$, which differs from the usual scalar $F_{\mu\nu}F^{\alpha\beta}$ in that it does not rely on the metric for raising or lowering tensor indices. This term is not time-reversal invariant because it involves the duality operator, requiring the introduction of another field $\theta(\boldsymbol{r},t)$ to achieve this symmetry. This results in the modified term $\frac{e^2}{16\pi^2}\,\theta(\boldsymbol{r},t)\epsilon^{\mu\nu\alpha\beta}F_{\mu\nu}F_{\alpha\beta}$. The new pseudo-scalar field is what gives rise to axionic electromagnetism. This leads to an electromagnetism where electric and magnetic fields are confined within tori in each Brillouin zone, which naturally leads to a quantized action, reflecting its topological nature. The key concept here is the duality of electromagnetic fields, which is related to the symmetry of dual rotations, $SO(2)$. This symmetry can be generalized to the Yang–Mills equations to find topological solutions, such as instantons or anti-instantons, with self-dual or anti-self-dual fields, respectively, in Euclidean space. These solutions exhibit quantized action and are topological. In this context, we have defined them in the space of k-points using the non-Abelian Berry phase to account for the degeneracy of states. In summary, topological materials exhibit a vacuum with fields distinct from those of materials with trivial topology.

Furthermore, the Lorentz pseudoscalar associated with the fields can be expressed as the divergence of a term in terms of the potentials, known as the Chern–Simons term, $\epsilon_{\mu\nu\alpha\beta}F^{\mu\nu}F^{\alpha\beta} = \epsilon_{\mu\nu\alpha\beta}\partial^{\mu}(A^{\nu}\partial^{\alpha}A^{\beta})$. This relates bulk electromagnetism to an equivalent one at the boundary, except for gauge transformations. The electric currents associated with this term at the surface of topological insulators are quantized in half-integer values in the lowest state $n = 0$, which is anomalous since integer quantization is expected in integers, since they must be Chern numbers. However, considering the Fermi zero modes near the surface, where the Dirac equation has massless fermions and only half of the possible zero modes can be normalized, we observe that the Chern–Simons behavior and Fermi zero modes exhibit analogous behavior at the surface. Consequently, if both mechanisms contribute half of the electrons, the total current becomes an integer, as expected—i.e., spin and charge currents complement each other, as they should in the case of electrons(Anomaly Inflow). This behavior justifies the correspondence between spin-based and charge-based topological models for the topological materials in many respects, despite their very different origins. Understanding the behavior of these massless electrons is crucial because, unlike free electrons in metals, they are bound to the bulk atoms and follow their atomic mechanical oscillations. Thus, phonons directly influence these electrons, transferring thermal energy without requiring a temperature gradient, as in non-topological thermoelectrics. This connection allows us to relate the Coulomb electric potential to temperature, establishing the degree of freedom left by the Chern–Simons in its gauge transformations. This leads to a novel way of determining the Seebeck coefficient in these topological materials, where the electric field variation due to Thouless pumping is accompanied by a temperature variation, or vice versa. This effect is a key feature for understanding thermoelectricity in these materials, which would not be so high without the axionic electromagnetic behavior that has been described.

Taking into account all these conditions, it is possible to try to model how the transformation of thermal energy into electrical energy takes place near the surface of the topological insulator. We can imagine an external atomic layer on the surface and in contact with an internal one belonging to the volume, both with a slightly different periodicity and immersed in an electric field $\boldsymbol{E}$ due to the electric polarization $\boldsymbol{P}$ induced by axionic electrodynamics. We saw how a topological current arises, produced by Thouless pumping between both layers due to the atomic phase change between them, whose origin is produced by thermal oscillations within an adiabatic regime. We can observe that the Matsubara frequency of Thermofield Dynamics arises in this physical context in a natural way and helps to associate the instantons (or the self-dual or anti-self-dual solutions of the fields) with the thermal behavior that we already mentioned above. There

is strong tunneling between the bulk and the surface, i.e., topological massive electrons in trivial sectors and massless topological electrons.

This leaves us to apply the basic concepts of thermoelectricity to calculate the dimensionless figure of merit $ZT = n^2\overline{n}^3 \frac{\pi^2}{3\zeta(3)}$, which has a topological origin and is numerically very credible. This value, $ZT = 2.73$, is very close to the maximum experimental value found in Bi_2Te_3/Sb_2Te_3 superlattices, which minimize the thermal contributions of the lattice. But more importantly, it gives us an expression that depends on the first Chern numbers $\overline{n}$ and n, as quantized integer number of states. This opens the possibility of surpassing the efficiency of topological thermoelectrics if we can overcome their initial value $\overline{n} = n = 1$. A rather natural idea would be to combine different topological phases, in such a way that the winding numbers can surround the singularities more than once. In practice, we could think of a proximity effect between a topological superconductor and a topological insulator, whose currents have electronic trajectories whose winding number is two instead of one. In that case, $ZT = 10.948$, which would mean a drastic change in the technology of these materials.

This justifies the more general study of topological phases carried out in this review for topological thermoelectricity, although we finally focus on topological insulators and superconductors. We have presented a classification of the Hermitian Hamiltonians in only ten classes using the curvature, as Cartan did at the beginning of the 20th century, and we put as appendices the basic toy models for these candidate topological phases for topological thermoelectricity. The fundamental idea is to try to see the formal equivalence of the Hamiltonians of topological phases, so physically different, such as topological superconductivity and topological insulators, if formal equivalences are made between their fundamental magnitudes. A clear example could be the gap between bands and the pairing gap in superconductors. In one case, it must be annulled on the surface associated with a singular Dirac point, while in the other, superconductivity would not exist without its existence. In both Hamiltonians, these magnitudes play a fairly similar role and are key to understanding their topological behavior. Another, also very important, is to see the existence of zero states on the surface for both phases and their direct relationship with the winding number. Their location could allow their manipulation to play with the electric and thermal currents optimally. We are aware of the experimental challenges associated with implementing these fundamental theoretical concepts in real materials. Nevertheless, the theoretical framework we have discussed may inspire new approaches to overcoming such difficulties. In any case, our goal has been to explore the principal ways in which physical mechanisms intertwine with topology to better understand the complexity underlying these emerging topological materials.

Finally, we present in the appendices the fundamental models of topological materials to concisely illustrate how their global phases are established, which are fundamentally related to spin. However, it has been shown that for thermoelectricity, it is the electric charge through the Thouless pumping, rather than the spin, that plays the fundamental role. Therefore, the importance of these models for this phenomenon is somewhat restricted. Nevertheless, the topological invariants they exhibit are essential and are reflected in the figure of merit obtained. We hope that the reader of this review will gain a broad understanding of the fundamental ingredients surrounding topological materials-based thermoelectricity and that it will serve as a stimulus to explore this fascinating scientific and technical topic further.

CRediT authorship contribution statement

Daniel Baldomir: Data curation, Conceptualization, Writing – original draft, Investigation. **Daniel Failde:** Formal analysis.

Declaration of competing interest

The authors declare that they have no known competing financial interests or personal relationships that could have appeared to influence the work reported in this paper.

Acknowledgments

D.B was supported by the project PID2022-138883NB-I00 funded by the Spanish Ministry of Science, Innovation and Universities, and by the European Union project MiniStor (H2020 GA No 869821). D.F was supported by MICIN through the European Union NextGenerationEU recovery plan (PRTR-C17.I1), and by the Galician Regional Government through the "Planes Complementarios de I+D+I con las Comunidades Autónomas" in Quantum Communication.

Appendix A. Basic topological toy models for non-interacting fermions

The general Hamiltonian of materials is often written in a Fock space, rather than in a Hilbert space, to use a basis based on the atoms of the crystal lattice and their symmetries. This allows defining the tight-binding models for electron transport located in covalently bonded states of said atoms, within a Coulomb potential U and with a jump probability t. More specifically, the Hamiltonian operator is represented by

$$\hat{\mathcal{H}} = \sum_{i,j} \hat{c}_i^\dagger \mathcal{H}_{ij} \hat{c}_j, \tag{A.1}$$

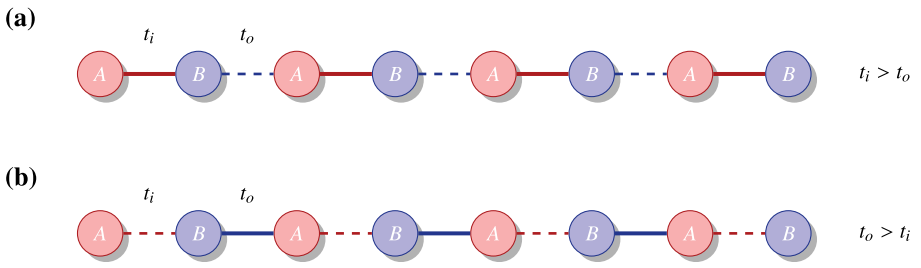

Fig. A.8. (a) Dimerized chain with intra-cell hopping $t_i > t_o$, in the topologically non-trivial phase, hosting localized edge modes. (b) Dimerized chain with inter-cell hopping $t_o > t_i$, in the topologically trivial phase, lacking edge modes.

where $\mathcal{H}_{ij} = \langle\psi|H|\psi\rangle$ is the expectation value with $|\psi\rangle = \sum_i \hat{c}_i\phi_i$, and $|\phi_i\rangle$ is an orthonormal and complete basis associated with the atomic Hamiltonian

$$H = \frac{p^2}{2m} + U(\boldsymbol{r}). \tag{A.2}$$

The $\hat{c}_i^\dagger$, $\hat{c}_i$ are the creation and annihilation operators at site i, defined to follow the Pauli exclusion principle: $\hat{c}_i^\dagger|0\rangle = |1\rangle$, $\hat{c}_i|0\rangle = 0$, $\hat{c}_i^\dagger|1\rangle = 0$, $\hat{c}_i|1\rangle = |0\rangle$, and the number operator $\hat{n}_i = \hat{c}_i^\dagger\hat{c}_i$, with $i = 0, 1$. The commutation rules of these operators are $\{\hat{c}_i, \hat{c}_j\} = \{\hat{c}_i^\dagger, \hat{c}_j^\dagger\} = 0$ and $\{\hat{c}_i, \hat{c}_j^\dagger\} = \delta_{ij}$.

Applying this to a chain of N atoms, separated by a distance a from each other, with translation symmetry and nearest-neighbor interaction, it is straightforward to find a new analytical representation in the Fock space given by

$$\hat{\mathcal{H}} = \sum_{n=1}^{N} t_n\hat{c}_n^\dagger\hat{c}_{n+1} + t_n^*\hat{c}_{n+1}^\dagger\hat{c}_n + \mu\hat{n}_i, \tag{A.3}$$

where the second term is the Hermitian conjugate (h.c.) of the first, and the third term adds the chemical potential μ times the number operator $\hat{n}_i$. Performing the Fourier transformation of the operators, $\hat{c}_n = \frac{1}{\sqrt{N}}\sum_k e^{ikx_n}\hat{c}_k$, we obtain the Bloch Hamiltonian

$$\hat{\mathcal{H}}(k) = \sum_k \left(te^{ika} + t^*e^{-ika} + \mu\right)\hat{c}_k^\dagger\hat{c}_k = \sum_k \xi(k)\hat{c}_k^\dagger\hat{c}_k, \tag{A.4}$$

which leads to the dispersion relation

$$\xi(k) = 2t\cos(ka), \tag{A.5}$$

assuming that $t = t^*$ is real. However, this system is not stable if there is one electron per ion in the chain, i.e., at half-filling. In such a case, a Peierls distortion arises, creating an energy gap for $ka = \pm\frac{\pi}{2}$ in the ground state. This changes the periodicity of the lattice by assuming that one of the atoms remains fixed, leading to dimerization.

This model was originally proposed by Su, Schrieffer, and Heeger (SSH) [306–308] to describe the electronic properties of polyacetylene (C_2H_2). The SSH model provides a minimal yet insightful illustration of a topological phase transition between two insulating phases. Mathematically, this arises from the breaking of translational symmetry due to dimerization, which introduces two distinct nearest-neighbor hopping amplitudes: t_i (intra-cell) and t_o (inter-cell) (see Fig. A.8).

Given that the Hamiltonian is Hermitian, we can rewrite it in a 2×2 simple form using the Pauli matrices:

$$\hat{\mathcal{H}}(k) = \sum_i d_i(k)\sigma^i, \tag{A.6}$$

where $d_x(k) = t_i + t_o\cos(ka)$, $d_y(k) = t_o\sin(ka)$, and $d_z(k) = 0$. Thus, there exists a mapping from the Brillouin torus to the sphere, $d(k) : T^1 \to S^2$, which may not be topologically trivial under certain conditions. Given the periodicity and translational symmetry of the chain, which allow the Fourier transformations, the tight-binding model in k-space can be written as

$$\sum_k \left((t_i + e^{ik}t_o)|k, A\rangle\langle B, k| + (t_i + e^{-ik}t_o)|k, B\rangle\langle A, k|\right) = \sum_k |k\rangle H(k)\langle k|, \tag{A.7}$$

where the basis of the Hamiltonian is $|k, A\rangle = |k\rangle \otimes |A\rangle$, $|k, B\rangle = |k\rangle \otimes |B\rangle$, and

$$H(k) = \begin{pmatrix} 0 & t_i + e^{ik}t_o \\ t_i + e^{-ik}t_o & 0 \end{pmatrix} \tag{A.8}$$

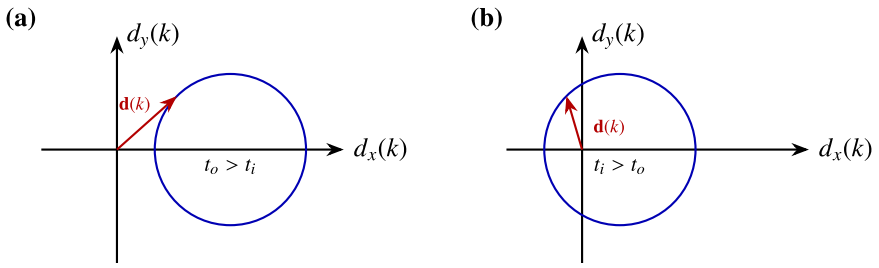

Fig. A.9. Winding number representation. (a) Trivial regime ($t_o > t_i$): the parameter trajectory does not enclose the origin. (b) Nontrivial regime ($t_i > t_o$): the parameter trajectory encloses the origin.

is the band Hamiltonian to be diagonalized. It is straightforward to calculate the eigenvalues

$$\xi_{\pm}(k) = \pm\sqrt{t_i^2 + 2t_i t_o \cos(ka) + t_o^2}, \tag{A.9}$$

and the eigenvectors, for $\theta(k) = \frac{\pi}{2}$,

$$|{\pm}u(k)\rangle = \frac{1}{\sqrt{2}}\begin{pmatrix} \pm e^{-i\phi(k)} \\ 1 \end{pmatrix}, \tag{A.10}$$

where the phase is given by

$$\phi(k) = \tan^{-1}\left(\frac{t_o \sin(ka)}{t_i + t_o \cos(ka)}\right). \tag{A.11}$$

in the Bloch sphere. It is easy to make a physical interpretation of this model by considering the different hopping terms. When the hopping terms are equal, no preferred electronic trajectory is determined, as in metals. If they are very different, insulators appear since there would be no significant hopping. However, the interesting aspect is that these two insulators are fundamentally different: one is topologically trivial, and the other is not. By calculating the winding number for these trajectories, we have

$$w = \frac{1}{2\pi i}\int_{-\pi}^{\pi} dk\, \ln(d(k)) = \frac{1}{2\pi}\left[\phi(k)\right]_{-\pi}^{\pi}, \tag{A.12}$$

which gives 1 or 0. That is, the system is non-trivial for $t_i > t_o$ and trivial for $t_o > t_i$ (Fig. A.9).

Another type of non-trivial topological model is known as Chern insulators, which involve two bands with similar Hamiltonian but different parameters

$$d(k) = (A\sin(k_x a), -A\sin(k_y a), \mathcal{M}(k)), \tag{A.13}$$

where $\mathcal{M}(k) = M + 2B(2 - \cos(k_x a) - \cos(k_y a))$, and A, B, and M are parameters that can be physically interpreted based on the chosen material. This model is often solved by expanding it around the point $k = 0$ to avoid trigonometric terms, approximating $\sin(ka) \approx ka$ and $\cos(ka) \approx 1 - (ka)^2/2$. The topology of this model is characterized by the TKNN Hall conductivity, which can be written as

$$\sigma_{xy} = \frac{e^2}{h}\frac{1}{4\pi}\iint dk_x dk_y\, \hat{d}\cdot\left(\frac{\partial\hat{d}}{\partial k_x}\times\frac{\partial\hat{d}}{\partial k_y}\right). \tag{A.14}$$

Haldane proposed a more sophisticated model using a honeycomb lattice expanded by a two-atom basis A and B

$$\hat{\mathcal{H}} = 2t_2\cos\phi\left(\sum_i \cos(kb_i)\right)\mathbb{I}_2 + \sum_j d^j\sigma_j, \tag{A.15}$$

where $\mathbb{I}_2$ is the 2×2 identity matrix, σ_j are the Pauli matrices, $d^j = (t_1\cos(ka_i), t_1\sin(ka_i), M - 2t_2\sin\phi\sum_i\sin(kb_i))$, t_1 is the nearest-neighbor hopping, t_2 is the complex second-neighbor hopping (associated with the Aharonov–Bohm effect in the case of a periodic magnetic field), ϕ is the phase accumulated by the t_2 hopping, and M is the on-site energy difference between the A and B sublattices. It is immediately clear that introducing the new hopping terms breaks time-reversal symmetry; under time reversal T, $k \to -k$, which changes the sign of terms involving $\sin(kb_i)$. The term $\sin(ka_i)$ does not affect the Hamiltonian because it is multiplied by the Dirac matrix σ_2. To preserve the C_3 symmetry of the lattice, the masses at points K and K' must have opposite signs, $M = -M'$, and the gap closes at one of these points.

For greater clarity, consider the honeycomb lattice with $a_1 = \frac{1}{2}\begin{pmatrix}\sqrt{3}\\1\end{pmatrix}$, $a_2 = \frac{1}{2}\begin{pmatrix}\sqrt{3}\\-1\end{pmatrix}$, and the Dirac points K, K' given by $\frac{2\pi}{3}(\sqrt{3}, \pm 1)$. Using the conditions $k \cdot a_1 = \frac{4\pi}{3}$, $k \cdot (a_1 - a_2) = \frac{2\pi}{3}$ for K, and $k \cdot a_1 = \frac{2\pi}{3}$, $k \cdot (a_1 - a_2) = \frac{4\pi}{3}$ for K', the gap at K closes when $M - 3\sqrt{3}|t_2| \sin\phi = 0$, and similarly at K' with quantized Hall conductivity $\sigma_{xy} = \mp\frac{e^2}{h}$.

The phase diagram in the Brillouin zone is represented by the expression

$$M = \pm 3\sqrt{3}|t_2| \sin\phi, \tag{A.16}$$

for ϕ ranging from $-\pi$ to π, after calculating the Chern number C.

The Haldane model [49] can be simplified without explicitly referring to graphene by considering a square lattice with $d_1 = \sin(k_x)$, $d_2 = \sin(k_y)$, $d_3 = 2 - M - \cos(k_x) - \cos(k_y)$, as made by Qi–Wu–Zhang [309]. The non-trivial topological phases occur for $0 < M < 2$ and $2 < M < 4$, corresponding to Chern numbers $+1$ and -1, respectively. In real space, this model in the second quantization formalism is given by

$$H = t_1 \sum_{\langle i,j\rangle} c_i^\dagger c_j + t_2 \sum_{\ll i,j \gg} e^{\pm i\phi} c_i^\dagger c_j + M \sum_i \xi_i c_i^\dagger c_i \tag{A.17}$$

where $\xi_i = +1$ for sublattice A and $\xi_i = -1$ for sublattice B. This makes it easier to compare with the following model [310].

Kane and Mele [50,311] presented for the first time a model of topological insulators that allows time-reversal symmetry and is equivalent to a duplication of the Haldane model. The Hamiltonian is

$$H = t \sum_{\langle i,j\rangle} c_i^\dagger c_j + i\lambda_{SO} \sum_{\ll i,j \gg} \nu_{ij} c_i^\dagger c_j s_z + i\lambda_R \sum_{\langle i,j\rangle} (\boldsymbol{s} \times \hat{\boldsymbol{d}}_{\boldsymbol{ij}})_z c_i^\dagger c_j + \lambda_v \sum_i \xi_i c_i^\dagger c_i \tag{A.18}$$

If we compare it with the Haldane Hamiltonian, we observe that we have introduced the spin s_i, the spin–orbit interaction λ_{SO}, the Rashba interaction λ_R, and λ_v, which represents an alternating on-site potential with opposite values in each sublattice. Additionally, $\hat{d}_{ij}$ is a unit vector connecting the nearest-neighbor edge i to edge j in the $x-y$ plane, and $\nu_{ij} = \frac{\sqrt{2}}{3}(\mathbf{d}_i \times \mathbf{d}_j)_z = \pm 1$, where $\mathbf{d}_i$ and $\mathbf{d}_j$ are two unit vectors along the bonds that the electron traverses when moving from site j to site i.

If we neglect the Rashba term and reinterpret each interaction, we find that the system consists of two copies of the Haldane model, where we choose $s_z = \pm 1$ and $\phi = \pm\frac{\pi}{2}$. The first Kane–Mele model was presented in this form as two copies of Haldane, leaving the Hamiltonian with time-reversal symmetry. Later, the Rashba term was added to take into account the interaction of the spin with the background electric field $\boldsymbol{E}$, which is also a spin–orbit that does not introduce a gap, but modifies it by making non-conservation of spin.

The Hamiltonian, in the k-space, of this 4-band model is

$$\begin{aligned} H(k) =& t\left[\left(1 + 2\cos\frac{k_x}{2}\cos\frac{\sqrt{3}k_y}{2}\right)\sigma_x \otimes s_0 - 2\cos\frac{k_x}{2}\sin\frac{\sqrt{3}k_y}{2}\sigma_y \otimes s_0\right] \\ &+ \lambda_{SO}\left(2\sin k_x - 4\sin\frac{k_x}{2}\cos\frac{\sqrt{3}k_y}{2}\right)\sigma_z \otimes s_z + \lambda_v \sigma_z \otimes s_0 \\ &+ \lambda_R\left[-\cos\frac{k_x}{2}\sin\frac{\sqrt{3}k_y}{2}\sigma_x \otimes s_x + \sqrt{3}\sin\frac{k_x}{2}\cos\frac{\sqrt{3}k_y}{2}\sigma_x \otimes s_y\right. \\ &\left.+ \left(1 - \cos\frac{k_x}{2}\cos\frac{\sqrt{3}k_y}{2}\right)\sigma_y \otimes s_x - \sqrt{3}\sin\frac{k_x}{2}\sin\frac{\sqrt{3}k_y}{2}\sigma_y \otimes s_y\right]. \end{aligned} \tag{A.19}$$

The non-topological phase can be found directly by neglecting the Rashba term $\lambda_R = 0$, which splits the Hamiltonian into two independent parts. To get the energy $\xi = 0$ in the Dirac points, we have the algebraic system of equations taking the hopping $t = 1$

$$1 + 2\cos\frac{k_x}{2}\cos\frac{\sqrt{3}k_y}{2} = 0 \tag{A.20}$$

$$\cos\frac{k_x}{2}\sin\frac{\sqrt{3}k_y}{2} = 0 \tag{A.21}$$

$$2\lambda_{SO}\left(\sin k_x - 2\sin\frac{k_x}{2}\cos\frac{\sqrt{3}k_y}{2}\right) + \lambda_v = 0 \tag{A.22}$$

give us the condition $\lambda_v/\lambda_{SO} = \pm 3\sqrt{3}$, taking into account the second equation, which gives $k_y = 0$ and $k_y = \frac{2\pi}{\sqrt{3}}$. This leads to

$$-3\sqrt{3} \le \frac{\lambda_v}{\lambda_{SO}} \le 3\sqrt{3}, \tag{A.23}$$

as the interval where the Chern number is nonzero. Expanding the Hamiltonian to first order near the Dirac points and choosing $s_z = +1$, we obtain

$$H(k) \simeq \frac{\sqrt{3}}{2}(\sigma_x k_x + \sigma_y k_y) + \sigma_z(\lambda_v - 3\sqrt{3}\lambda_{SO}). \tag{A.24}$$

For $k_y \simeq 0$, we can derive the zero mode

$$\phi\left(\frac{k_x}{2}\right) = \phi(0)\exp\left[-\frac{1}{2}\int_0^{\frac{k_x}{2}} dk_x' M\left(\frac{k_x'}{2}\right)\right], \tag{A.25}$$

where the mass term is defined as

$$M\left(\frac{k_x}{2}\right) = \frac{2}{\sqrt{3}}\left(\lambda_v - 3\sqrt{3}\lambda_{SO}\right). \tag{A.26}$$

The solution with $s_z = -1$ corresponds to the Hamiltonian

$$H(-k) \simeq \frac{\sqrt{3}}{3}(\sigma_x k_x + \sigma_y k_y) - \sigma_z(\lambda_v - 3\sqrt{3}\lambda_{SO}), \tag{A.27}$$

which represents the time-reversal counterpart of the solution calculated for $s_z = +1$. Note that we could also find zero modes for $k_y \simeq 0$, leading to additional states that may couple with those of the topological superconductor mentioned in the previous section [28,80,312].

In this model, where spin–orbit plays a key role, we need a new topological index to distinguish its two phases. Due to Kramers' theorem, all bands must cross at the center of the Brillouin zone (BZ), and it is possible to define time-reversal invariant momenta (TRIM). For the Bloch Hamiltonian, $H(-k) = \hat{\mathcal{T}}H(k)\hat{\mathcal{T}}^{-1}$, the bands in the BZ appear as Kramers pairs. We can define the matrix element between states α and β at time-conjugate momenta as

$$B_{\alpha\beta} = \langle -k, \alpha|\hat{\mathcal{T}}|k, \beta\rangle. \tag{A.28}$$

At the TRIM $k = \Gamma_i$, $B_{\alpha\beta}(\Gamma_i)$ is antisymmetric, allowing us to define

$$\delta_i = \frac{\sqrt{\det[B(\Gamma_i)]}}{\mathrm{Pf}[B(\Gamma_i)]}, \tag{A.29}$$

as an invariant quantity associated with the TRIM points Γ_i. In fact, in 1-D, this corresponds to the product of these δ values, which extends to four in 2-D and eight in 3-D. This ultimately allows us to define a $\mathcal{Z}_2$ Pfaffian index that accounts for the band topological structure of the BZ when Kramers degeneracy exists due to time-reversal symmetry.

It is immediately apparent that we can leave the λ_v to consider the Rashba parameter λ_R. This calculation would lead us to the non-trivial topological interval

$$-2\sqrt{3} \leq \frac{\lambda_R}{\lambda_{SO}} \leq 2\sqrt{3} \tag{A.30}$$

which would allow us to represent a phase diagram for the parameters of the Kane–Mele model as a function of these three parameters.

Finally, in the seminal paper [313] presented by Bernevig, Hughes, and Zhang (BHZ), they propose a model describing the vicinity of a gap closing at $\Gamma = (0, 0)$ for a *HgTe/CdTe* quantum well as a topological insulator in $2 - D$. Assuming a square unit cell with coordinates x, y, the on-site Coulomb energy U, hopping coefficients t_x, t_y, and translational symmetry, it is possible to write a tight-binding Hamiltonian

$$H(x, y) = \sum_{x,y} \frac{U}{2} c^\dagger_{x,y} c_{x,y} + t_x c^\dagger_{x+1,y} c_{x,y} + t_y c^\dagger_{x,y+1} c_{x,y} + h.c. \tag{A.31}$$

After performing a Fourier transformation for the creation and annihilation operators, we obtain

$$H(x, y) = \sum_{k_x,k_y} c^\dagger_{k_x,k_y} H(k) c_{k_x,k_y}, \tag{A.32}$$

where $h(k) = \frac{U}{2} + t_x e^{ik_x} + t_y e^{ik_y} + h.c.$, and $U = \triangle\sigma_z$, $t_x = \frac{1}{2}\sigma_z + \frac{i}{2}\sigma_x$, $t_y = \frac{1}{2}\sigma_z + \frac{i}{2}\sigma_y$. This leads us to the simple Hamiltonian

$$h(k) = \sigma_1 k_x + \sigma_2 k_y + (\triangle + \cos k_x + \cos k_y)\sigma_3 = \sum_i d^i \sigma_i. \tag{A.33}$$

The bands will cross at $d = 0$, with solutions $k(\pi, \pi), \triangle = -2$; $k(0, \pi), \triangle = 0$; $k(\pi, 0), \triangle = 0$; $k(0, 0), \triangle = 2$. These provide non-trivial topological regions that can be calculated straightforwardly. The energy is given by

$$\xi(k) = \pm|d(k)| = \pm\sqrt{\sin^2 k_x + \sin^2 k_y + (\triangle + \cos k_x + \cos k_y)^2}. \tag{A.34}$$

When $\triangle \ll -2$, we have $h \simeq -\triangle\sigma_z$, meaning this region corresponds to a trivial mapping of the BZ onto d_z, which cannot surround the Dirac point. Thus, this region must have a Chern number equal to zero, $C = 0$, and similarly for $\triangle \gg 2$. These regions are therefore topologically trivial. Close to the point $\Gamma = (0, 0)$, for the parameter $\triangle = -2$, the Hamiltonian becomes

$$H_\Gamma \simeq k_x\sigma_x + k_y\sigma_y + (\triangle + 2). \tag{A.35}$$

We can calculate the Berry curvature for these parameters

$$\Omega_{ij} = \frac{m}{2(k_x^2 + k_y^2 + m^2)^{\frac{3}{2}}}, \tag{A.36}$$

where $m = \triangle + 2$, and we have used the definition $\Omega_{ij} = \frac{1}{2}\hat{d} \cdot (\partial_i\hat{d} \times \partial_j\hat{d})$, which gives the Chern number

$$C = \int \Omega_{ij} dk_x dk_y = \frac{\text{sign}(m)}{2}. \tag{A.37}$$

This result is incorrect because the Chern number must be an integer, but this arises because the integration is performed over a non-compact manifold. To address this issue, we consider two regions bounded in k-space

$$C = \frac{\text{sign}(m > 0)}{2} - \frac{\text{sign}(m < 0)}{2} = +1, \tag{A.38}$$

for $2 > \triangle > 0$. Similarly, for $0 > \triangle > -2$, $C = -1$, and $C = 0$ for $|\triangle| > 2$.

Following the Kane–Mele model, we extend this Hamiltonian to account for time-reversal symmetry:

$$\mathcal{H} = \begin{pmatrix} h(k) & 0 \\ 0 & h^*(-k) \end{pmatrix}, \tag{A.39}$$

where

$$h^*(-k) = -\sigma_x k_x + \sigma_y k_y + (\triangle + \cos k_x + \cos k_y)\sigma_z. \tag{A.40}$$

Thus, the full Hamiltonian of the BHZ model can be written as

$$\mathcal{H} = \sin k_y\sigma_y + (\triangle + \cos k_x + \cos k_y)\sigma_z \otimes \mathbb{I}_2 + \sin k_x\sigma_x \otimes \tau_z, \tag{A.41}$$

where the τ matrices are defined as

$$\tau_y = \begin{pmatrix} 0 & -i\mathbb{I}_2 \\ i\mathbb{I}_2 & 0 \end{pmatrix}, \qquad \tau_z = \begin{pmatrix} \mathbb{I}_2 & 0 \\ 0 & -\mathbb{I}_2 \end{pmatrix}. \tag{A.42}$$

Now the Hamiltonian is time-reversal symmetric:

$$\hat{T}\mathcal{H}(k)\hat{T}^{-1} = \mathcal{H}(-k), \tag{A.43}$$

with $\hat{T} = i\tau_y K$ being the time-reversal operator.

Let us examine the simplest propagation states on the surface. Taking $x = 0$, where there is a change from trivial topology ($C = 0$) to a non-trivial one ($C = -1$), with parameters transitioning from $|\triangle| > 2, m(x) > 0$ to $-2 < \triangle < 0, m(x) < 0$. In this case, we have a simple Dirac equation:

$$(i\sigma_x\partial_x + i\sigma_y\partial_y + m(x)\sigma_z)\psi(x, y) = \xi\,\psi(x, y). \tag{A.44}$$

Using translation symmetry and spatial periodicity, we set $\psi(x, y) = e^{ik_y}\phi(x)$ and consider zero energy $\xi = 0$, $k_y = 0$, leading to:

$$\frac{d}{dx}\phi(x) = -im(x')dx'. \tag{A.45}$$

The solution is given by

$$|\phi_k(x)\rangle = \exp\left[\int_\infty^x m(x')dx'\right]\begin{pmatrix} 1 \\ i \end{pmatrix}, \tag{A.46}$$

which represents a zero mode. We can extend this solution to the y-axis, where propagation occurs at the Fermi velocity $v_F = 1$ ($\hbar = 1$):

$$|\phi(k_y)\rangle = e^{ik_y y}\exp\left[-\int_\infty^x m(x')dx'\right]\begin{pmatrix} 1 \\ i \end{pmatrix}. \tag{A.47}$$

Introducing constants, we obtain:

$$h(|\psi(k_y)\rangle) = \hbar k_y v_F|\psi(k_y)\rangle. \tag{A.48}$$

The existence of these chiral states on the surface demonstrates that electronic transport behaves very differently from conventional systems, as it is immune to crystalline defects and does not localize. This phenomenon can be generalized: the contact of two materials characterized by different topological Chern invariants, C_1 and C_2, implies the emergence of $|C_1 - C_2|$ gapless edge modes. This feature must be considered in phenomena such as thermoelectricity due to its subtle relationship with these currents.

Appendix B. 2-D topological superconductivity

In a $2-D$ lattice, the Hamiltonian of a p-wave superconductor can be written as

$$\mathcal{H} = \sum_{i,j} -t\left(c^{\dagger}_{i+1,j}c_{i,j} + c^{\dagger}_{i,j+1}c_{i,j}\right) + \triangle\left(c^{\dagger}_{i+1,j}c^{\dagger}_{i,j} + ic^{\dagger}_{i,j+1}c^{\dagger}_{i,j} + h.c.\right) - (\mu - 4t)c^{\dagger}_{i,j}c_{i,j}, \tag{B.1}$$

where the operators act at the site (i, j) of the lattice. This leads to the Bloch Hamiltonian

$$\mathcal{H}(k) = \begin{pmatrix} \epsilon(k) & 2i(\sin k_x + \sin k_y) \\ -2i(\sin k_x + \sin k_y) & -\epsilon(k) \end{pmatrix} = \sum_i d^i\sigma_i, \tag{B.2}$$

with $\epsilon(k) = -2t(\cos k_x + \cos k_y) + (4t - \mu)$.

To avoid the complex parameter $\triangle = |\triangle|e^{i\Lambda}$, we perform a gauge transformation of the operators $c_k \rightarrow e^{-i\Lambda}c_k$, $c^{\dagger}_k \rightarrow e^{-i\Lambda}c^{\dagger}_k$, obtaining:

$$\mathcal{H}(k) = -2\triangle(\sin k_y\tau_x + \sin k_x\tau_y) + \epsilon(k)\tau_z = \overrightarrow{d}\cdot\overrightarrow{\tau}, \tag{B.3}$$

where the matrices τ are associated with particle–hole elements. The eigenvalues are then given by:

$$\xi_{\pm} = \pm|\overrightarrow{d}| = \pm\sqrt{\epsilon(k)^2 + 4|\triangle|^2(\sin^2 k_x + \sin^2 k_y)}. \tag{B.4}$$

This energy spectrum is gapped if we choose $t = \triangle = \frac{1}{2}$, except for the critical values $(k_x, k_y, \mu) = (0, 0, 0)$, $(\pi, 0, 2)$, $(0, \pi, 2)$, and $(\pi, \pi, 4)$. Thus, there are four phases to distinguish their topology, and we must calculate the Chern number

$$C = \frac{1}{8\pi}\int_{-\pi}^{\pi} dk_x \int_{-\pi}^{\pi} dk_y\, \hat{d}\cdot\left(\frac{\partial\hat{d}}{\partial k_x}\times\frac{\partial\hat{d}}{\partial k_y}\right). \tag{B.5}$$

In the limit $k \rightarrow 0$, we find $C = 1$ for $0 < \mu < 2$ and $C = -1$ for $2 < \mu < 4$, corresponding to non-trivial phases. For $\mu < 0$ and $\mu > 4$, the Chern number $C = 0$, indicating trivial topology [80,314,315].

From a more physical perspective, we can consider the gap parameter $\triangle_{ab}(k) = \triangle_0\langle c_a(k)c_b(-k)\rangle$ as an electron correlation, where a and b are spin indices. It arises due to instabilities on the Fermi surface, creating an effective energy gap for superconducting carriers. Furthermore, it must obey the Pauli exclusion principle by acting on fermions, implying $\triangle_{ab}(k) + \triangle_{ba}(-k) = 0$. If there is no spin–orbit coupling, we can treat spin and momentum as good quantum numbers and write $\triangle_{ab}(k) = \chi_{ab}\triangle(k)$, where $\chi_{ab} = \pm\chi_{ba}$ and $\triangle(k) = \pm\triangle(-k)$. This leads to singlet or triplet pairings: singlets when $\chi_{ab} = -\chi_{ba}$ and $\triangle(k) = \triangle(-k)$, and triplets when $\chi_{ab} = \chi_{ba}$ and $\triangle(k) = -\triangle(-k)$.

Thus, s- and d-wave superconductors correspond to singlets, while p- and f-wave ones correspond to triplets. Note that if we have a singlet, time-reversal symmetry is preserved, and by Kramers' theorem, states are degenerate. Consequently, Majorana modes cannot be separated. This classification is an oversimplification, as other factors, such as lattice symmetries or the relative orientation of states, also influence these conditions [316–318].

Appendix C. SSH and Kitaev Peierls formal similarities

A paradigmatic example of this point of view is given by the Kitaev chain

$$\mathcal{H}_K = \sum_n (tc^{\dagger}_n c_{n+1} - i\Delta c_n c_{n+1} + h.c) + \mu c^{\dagger}_n c_n \tag{C.1}$$

where t is the hopping energy, Δ the p-wave pairing amplitude and μ the chemical potential. On the other hand, the *SSH* Hamiltonian can be written as

$$\mathcal{H}_S = \sum_n (t_i c^{\dagger}_{2n-1}c_{2n} + t_o c^{\dagger}_{2n}c_{2n+1} + h.c) \tag{C.2}$$

where the hopping are related by the expression $t_i = t(1 - \delta cos\alpha)$ and $t_o = t(1 + \delta cos\alpha)$. In such a form that the hopping changes from $-t\delta$ to $+t\delta$, being t the hopping between nearest neighbors, n the lattice side, and δ the Peierls dimerization strength. If we choose the chemical potential to be zero, $\mu = 0$, the analogy of both Hamiltonians is very clear and justifies the parallel topological study for both models.

References

[1] H.J. Goldsmid, R.W. Douglas, The use of semiconductors in thermoelectric refrigeration, Br. J. Appl. Phys. 5 (12) (1954) 458, http://dx.doi.org/10.1088/0508-3443/5/12/513.

[2] J.R. Sootsman, D.Y. Chung, M.G. Kanatzidis, New and old concepts in thermoelectric materials, Angew. Chem. Int. Ed. 48 (46) (2009) 8616–8639, http://dx.doi.org/10.1002/anie.200900598.

[3] T.M. Tritt, M.A. Subramanian, Thermoelectric materials, phenomena, and applications: A bird's eye view, MRS Bull. 31 (3) (2006) 188–198, http://dx.doi.org/10.1557/mrs2006.44.

[4] G. Mahan, B. Sales, J. Sharp, Thermoelectric Materials: New Approaches to an Old Problem, Phys. Today 50 (3) (1997) 42–47, http://dx.doi.org/10.1063/1.881752.

[5] G. Nolas, J. Sharp, J. Goldsmid, Thermoelectrics: Basic Principles and New Materials Developments, in: Springer Series in Materials Science, Springer Berlin Heidelberg, 2001, URL https://books.google.es/books?id=0q5mi2XKbFAC.

[6] I.T. Witting, F. Ricci, T.C. Chasapis, G. Hautier, G.J. Snyder, The Thermoelectric Properties of n-Type Bismuth Telluride–Bismuth Selenide Alloys $Bi_2Te_{3-x}Se_x$, Research 2020 (2020) http://dx.doi.org/10.34133/2020/4361703.

[7] L.V. Prokofieva, D.A. Pshenay-Severin, P. Konstantinov, A.A. Shabaldin, Optimum composition of a $Bi_2Te_{3-x}Se_x$ alloy for the n-type leg of a thermoelectric generator, Semiconductors 43 (2009) 973–976.

[8] H. Goldsmid, Introduction to thermoelectricity, in: Springer Series in Materials Science, Springer Berlin Heidelberg, 2009, URL https://books.google.es/books?id=LYN3nDy0FccC.

[9] H. Goldsmid, Thermoelectric refrigeration, in: The International Cryogenics Monograph Series, Springer US, 2013, URL https://books.google.es/books?id=YP8ICAAAQBAJ.

[10] W. Liu, Q. Jie, H.S. Kim, Z. Ren, Current progress and future challenges in thermoelectric power generation: From materials to devices, Acta Mater. 87 (2015) 357–376, http://dx.doi.org/10.1016/j.actamat.2014.12.042, URL https://www.sciencedirect.com/science/article/pii/S1359645414009689.

[11] M. Castañeda, E.I. Gutiérrez-Velásquez, C.E. Aguilar, S. Neves Monteiro, A.A. Amell, H.A. Colorado, Sustainability and circular economy perspectives of materials for thermoelectric modules, Sustainability 14 (2022) 5987, http://dx.doi.org/10.3390/su14105987.

[12] G.J. Snyder, E.S. Toberer, Complex thermoelectric materials, Nat. Mater. 7 (2) (2008) 105–114, http://dx.doi.org/10.1038/nmat2090.

[13] L.E. Bell, Cooling, heating, generating power, and recovering waste heat with thermoelectric systems, Science 321 (5885) (2008) 1457–1461, http://dx.doi.org/10.1126/science.1158899.

[14] C. Fu, Y. Sun, C. Felser, Topological thermoelectrics, APL Mater. 8 (4) (2020) 040913, http://dx.doi.org/10.1063/5.0005481.

[15] Y. Dubi, M. Di Ventra, Colloquium: Heat flow and thermoelectricity in atomic and molecular junctions, Rev. Modern Phys. 83 (1) (2011) 131–155, http://dx.doi.org/10.1103/RevModPhys.83.131, URL https://link.aps.org/doi/10.1103/RevModPhys.83.131.

[16] T. Takabatake, K. Suekuni, T. Nakayama, E. Kaneshita, Phonon-glass electron-crystal thermoelectric clathrates: Experiments and theory, Rev. Modern Phys. 86 (2) (2014) 669–716, http://dx.doi.org/10.1103/RevModPhys.86.669, URL https://link.aps.org/doi/10.1103/RevModPhys.86.669.

[17] J. He, T.M. Tritt, Advances in thermoelectric materials research: Looking back and moving forward, Science 357 (6358) (2017) eaak9997, http://dx.doi.org/10.1126/science.aak9997, URL https://www.science.org/doi/10.1126/science.aak9997.

[18] P. Gorai, V. Stevanović, E.S. Toberer, Computationally guided discovery of thermoelectric materials, Nat. Rev. Mater. 2 (2017) 17053, http://dx.doi.org/10.1038/natrevmats.2017.53, URL https://www.nature.com/articles/natrevmats.2017.53.

[19] B. Kozinsky, Thermoelectrics by computational design: progress and opportunities, Annu. Rev. Mater. Res. 51 (2021) 565–590, http://dx.doi.org/10.1146/annurev-matsci-100520-015716, URL https://www.annualreviews.org/doi/10.1146/annurev-matsci-100520-015716.

[20] M. Jonson, G.D. Mahan, Mott's formula for the thermopower and the Wiedemann-Franz law, Phys. Rev. B 21 (1980) 4223–4229, http://dx.doi.org/10.1103/PhysRevB.21.4223, URL https://link.aps.org/doi/10.1103/PhysRevB.21.4223.

[21] G. Wang, T. Cagin, Electronic structure of the thermoelectric materials Bi_2Te_3 and Sb_2Te_3 from first-principles calculations, Phys. Rev. B 76 (2007) 075201, http://dx.doi.org/10.1103/PhysRevB.76.075201, URL https://link.aps.org/doi/10.1103/PhysRevB.76.075201.

[22] R.J. Cava, H. Ji, M.K. Fuccillo, Q.D. Gibson, Y.S. Hor, Crystal structure and chemistry of topological insulators, J. Mater. Chem. C 1 (19) (2013) 3176–3189, http://dx.doi.org/10.1039/C3TC30186A.

[23] G. Slack, Design concepts for improved thermoelectric materials, MRS Online Proc. Libr. 478 (1997) 47–54, http://dx.doi.org/10.1557/PROC-478-47.

[24] G.A. Slack, New Materials and Performance Limits for Thermoelectric Cooling, CRC Press, 1995.

[25] G.A. Slack, The thermal conductivity of nonmetallic crystals, J. Phys. C: Solid State Phys. 34 (1979) 1–71, URL https://api.semanticscholar.org/CorpusID:117771715.

[26] F. Seitz, D. Turnbull, H. Ehrenreich, Solid state physics, in: ISSN, Elsevier Science, 1968, URL https://books.google.es/books?id=09BryaGQtYsC.

[27] T. Tritt, Thermal conductivity: Theory, properties, and applications, in: Physics of Solids and Liquids, Springer US, 2005, URL https://books.google.es/books?id=whJNfKmziIC.

[28] S.-Q. Shen, Topological Insulators, vol. 174, Springer, 2012.

[29] L.I. Magarill, M.V. Entin, Backscattering in a 2D topological insulator and the conductivity of a 2D strip, JETP Lett. 100 (9) (2015) 561–565, http://dx.doi.org/10.1134/S0021364014210097.

[30] P. Roushan, J. Seo, C.V. Parker, Y.S. Hor, D. Hsieh, D. Qian, A. Richardella, M.Z. Hasan, R.J. Cava, A. Yazdani, Topological surface states protected from backscattering by chiral spin texture, Nature 460 (7259) (2009) 1106–1109, http://dx.doi.org/10.1038/nature08308.

[31] D. Baldomir, D. Faílde, On behind the physics of the thermoelectricity of topological insulators, Sci. Rep. 9 (2019) 6324, http://dx.doi.org/10.1038/s41598-019-42744-3.

[32] M. Stone, Gravitational anomalies and thermal Hall effect in topological insulators, Phys. Rev. B 85 (2012) 184503, http://dx.doi.org/10.1103/PhysRevB.85.184503, URL https://link.aps.org/doi/10.1103/PhysRevB.85.184503.

[33] N. Xu, Y. Xu, J. Zhu, Topological insulators for thermoelectrics, Npj Quantum Mater. 2 (1) (2017) 51, http://dx.doi.org/10.1038/s41535-017-0054-3.

[34] J. Zhang, X. Feng, Y. Xu, M. Guo, Z. Zhang, Y. Ou, Y. Feng, K. Li, H. Zhang, L. Wang, X. Chen, Z. Gan, S.-C. Zhang, K. He, X. Ma, Q.-K. Xue, Y. Wang, Disentangling the magnetoelectric and thermoelectric transport in topological insulator thin films, Phys. Rev. B 91 (2015) 075431, http://dx.doi.org/10.1103/PhysRevB.91.075431.

[35] M. Guo, Z. Wang, Y. Xu, H. Huang, Y. Zang, C. Liu, W. Duan, Z. Gan, S.-C. Zhang, K. He, X. Ma, Q. Xue, Y. Wang, Tuning thermoelectricity in a Bi_2Se_3 topological insulator via varied film thickness, New J. Phys. 18 (1) (2016) 015008, http://dx.doi.org/10.1088/1367-2630/18/1/015008.

[36] Y.-Y. Li, G. Wang, X.-G. Zhu, M.-H. Liu, C. Ye, X. Chen, Y.-Y. Wang, K. He, L.-L. Wang, X.-C. Ma, H.-J. Zhang, X. Dai, Z. Fang, X.-C. Xie, Y. Liu, X.-L. Qi, J.-F. Jia, S.-C. Zhang, Q.-K. Xue, Intrinsic topological insulator Bi_2Te_3 thin films on Si and their thickness limit, Adv. Mater. 22 (36) (2010) 4002–4007, http://dx.doi.org/10.1002/adma.201000368.

[37] B. Poudel, Q. Hao, Y. Ma, Y. Lan, A. Minnich, B. Yu, X. Yan, D. Wang, A. Muto, D. Vashaee, X. Chen, J. Liu, M.S. Dresselhaus, G. Chen, Z. Ren, High-thermoelectric performance of nanostructured bismuth antimony telluride bulk alloys, Science 320 (5876) (2008) 634–638, http://dx.doi.org/10.1126/science.1156446, URL https://www.science.org/doi/abs/10.1126/science.1156446.

[38] K. Biswas, J. He, I.D. Blum, C.-I. Wu, T.P. Hogan, D.N. Seidman, V.P. Dravid, M.G. Kanatzidis, High-performance bulk thermoelectrics with all-scale hierarchical architectures, Nature 489 (7416) (2012) 414–418, http://dx.doi.org/10.1038/nature11439.

[39] R. Takahashi, S. Murakami, Thermoelectric transport in topological insulators, Semicond. Sci. Technol. (2012) http://dx.doi.org/10.1088/0268-1242/27/12/124005.

[40] P. Ghaemi, R.S.K. Mong, J.E. Moore, In-plane transport and enhanced thermoelectric performance in thin films of the topological insulators Bi_2Te_3 and Bi_2Se_3, Phys. Rev. Lett. 105 (2010) 166603, http://dx.doi.org/10.1103/PhysRevLett.105.166603, URL https://link.aps.org/doi/10.1103/PhysRevLett.105.166603.

[41] O.V. Yazyev, J.E. Moore, S.G. Louie, Spin polarization and transport of surface states in the topological insulators Bi_2Se_3 and Bi_2Te_3 from first principles, Phys. Rev. Lett. 105 (2010) 266806, http://dx.doi.org/10.1103/PhysRevLett.105.266806, URL https://link.aps.org/doi/10.1103/PhysRevLett.105.266806.

[42] Y. Min, J.W. Roh, H. Yang, M. Park, S.I. Kim, S. Hwang, S.M. Lee, K.H. Lee, U. Jeong, Surfactant-free scalable synthesis of Bi_2Te_3 and Bi_2Se_3 nanoflakes and enhanced thermoelectric properties of their nanocomposites, Adv. Mater. 25 (10) (2013) 1425–1429, http://dx.doi.org/10.1002/adma.201203764.

[43] G.L. Sun, L.L. Li, X.Y. Qin, D. Li, T.H. Zou, H.X. Xin, B.J. Ren, J. Zhang, Y.Y. Li, X.J. Li, Enhanced thermoelectric performance of nanostructured topological insulator Bi_2Se_3, Appl. Phys. Lett. 106 (5) (2015) 053102, http://dx.doi.org/10.1063/1.4907252.

[44] Y. Xia, D. Qian, D. Hsieh, L. Wray, A. Pal, H. Lin, A. Bansil, D. Grauer, Y.S. Hor, R.J. Cava, M.Z. Hasan, Observation of a large-gap topological-insulator class with a single Dirac cone on the surface, Nat. Phys. 5 (6) (2009) 398–402, http://dx.doi.org/10.1038/nphys1274.

[45] Y. Xu, Z. Gan, S.-C. Zhang, Enhanced thermoelectric performance and anomalous seebeck effects in topological insulators, Phys. Rev. Lett. 112 (2014) 226801, http://dx.doi.org/10.1103/PhysRevLett.112.226801, URL https://link.aps.org/doi/10.1103/PhysRevLett.112.226801.

[46] L. Müchler, F. Casper, B. Yan, S. Chadov, C. Felser, Topological insulators and thermoelectric materials, Phys. Status Solidi (RRL) – Rapid Res. Lett. 7 (1–2) (2013) 91–100, http://dx.doi.org/10.1002/pssr.201206411.

[47] K.v. Klitzing, G. Dorda, M. Pepper, New method for high-accuracy determination of the fine-structure constant based on quantized Hall resistance, Phys. Rev. Lett. 45 (1980) 494–497, http://dx.doi.org/10.1103/PhysRevLett.45.494, URL https://link.aps.org/doi/10.1103/PhysRevLett.45.494.

[48] D.J. Thouless, M. Kohmoto, M.P. Nightingale, M. den Nijs, Quantized Hall conductance in a two-dimensional periodic potential, Phys. Rev. Lett. 49 (1982) 405–408, http://dx.doi.org/10.1103/PhysRevLett.49.405, URL https://link.aps.org/doi/10.1103/PhysRevLett.49.405.

[49] F.D.M. Haldane, Model for a quantum Hall effect without Landau levels: Condensed-matter realization of the "parity anomaly", Phys. Rev. Lett. 61 (1988) 2015–2018, http://dx.doi.org/10.1103/PhysRevLett.61.2015, URL https://link.aps.org/doi/10.1103/PhysRevLett.61.2015.

[50] C.L. Kane, E.J. Mele, Quantum spin Hall effect in graphene, Phys. Rev. Lett. 95 (2005) 226801, http://dx.doi.org/10.1103/PhysRevLett.95.226801, URL https://link.aps.org/doi/10.1103/PhysRevLett.95.226801.

[51] B.A. Bernevig, S.-C. Zhang, Quantum spin Hall effect, Phys. Rev. Lett. 96 (2006) 106802, http://dx.doi.org/10.1103/PhysRevLett.96.106802, URL https://link.aps.org/doi/10.1103/PhysRevLett.96.106802.

[52] M. König, S. Wiedmann, C. Brüne, A. Roth, H. Buhmann, L.W. Molenkamp, X.-L. Qi, S.-C. Zhang, Quantum Spin Hall Insulator State in HgTe Quantum Wells, Science 318 (5851) (2007) 766–770, http://dx.doi.org/10.1126/science.1148047.

[53] X.-L. Qi, T.L. Hughes, S.-C. Zhang, Topological field theory of time-reversal invariant insulators, Phys. Rev. B 78 (2008) 195424, http://dx.doi.org/10.1103/PhysRevB.78.195424, URL https://link.aps.org/doi/10.1103/PhysRevB.78.195424.

[54] M.F. Atiyah, I.M. Singer, The index of elliptic operators: I, Ann. Math. 87 (3) (1968) 484–530, URL http://www.jstor.org/stable/1970715.

[55] N. Berline, E. Getzler, M. Vergne, Heat kernels and Dirac operators, in: Grundlehren der mathematischen Wissenschaften, vol. 298, Springer, 1992, http://dx.doi.org/10.1007/978-3-662-21739-9.

[56] Y. Nambu, G. Jona-Lasinio, Dynamical model of elementary particles based on an analogy with superconductivity. I, Phys. Rev. 122 (1) (1961) 345–358, http://dx.doi.org/10.1103/PhysRev.122.345.

[57] M. Gell-Mann, M. Levy, Axial vector current conservation in weak interactions, Il Nuovo Cimento 16 (4) (1960) 705–726, http://dx.doi.org/10.1007/BF02859738.

[58] T. Hatsuda, T. Kunihiro, QCD phenomenology based on a chiral effective Lagrangian, Phys. Rep. 247 (5–6) (1994) 221–367, http://dx.doi.org/10.1016/0370-1573(94)90022-1.

[59] R. Citro, M. Aidelsburger, Thouless pumping and topology, Nat. Rev. Phys. 5 (2) (2023) 87–101, http://dx.doi.org/10.1038/s42254-022-00545-0.

[60] F. Zhou, B. Spivak, B. Altshuler, Mesoscopic mechanism of adiabatic charge transport, Phys. Rev. Lett. 82 (1999) 608–611, http://dx.doi.org/10.1103/PhysRevLett.82.608, URL https://link.aps.org/doi/10.1103/PhysRevLett.82.608.

[61] C.W. Wächtler, J. Cerrillo, Electron shuttle as an autonomous single-electron source, Phys. Rev. Appl. 18 (2022) 014011, http://dx.doi.org/10.1103/PhysRevApplied.18.014011, URL https://link.aps.org/doi/10.1103/PhysRevApplied.18.014011.

[62] Q. Niu, Towards a quantum pump of electric charges, Phys. Rev. Lett. 64 (1990) 1812–1815, http://dx.doi.org/10.1103/PhysRevLett.64.1812, URL https://link.aps.org/doi/10.1103/PhysRevLett.64.1812.

[63] Y. Xia, E. Riva, M.I.N. Rosa, G. Cazzulani, A. Erturk, F. Braghin, M. Ruzzene, Experimental observation of temporal pumping in electromechanical waveguides, Phys. Rev. Lett. 126 (2021) 095501, http://dx.doi.org/10.1103/PhysRevLett.126.095501, URL https://link.aps.org/doi/10.1103/PhysRevLett.126.095501.

[64] D. Failde, D. Baldomir, Emergent topological fields and relativistic phonons within the thermoelectricity in topological insulators, Sci. Rep. 11 (2021) http://dx.doi.org/10.1038/s41598-021-93667-x.

[65] S. Ryu, A.P. Schnyder, A. Furusaki, A.W.W. Ludwig, Topological insulators and superconductors: tenfold way and dimensional hierarchy, New J. Phys. 12 (2010) 0655010, http://dx.doi.org/10.1088/1367-2630/12/6/065010.

[66] C.-K. Chiu, J.C.Y. Teo, A.P. Schnyder, S. Ryu, Classification of topological quantum matter with symmetries, Rev. Modern Phys. 88 (2016) 035005, http://dx.doi.org/10.1103/RevModPhys.88.035005, URL https://link.aps.org/doi/10.1103/RevModPhys.88.035005.

[67] A. Altland, M.R. Zirnbauer, Nonstandard symmetry classes in mesoscopic normal-superconducting hybrid structures, Phys. Rev. B 55 (1997) 1142–1161, http://dx.doi.org/10.1103/PhysRevB.55.1142, URL https://link.aps.org/doi/10.1103/PhysRevB.55.1142.

[68] M.Z. Hasan, C.L. Kane, Colloquium: Topological insulators, Rev. Modern Phys. 82 (2010) 3045–3067, http://dx.doi.org/10.1103/RevModPhys.82.3045, URL https://link.aps.org/doi/10.1103/RevModPhys.82.3045.

[69] X.-L. Qi, S.-C. Zhang, Topological insulators and superconductors, Rev. Modern Phys. 83 (2011) 1057–1110, http://dx.doi.org/10.1103/RevModPhys.83.1057, URL https://link.aps.org/doi/10.1103/RevModPhys.83.1057.

[70] M. Sato, Y. Ando, Topological superconductors: a review, Rep. Progr. Phys. 80 (2017) 076501, http://dx.doi.org/10.1088/1361-6633/aa6ac7.

[71] A. Kumar, et al., Topological quantum materials from the viewpoint of chemistry, Chem. Rev. 120 (22) (2020) 12570–12675, http://dx.doi.org/10.1021/acs.chemrev.0c00732.

[72] K. Manna, Y. Sun, L. Muechler, J. Kübler, C. Felser, Heusler, Weyl and Berry, Nature Rev. Mater. 3 (8) (2018) 244–256, http://dx.doi.org/10.1038/s41578-018-0036-5.

[73] M. Mandal, N.C. Drucker, P. Siriviboon, T. Nguyen, A. Boonkird, T.N. Lamichhane, R. Okabe, A. Chotrattanapituk, M. Li, Topological superconductors from a materials perspective, Chem. Mater. 35 (16) (2023) 6184–6200, http://dx.doi.org/10.1021/acs.chemmater.3c00713.

[74] R. Lo Conte, J. Wiebe, S. Rachel, D.K. Morr, R. Wiesendanger, Magnet–superconductor hybrid quantum systems: a materials platform for topological superconductivity, La Riv. Del Nuovo Cimento 47 (8) (2024) 453–554, http://dx.doi.org/10.1007/s40766-024-00060-1.
[75] P.C. Adak, S. Sinha, A. Agarwal, M.M. Deshmukh, Tunable Moiré materials for probing Berry physics and topology, Nat. Rev. Mater. 9 (7) (2024) 481–498, http://dx.doi.org/10.1038/s41578-024-00671-4.
[76] C. Hu, T. Qian, N. Ni, Recent progress in $MnBi_{2n}Te_{3n+1}$ intrinsic magnetic topological insulators: crystal growth, magnetism and chemical disorder, Natl. Sci. Rev. 11 (2) (2023) nwad282, http://dx.doi.org/10.1093/nsr/nwad282, arXiv:https://academic.oup.com/nsr/article-pdf/11/2/nwad282/55284821/nwad282.pdf.
[77] Y. Chen, X. Gu, Y. Li, X. Du, L. Yang, Y. Chen, Recent advances in topological quantum materials by angle-resolved photoemission spectroscopy, Matter 3 (4) (2020) 1114–1141, http://dx.doi.org/10.1016/j.matt.2020.07.007.
[78] E. Witten, Dyons of charge $e\theta/2\pi$, Phys. Lett. B 86 (1979) 283–287, http://dx.doi.org/10.1016/0370-2693(79)90838-4.
[79] F. Wilczek, Two applications of axion electrodynamics, Phys. Rev. Lett. 58 (1987) 1799–1802, http://dx.doi.org/10.1103/PhysRevLett.58.1799, URL https://link.aps.org/doi/10.1103/PhysRevLett.58.1799.
[80] B.A. Bernevig, T.L. Hughes, Topological Insulators and Topological Superconductors, Princeton University Press, Princeton, 2013, http://dx.doi.org/10.1515/9781400846733.
[81] A.M. Essin, J.E. Moore, D. Vanderbilt, Magnetoelectric polarizability and axion electrodynamics in crystalline insulators, Phys. Rev. Lett. 102 (14) (2009) 146805, http://dx.doi.org/10.1103/PhysRevLett.102.146805.
[82] R. Li, J. Wu, X.-C. Wang, J. Xia, Q.-K. Xue, Dynamical axion field in topological magnetic insulators, Nat. Phys. 6 (2010) 284–288, http://dx.doi.org/10.1038/nphys1534, URL https://www.nature.com/articles/nphys1534.
[83] L. Wu, M. Salehi, N. Koirala, J. Moon, S. Oh, N.P. Armitage, Quantized Faraday and Kerr rotation and axion electrodynamics of the surface states of three-dimensional topological insulators, Science 354 (6316) (2016) 1124–1127, http://dx.doi.org/10.1126/science.aaf5541, URL https://www.science.org/doi/10.1126/science.aaf5541.
[84] Y. Tokura, K. Yasuda, A. Tsukazaki, Magnetic topological insulators, Nat. Rev. Phys. 1 (2019) 126–143, http://dx.doi.org/10.1038/s42254-018-0011-5.
[85] H.-P. Wang, H. Ding, G.-Y. Xu, Q.-K. Xue, Y.X. Wang, Topological magnetoelectric response in ferromagnetic axion insulators, Natl. Sci. Rev. 11 (2) (2022) nwac138, http://dx.doi.org/10.1093/nsr/nwac138, URL https://academic.oup.com/nsr/article/11/2/nwac138/6648715.
[86] B. Felsager, C. Claussen, Geometry, particles, and fields, Graduate texts in contemporary physics, Springer, 1981, URL https://books.google.es/books?id=T9TvAAAAMAAJ.
[87] S. Deser, C. Teitelboim, Duality transformations of Abelian and non-Abelian gauge fields, Phys. Rev. D 13 (1976) 1592–1597, http://dx.doi.org/10.1103/PhysRevD.13.1592, URL https://link.aps.org/doi/10.1103/PhysRevD.13.1592.
[88] I. Agullo, A. del Rio, J. Navarro-Salas, Classical and quantum aspects of electric-magnetic duality rotations in curved spacetimes, Phys. Rev. D 98 (2018) 125001, http://dx.doi.org/10.1103/PhysRevD.98.125001, URL https://link.aps.org/doi/10.1103/PhysRevD.98.125001.
[89] C.W. Misner, J. Wheeler, Classical physics as geometry, Ann. Physics 2 (1957) 525–603, http://dx.doi.org/10.1016/0003-4916(57)90049-0.
[90] I. Fernandez-Corbaton, X. Zambrana-Puyalto, N. Tischler, X. Vidal, M.L. Juan, G. Molina-Terriza, Electromagnetic duality symmetry and helicity conservation for the macroscopic Maxwell's equations, Phys. Rev. Lett. 111 (2013) 060401, http://dx.doi.org/10.1103/PhysRevLett.111.060401, URL https://link.aps.org/doi/10.1103/PhysRevLett.111.060401.
[91] L. Wu, M. Salehi, N. Koirala, J. Moon, S. Oh, N.P. Armitage, Quantized faraday and Kerr rotation and axion electrodynamics of a 3D topological insulator, Science 354 (6316) (2016) 1124–1127, http://dx.doi.org/10.1126/science.aaf5541, URL https://www.science.org/doi/abs/10.1126/science.aaf5541.
[92] D. Baldomir, P. Hammond, Geometry of electromagnetic systems, in: Monographs in electrical and electronic engineering;39, Oxford University Press, 1996.
[93] F.W. Hehl, Y.N. Obukhov, Foundations of classical electrodynamics: Charge, flux, and metric, in: Progress in Mathematical Physics, vol. 33, Birkhäuser / Springer, Boston, MA, 2003, URL https://www.springer.com/gp/book/9780817645589.
[94] Y. Itin, Hilbert's energy-momentum tensor extended, Ann. Physics 459 (2024) 169504, https://doi.org/10.1016/j.aop.2023.169504.
[95] D. Bleecker, Gauge Theory and Variational Principles, 0486445461, Dover Publications Inc. 2005-12-30, Mineola, N.Y., 2005.
[96] M. Nakahara, Geometry,Topology and Physics, CRC Press, 2017, http://dx.doi.org/10.1201/9781315275826.
[97] J.D. Jackson, Classical Electrodynamics, John Wiley and Sons, 1999.
[98] X.-L. Qi, S.-C. Zhang, Topological insulators and superconductors, Rev. Modern Phys. 83 (4) (2011) 1057–1110, http://dx.doi.org/10.1103/RevModPhys.83.1057, URL https://doi.org/10.1103/RevModPhys.83.1057.
[99] D.M. Nenno, C.A.C. Garcia, J. Gooth, C. Felser, P. Narang, Axion physics in condensed-matter systems, Nat. Rev. Phys. 2 (2020) 682–696, http://dx.doi.org/10.1038/s42254-020-0240-2, URL https://www.nature.com/articles/s42254-020-0240-2.
[100] Z.-X. Li, Y. Cao, P. Yan, Topological insulators and semimetals in classical magnetic systems, Phys. Rep. 915 (2021) 1–64, http://dx.doi.org/10.1016/j.physrep.2021.02.003, URL https://www.sciencedirect.com/science/article/pii/S0370157321000703.
[101] A. Sekine, K. Nomura, Axion electrodynamics in topological materials, J. Appl. Phys. 129 (14) (2021) 141101, http://dx.doi.org/10.1063/5.0032946, arXiv:2011.13601.
[102] Y. Tokura, K. Yasuda, A. Tsukazaki, Magnetic topological insulators, Nat. Rev. Phys. 1 (2019) 126–143, http://dx.doi.org/10.1038/s42254-018-0011-5, URL https://doi.org/10.1038/s42254-018-0011-5.
[103] P. Sikivie, Invisible axion search methods, Rev. Modern Phys. 93 (1) (2021) 015004, http://dx.doi.org/10.1103/RevModPhys.93.015004.
[104] J.S. Bell, R. Jackiw, A PCAC puzzle: $\pi^0 \to \gamma\ \gamma$ in the σ-model, Il Nuovo Cimento A (1965-1970) 60 (1) (1969) 47–61, http://dx.doi.org/10.1007/BF02823296.
[105] K. Fujikawa, Path integral for gauge theories with fermions, Phys. Rev. D 21 (1980) 2848–2858, http://dx.doi.org/10.1103/PhysRevD.21.2848, URL https://link.aps.org/doi/10.1103/PhysRevD.21.2848.
[106] D. Tong, Gauge theory, Lect. Notes DAMTP Camb. 10 (2018) 8.
[107] X.-G. Wen, Quantum Field Theory of Many-Body Systems, Oxford University Press, 2004.
[108] E. Fradkin, Field Theories of Condensed Matter Physics, Cambridge University Press, 2013.
[109] S. Deser, R. Jackiw, S. Templeton, Topologically massive gauge theories, Ann. Physics 140 (2) (1982) 372–411, http://dx.doi.org/10.1016/0003-4916(82)90164-6.
[110] P.A. Horváthy, C. Nash, Geometric view on topologically massive gauge theories, Phys. Rev. D 33 (6) (1986) 1822–1828, http://dx.doi.org/10.1103/PhysRevD.33.1822.
[111] E.A. Bergshoeff, O. Hohm, Topologically massive gauge theory with 32 supercharges, Phys. Rev. D 78 (12) (2008) 125017, http://dx.doi.org/10.1103/PhysRevD.78.125017.
[112] S.M. Kuzenko, M. Ponds, Topologically massive higher spin gauge theories, J. High Energy Phys. 2018 (10) (2018) 160, http://dx.doi.org/10.1007/JHEP10(2018)160.
[113] N. Yamamoto, R. Yokokura, Topological mass generation in gapless systems, Phys. Rev. D 104 (2) (2021) 025010, http://dx.doi.org/10.1103/PhysRevD.104.025010.

[114] T.J. ALLEN, M.J. BOWICK, A. LAHIRI, Topological mass generation in 3+1 dimensions, Modern Phys. Lett. A 06 (07) (1991) 559–571, http://dx.doi.org/10.1142/S0217732391000580.
[115] F. Wilczek, Two applications of axion electrodynamics, Phys. Rev. Lett. 58 (18) (1987) 1799–1802, http://dx.doi.org/10.1103/PhysRevLett.58.1799.
[116] M.M. Vazifeh, M. Franz, Quantization and 2π periodicity of the axion action in topological insulators, Phys. Rev. B 82 (2010) 233103, http://dx.doi.org/10.1103/PhysRevB.82.233103.
[117] I.H. Brevik, M.M. Chaichian, Axion electrodynamics: Energy–momentum tensor, and possibilities for experimental tests, Internat. J. Modern Phys. A 37 (24) (2022) 2250151, http://dx.doi.org/10.1142/S0217751X22501512.
[118] C. Nash, Differential Topology and Quantum Field Theory, Elsevier Science, 1991, URL https://books.google.es/books?id=t5ptUuv0OGwC.
[119] K.N. Akihiko Sekine, Axion electrodynamics in topological materials, J. Appl. Phys. 129 (2021) 141101, URL https://doi.org/10.1063/5.0038804.
[120] Y. Hatsugai, Topological aspects of the quantum Hall effect, J. Phys.: Condens. Matter. 9 (1997) 2507, http://dx.doi.org/10.1088/0953-8984/9/12/003.
[121] R.A. Bertlmann, Anomalies in Quantum Field Theory, Clarendon Press, 2001.
[122] N.P. Ong, S. Liang, Experimental signatures of the chiral anomaly in Dirac–Weyl semimetals, Nat. Rev. Phys. 3 (6) (2021) 394–404, http://dx.doi.org/10.1038/s42254-021-00310-9.
[123] S.-Y. Xu, M. Neupane, C. Liu, D. Zhang, A. Richardella, L. Andrew Wray, N. Alidoust, M. Leandersson, T. Balasubramanian, J. Sánchez-Barriga, O. Rader, G. Landolt, B. Slomski, J. Hugo Dil, J. Osterwalder, T.-R. Chang, H.-T. Jeng, H. Lin, A. Bansil, N. Samarth, M. Zahid Hasan, Hedgehog spin texture and Berry's phase tuning in a magnetic topological insulator, Nat. Phys. 8 (8) (2012) 616–622, http://dx.doi.org/10.1038/nphys2351.
[124] L. Bao, W. Wang, N. Meyer, Y. Liu, C. Zhang, K. Wang, P. Ai, F. Xiu, Quantum corrections crossover and ferromagnetism in magnetic topological insulators, Sci. Rep. 3 (1) (2013) 2391, http://dx.doi.org/10.1038/srep02391.
[125] R.D. Peccei, H.R. Quinn, CP conservation in the presence of pseudoparticles, Phys. Rev. Lett. 38 (1977) 1440–1443, http://dx.doi.org/10.1103/PhysRevLett.38.1440, URL https://link.aps.org/doi/10.1103/PhysRevLett.38.1440.
[126] S. Weinberg, A new light boson? Phys. Rev. Lett. 40 (1978) 223–226, http://dx.doi.org/10.1103/PhysRevLett.40.223, URL https://link.aps.org/doi/10.1103/PhysRevLett.40.223.
[127] F. Wilczek, Problem of strong P and T invariance in the presence of instantons, Phys. Rev. Lett. 40 (1978) 279–282, http://dx.doi.org/10.1103/PhysRevLett.40.279, URL https://link.aps.org/doi/10.1103/PhysRevLett.40.279.
[128] J. Gooth, B. Bradlyn, S. Honnali, C. Schindler, N. Kumar, J. Noky, Y. Qi, C. Shekhar, Y. Sun, Z. Wang, B.A. Bernevig, C. Felser, Axionic charge-density wave in the Weyl semimetal $(TaSe_4)_2I$, Nature 575 (7782) (2019) 315–319, http://dx.doi.org/10.1038/s41586-019-1630-4.
[129] M. Tobar, B. McAllister, M. Goryachev, Modified axion electrodynamics as impressed electromagnetic sources through oscillating background polarization and magnetization, Phys. Dark Universe 26 (2019) 100339, http://dx.doi.org/10.1016/j.dark.2019.100339.
[130] D. Faílde, D. Baldomir, On the inner topological pressure within the topological insulators, Ann. Phys., Lpz. 534 (1) (2022) 2100313, http://dx.doi.org/10.1002/andp.202100313, URL https://onlinelibrary.wiley.com/doi/abs/10.1002/andp.202100313.
[131] J.P. Reed, B. Uchoa, Y.I. Joe, Y. Gan, D. Casa, E. Fradkin, P. Abbamonte, The effective fine-structure constant of freestanding graphene measured in graphite, Science 330 (6005) (2010) 805, http://dx.doi.org/10.1126/science.1190920.
[132] C. Jang, S. Adam, J.-H. Chen, E.D. Williams, S. Das Sarma, M.S. Fuhrer, Tuning the effective fine structure constant in graphene: Opposing effects of dielectric screening on short- and long-range potential scattering, Phys. Rev. Lett. 101 (2008) 146805, http://dx.doi.org/10.1103/PhysRevLett.101.146805, URL https://link.aps.org/doi/10.1103/PhysRevLett.101.146805.
[133] J. Schwinger, L.L. DeRaad, K.A. Milton, Casimir effect in dielectrics, Ann. Physics 115 (1) (1978) 1, http://dx.doi.org/10.1016/0003-4916(78)90172-0.
[134] G.L. Klimchitskaya, What is the temperature dependence of the Casimir force between real metals? Internat. J. Modern Phys. A 17 (06n07) (2002) 751–760, http://dx.doi.org/10.1142/S0217751X02010078.
[135] E. Lifshitz, The theory of molecular attractive forces between solid bodies, J. Exp. Theor. Phys. 29 (1955) 94.
[136] P. Sikivie, Experimental tests of the "invisible" axion, Phys. Rev. Lett. 51 (1983) 1415–1417, http://dx.doi.org/10.1103/PhysRevLett.51.1415, URL https://link.aps.org/doi/10.1103/PhysRevLett.51.1415.
[137] B.M. V., Quantal phase factors accompanying adiabatic changes, Proc. R. Soc. Lond. Ser. A Math. Phys. Sci. 392 (1984) 45–57, http://dx.doi.org/10.1098/rspa.1984.0023.
[138] D. Xiao, M.-C. Chang, Q. Niu, Berry phase effects on electronic properties, Rev. Modern Phys. 82 (3) (2010) 1959–2007, http://dx.doi.org/10.1103/RevModPhys.82.1959.
[139] J. Zak, Berry's phase for energy bands in solids, Phys. Rev. Lett. 62 (1989) 2747–2750, http://dx.doi.org/10.1103/PhysRevLett.62.2747, URL https://link.aps.org/doi/10.1103/PhysRevLett.62.2747.
[140] Y. Hatsugai, Chern number and edge states in the integer quantum Hall effect, Phys. Rev. Lett. 71 (1993) 3697–3700, http://dx.doi.org/10.1103/PhysRevLett.71.3697, URL https://link.aps.org/doi/10.1103/PhysRevLett.71.3697.
[141] L. Li, Z. Xu, S. Chen, Topological phases of generalized Su-Schrieffer-Heeger models, Phys. Rev. B 89 (2014) 085111, http://dx.doi.org/10.1103/PhysRevB.89.085111, URL https://link.aps.org/doi/10.1103/PhysRevB.89.085111.
[142] C.L. Kane, E.J. Mele, Z_2 topological order and the quantum spin Hall effect, Phys. Rev. Lett. 95 (2005) 146802, http://dx.doi.org/10.1103/PhysRevLett.95.146802, URL https://link.aps.org/doi/10.1103/PhysRevLett.95.146802.
[143] D. Faílde, D. Baldomir, Orbital dynamics in 2D topological and Chern insulators, New J. Phys. 23 (11) (2021) 113002, http://dx.doi.org/10.1088/1367-2630/ac29fc.
[144] E. Witten, Quantum field theory and the Jones polynomial, Comm. Math. Phys. 121 (3) (1989) 351–399, http://dx.doi.org/10.1007/BF01217730, URL https://projecteuclid.org/euclid.cmp/1104178138.
[145] A.A. Migdal, Loop equations and $1/N$ expansion, Phys. Rep. 102 (4) (1983) 199–290, http://dx.doi.org/10.1016/0370-1573(83)90007-5.
[146] N. Drukker, Roadmap on Wilson loops in 3d Chern–Simons–matter theories, 2019, ArXiv Preprint. arXiv:1910.00588. URL https://arxiv.org/abs/1910.00588.
[147] D. Grabovsky, Chern–Simons theory in a knotshell, 2022, Pedagogical notes (arXiv/pdf).
[148] D.J. Thouless, M. Kohmoto, M.P. Nightingale, M. den Nijs, Quantized Hall conductance in a two-dimensional periodic potential, Phys. Rev. Lett. 49 (6) (1982) 405–408, http://dx.doi.org/10.1103/PhysRevLett.49.405.
[149] C.-Z. Chang, J. Zhang, X. Feng, J. Shen, Z. Zhang, M. Guo, K. Li, Y. Ou, P. Wei, L.-L. Wang, Z.-Q. Ji, Y. Feng, S. Ji, X. Chen, J. Jia, X. Dai, Z. Fang, S.-C. Zhang, K. He, Y. Wang, L. Lu, X.-C. Ma, Q.-K. Xue, Experimental observation of the quantum anomalous Hall effect in a magnetic topological insulator, Science 340 (6129) (2013) 167–170, http://dx.doi.org/10.1126/science.1234414.
[150] R. Yu, W. Zhang, H.-J. Zhang, S.-C. Zhang, X. Dai, Z. Fang, Quantized anomalous Hall effect in magnetic topological insulators, Science 329 (5987) (2010) 61–64, http://dx.doi.org/10.1126/science.1187485.
[151] Y. Tokura, K. Yasuda, A. Tsukazaki, Magnetic topological insulators, Nat. Rev. Phys. 1 (2) (2019) 126–143, http://dx.doi.org/10.1038/s42254-018-0011-5.
[152] N. Varnava, D. Vanderbilt, Surfaces of axion insulators, Phys. Rev. B 98 (2018) 245117, http://dx.doi.org/10.1103/PhysRevB.98.245117, URL https://link.aps.org/doi/10.1103/PhysRevB.98.245117.

[153] Y.S. Hor, P. Roushan, H. Beidenkopf, J. Seo, D. Qu, J.G. Checkelsky, L.A. Wray, D. Hsieh, Y. Xia, S.-Y. Xu, D. Qian, M.Z. Hasan, N.P. Ong, A. Yazdani, R.J. Cava, Development of ferromagnetism in the doped topological insulator $Bi_{2-x}Mn_xTe_3$, Phys. Rev. B 81 (2010) 195203, http://dx.doi.org/10.1103/PhysRevB.81.195203, URL https://link.aps.org/doi/10.1103/PhysRevB.81.195203.

[154] R. Yu, W. Zhang, H.-J. Zhang, S.-C. Zhang, X. Dai, Z. Fang, Quantized anomalous Hall effect in magnetic topological insulators, Science 329 (5987) (2010) 61–64, http://dx.doi.org/10.1126/science.1187485, URL https://www.science.org/doi/abs/10.1126/science.1187485.

[155] Y.L. Chen, J.G. Analytis, J.-H. Chu, Z.K. Liu, S.-K. Mo, X.L. Qi, H.J. Zhang, D.H. Lu, X. Dai, Z. Fang, S.C. Zhang, I.R. Fisher, Z. Hussain, Z.-X. Shen, Experimental realization of a three-dimensional topological insulator, Bi_2Te_3, Science 325 (5937) (2009) 178–181, http://dx.doi.org/10.1126/science.1173034.

[156] C. Liu, T.L. Hughes, X.-L. Qi, K. Wang, S.-C. Zhang, Quantum spin Hall effect in inverted type-II semiconductors, Phys. Rev. Lett. 100 (2008) 236601, http://dx.doi.org/10.1103/PhysRevLett.100.236601, URL https://link.aps.org/doi/10.1103/PhysRevLett.100.236601.

[157] B.-X. Li, Z. Song, Z. Fang, Z. Wang, H. Weng, Manipulation of topological phase transitions and the mechanism of magnetic interactions in Eu-based Zintl-phase materials, Phys. Rev. B 111 (2025) 205127, http://dx.doi.org/10.1103/PhysRevB.111.205127, URL https://link.aps.org/doi/10.1103/PhysRevB.111.205127.

[158] N.P. Ong, S. Liang, Experimental signatures of the chiral anomaly in Dirac–Weyl semimetals, Nat. Rev. Phys. 3 (2021) 394–404, http://dx.doi.org/10.1038/s42254-021-00310-9.

[159] K. Fukushima, D.E. Kharzeev, H.J. Warringa, Chiral magnetic effect, Phys. Rev. D 78 (7) (2008) 074033, http://dx.doi.org/10.1103/PhysRevD.78.074033.

[160] I.M. Atiyah, The index of elliptic operators on compact manifolds, Bull. Amer. Math. Soc. 69 (1963) 422–433, http://dx.doi.org/10.1090/S0002-9904-1963-10957-X.

[161] S. Weinberg, The Quantum Theory of Fields, vol. 2, Cambridge University Press, 2013.

[162] S.B. Treiman, R. Jackiw, B. Zumino, E. Witten, Current Algebra and Anomalies, Princeton University Press, 1985, http://dx.doi.org/10.2307/j.ctt7ztmc8.

[163] V.A. Miransky, I.A. Shovkovy, Quantum field theory in a magnetic field: From quantum chromodynamics to graphene and Dirac semimetals, Phys. Rep. 576 (2015) 1–209, http://dx.doi.org/10.1016/j.physrep.2015.02.003, arXiv:1503.00732.

[164] H.B. Nielsen, M. Ninomiya, The Adler–Bell–Jackiw anomaly and Weyl fermions in a crystal, Phys. Lett. B 130 (1983) 389–396, http://dx.doi.org/10.1016/0370-2693(83)91529-0, URL https://www.sciencedirect.com/science/article/pii/0370269383915290.

[165] E. Witten, K. Yonekura, Anomaly inflow and the η-invariant, 2020, arXiv:1909.08775. URL https://arxiv.org/abs/1909.08775.

[166] F.J. Burnell, T. Devakul, P. Gorantla, H.T. Lam, S.-H. Shao, Anomaly inflow for subsystem symmetries, Phys. Rev. B 106 (2022) 085113, http://dx.doi.org/10.1103/PhysRevB.106.085113, URL https://link.aps.org/doi/10.1103/PhysRevB.106.085113.

[167] K. Jensen, R. Loganayagam, A. Yarom, Anomaly inflow and thermal equilibrium, J. High Energy Phys. 2014 (5) (2014) 134, http://dx.doi.org/10.1007/JHEP05(2014)134.

[168] J. Fröhlich, Gauge invariance and anomalies in condensed matter physics, J. Math. Phys. 64 (2023) 031903, http://dx.doi.org/10.1063/5.0135142.

[169] E.W. Luis Alvarez-Gaumé, Gravitational anomalies, Nuclear Phys. B 234 (1984) 269–330, http://dx.doi.org/10.1016/0550-3213(84)90066-X.

[170] Y. Ferreiros, A.A. Zyuzin, J.H. Bardarson, Anomalous nernst and thermal hall effects in tilted Weyl semimetals, Phys. Rev. B 96 (2017) 115202, http://dx.doi.org/10.1103/PhysRevB.96.115202, URL https://link.aps.org/doi/10.1103/PhysRevB.96.115202.

[171] C. Zeng, S. Nandy, S. Tewari, Chiral anomaly induced nonlinear Nernst and thermal Hall effects in Weyl semimetals, Phys. Rev. B 105 (2022) 125131, http://dx.doi.org/10.1103/PhysRevB.105.125131, URL https://link.aps.org/doi/10.1103/PhysRevB.105.125131.

[172] A. Roy Karmakar, S. Nandy, A. Taraphder, G.P. Das, Giant anomalous thermal Hall effect in tilted type-I magnetic Weyl semimetal $Co_3Sn_2S_2$, Phys. Rev. B 106 (2022) 245133, http://dx.doi.org/10.1103/PhysRevB.106.245133, URL https://link.aps.org/doi/10.1103/PhysRevB.106.245133.

[173] H. Guo, R. Samajdar, M.S. Scheurer, S. Sachdev, Gauge theories for the thermal Hall effect, Phys. Rev. B 101 (2020) 195126, http://dx.doi.org/10.1103/PhysRevB.101.195126, URL https://link.aps.org/doi/10.1103/PhysRevB.101.195126.

[174] G. Grissonnanche, A. Legros, S. Badoux, E. Lefrançois, V. Zatko, M. Lizaire, F. Laliberté, A. Gourgout, J.-S. Zhou, S. Pyon, T. Takayama, H. Takagi, S. Ono, N. Doiron-Leyraud, L. Taillefer, Giant thermal Hall conductivity in the pseudogap phase of cuprate superconductors, Nature 571 (7765) (2019) 376–380, http://dx.doi.org/10.1038/s41586-019-1375-0.

[175] M.S. Scheurer, S. Chatterjee, W. Wu, M. Ferrero, A. Georges, S. Sachdev, Topological order in the pseudogap metal, Proc. Natl. Acad. Sci. 115 (16) (2018) E3665–E3672, http://dx.doi.org/10.1073/pnas.1720580115, URL https://www.pnas.org/doi/abs/10.1073/pnas.1720580115.

[176] E. Kröner, et al., Continuum theory of defects, Phys. Defects 35 (1981) 217–315.

[177] J.-J. E.Brezin, Fields, Strings and Critical Phenomena, North-Holland, Amsterdam, 1990.

[178] K.S. Novoselov, A.K. Geim, S.V. Morozov, D. Jiang, M.I. Katsnelson, I.V. Grigorieva, S.V. Dubonos, A.A. Firsov, Two-dimensional gas of massless Dirac fermions in graphene, Nature 438 (7065) (2005) 197–200, http://dx.doi.org/10.1038/nature04233.

[179] J.C. Meyer, A.K. Geim, M.I. Katsnelson, K.S. Novoselov, T.J. Booth, S. Roth, The structure of suspended graphene sheets, Nature 446 (7131) (2007) 60–63, http://dx.doi.org/10.1038/nature05545.

[180] M.A. Rieffel, The homotopy groups of the unitary groups of non-commutative tori, J. Operator Theory 17 (1987) 237–254, URL https://www.jstor.org/stable/24714841.

[181] J.E. Avron, R. Seiler, B. Simon, Homotopy and quantization in condensed matter physics, Phys. Rev. Lett. 51 (1983) 51–53, http://dx.doi.org/10.1103/PhysRevLett.51.51, URL https://link.aps.org/doi/10.1103/PhysRevLett.51.51.

[182] M.J. Klein, On a degeneracy theorem of kramers, Am. J. Phys. 20 (1952) 65–71, http://dx.doi.org/10.1119/1.1933118.

[183] S. Lieu, M. McGinley, O. Shtanko, N.R. Cooper, A.V. Gorshkov, Kramers' degeneracy for open systems in thermal equilibrium, Phys. Rev. B 105 (2022) L121104, http://dx.doi.org/10.1103/PhysRevB.105.L121104, URL https://link.aps.org/doi/10.1103/PhysRevB.105.L121104.

[184] J.N. Sakurai, Modern Quantum Mechanics, 0-8053-8291-7, Addison-Wesley, 1982.

[185] A.W.W. Ludwig, Topological phases: classification of topological insulators and superconductors of non-interacting fermions, and beyond, Phys. Scr. (2016).

[186] E. Cartan, Sur une classe remarquable d'espaces de Riemann i, Bull. Soc. Math. Fr. 54 (1926) 214–264., http://dx.doi.org/10.24033/bsmf.1105.

[187] E. Cartan, Sur une classe remarquable d'espaces de Riemann II, Bull. Soc. Math. Fr. 55 (1927) 114–134, http://dx.doi.org/10.24033/bsmf.1113.

[188] M.R. Zirnbauer, Riemannian symmetric superspaces and their origin in random-matrix theory, J. Math. Phys. 37 (1996) 4986–5018, http://dx.doi.org/10.1063/1.531675.

[189] A.H..M.Z. P. Heinzner, Symmetry classes of disordered Fermions, Comm. Math. Phys. 257 (2005) 725–771, http://dx.doi.org/10.1007/s00220-005-1330-9.

[190] A.P. Schnyder, S. Ryu, A. Furusaki, A.W.W. Ludwig, Classification of topological insulators and superconductors in three spatial dimensions, Phys. Rev. B 78 (2008) 195125, http://dx.doi.org/10.1103/PhysRevB.78.195125, URL https://link.aps.org/doi/10.1103/PhysRevB.78.195125.

[191] R. Bott, The stable homotopy of the classical groups, Ann. Math. 70 (1959) 313, URL http://www.jstor.org/stable/1970106.

[192] W.A. Benalcazar, B.A. Bernevig, T.L. Hughes, Quantized electric multipole insulators, Science 357 (6346) (2017) 61–66, http://dx.doi.org/10.1126/science.aah6442.

[193] F. Schindler, A.M. Cook, M.G. Vergniory, Z. Wang, S.S.P. Parkin, B.A. Bernevig, T. Neupert, Higher-order topological insulators, Sci. Adv. 4 (6) (2018) eaat0346, http://dx.doi.org/10.1126/sciadv.aat0346.

[194] Z. Song, Z. Fang, C. Fang, $(d-2)$-Dimensional edge states of rotation symmetry protected topological states, Phys. Rev. Lett. 119 (2017) 246402, http://dx.doi.org/10.1103/PhysRevLett.119.246402, URL https://link.aps.org/doi/10.1103/PhysRevLett.119.246402.

[195] J. Langbehn, Y. Peng, L. Trifunovic, F. von Oppen, P.W. Brouwer, Reflection-symmetric second-order topological insulators and superconductors, Phys. Rev. Lett. 119 (2017) 246401, http://dx.doi.org/10.1103/PhysRevLett.119.246401, URL https://link.aps.org/doi/10.1103/PhysRevLett.119.246401.

[196] I. Knez, R.-R. Du, G. Sullivan, Evidence for helical edge modes in inverted InAs/GaSb quantum wells, Phys. Rev. Lett. 107 (2011) 136603, http://dx.doi.org/10.1103/PhysRevLett.107.136603, URL https://link.aps.org/doi/10.1103/PhysRevLett.107.136603.

[197] L. Fu, C.L. Kane, E.J. Mele, Topological insulators in three dimensions, Phys. Rev. Lett. 98 (2007) 106803, http://dx.doi.org/10.1103/PhysRevLett.98.106803, URL https://link.aps.org/doi/10.1103/PhysRevLett.98.106803.

[198] R. Roy, Topological phases and the quantum spin Hall effect in three dimensions, Phys. Rev. B 79 (2009) 195322, http://dx.doi.org/10.1103/PhysRevB.79.195322, URL https://link.aps.org/doi/10.1103/PhysRevB.79.195322.

[199] J.E. Moore, L. Balents, Topological invariants of time-reversal-invariant band structures, Phys. Rev. B 75 (2007) 121306, http://dx.doi.org/10.1103/PhysRevB.75.121306, URL https://link.aps.org/doi/10.1103/PhysRevB.75.121306.

[200] D. Hsieh, D. Qian, L. Wray, Y. Xia, Y.S. Hor, R.J. Cava, M.Z. Hasan, A topological Dirac insulator in a quantum spin Hall phase, Nature 452 (7190) (2008) 970–974, http://dx.doi.org/10.1038/nature06843.

[201] M.J. Gilbert, Topological electronics, Commun. Phys. 4 (2021) 70, http://dx.doi.org/10.1038/s42005-021-00569-5.

[202] H. Luo, P. Yu, G. Li, K. Yan, Topological quantum materials for energy conversion and storage, Nat. Rev. Phys. 4 (9) (2022) 611–624, http://dx.doi.org/10.1038/s42254-022-00477-9.

[203] P. Bhalla, Intrinsic contribution to nonlinear thermoelectric effects in topological insulators, Phys. Rev. B 103 (2021) 115304, http://dx.doi.org/10.1103/PhysRevB.103.115304, URL https://link.aps.org/doi/10.1103/PhysRevB.103.115304.

[204] D.A. Wright, Thermoelectric properties of bismuth telluride and its alloys, Nature 181 (1958) 834, http://dx.doi.org/10.1038/181834a0.

[205] J. Zhang, X. Song, X. Zhang, Q. Zhang, H. Zhao, Performance analysis and optimization of the rough-contact Bi_2Te_3-based thermoelectric cooler via metallized layers, Case Stud. Therm. Eng. 40 (2022) 102522, http://dx.doi.org/10.1016/j.csite.2022.102522, URL https://www.sciencedirect.com/science/article/pii/S2214157X22007596.

[206] A.E. Seidzade, E.N. Orujlu, T. Doert, I.R. Amiraslanov, Z.S. Aliev, M.B. Babanly, An updated phase diagram of the SnTe-Sb_2Te_3 system and the crystal structure of the new compound $SnSb_4Te_7$, J. Phase Equilib. Diffus. 42 (3) (2021) 373–378, http://dx.doi.org/10.1007/s11669-021-00888-8.

[207] Y.A.W. Ahmed Subrati, et al., Monitoring the multiphasic evolution of bismuth telluride nanoplatelets, CrystEngComm 22 (2020) 7918–7928, http://dx.doi.org/10.1039/D0CE00719F.

[208] T.K. Dalui, P.K. Ghose, S. Majumdar, S. Giri, Interplay between positive magnetoresistance and thermoelectric properties by tuning carrier concentration in $Sb_{2-x}Sn_xTe_3$ ($x \leq 0.05$) crystals, J. Phys.: Condens. Matter. 32 (43) (2020) 435601, http://dx.doi.org/10.1088/1361-648X/aba386.

[209] L.N. Lukyanova, O.A. Usov, M.P. Volkov, I.V. Makarenko, Topological thermoelectric materials based on bismuth telluride, Nanobiotechnol. Rep. 16 (3) (2021) 282–293, http://dx.doi.org/10.1134/S2635167621030125.

[210] M. Gaffar, S.A. Wella, E.H. Hasdeo, Effects of topological band structure on thermoelectric transport of bismuthene, Phys. Rev. B 104 (2021) 205105, http://dx.doi.org/10.1103/PhysRevB.104.205105, URL https://link.aps.org/doi/10.1103/PhysRevB.104.205105.

[211] S. Sadhukhan, B. Sadhukhan, S. Kanungo, Pressure-driven tunable properties of the small-gap chalcopyrite topological quantum material $ZnGeSb_2$: A first-principles study, Phys. Rev. B 106 (2022) 125112, http://dx.doi.org/10.1103/PhysRevB.106.125112, URL https://link.aps.org/doi/10.1103/PhysRevB.106.125112.

[212] F. Hosseinzadeh, A. Boochani, S.M. Elahi, Z. Ghorannevis, Vanadium effect on the electronic and thermoelectric properties of ScPtBi compound, Int. Nano Lett. 10 (3) (2020) 225–234, http://dx.doi.org/10.1007/s40089-020-00310-0.

[213] J. Yadav, M. Anoop, R. Singh, N. Yadav, N.S. Rao, F. Singh, A. Jain, T. Ichikawa, K. Awasthi, M. Kumar, A reversible tuning of Fermi level in $BiSbTe_3$ thin films through ion implantation, Mater. Lett. 306 (2022) 130923, http://dx.doi.org/10.1016/j.matlet.2021.130923, URL https://www.sciencedirect.com/science/article/pii/S0167577X21016207.

[214] H. Zhang, C.-X. Liu, X.-L. Qi, X. Dai, Z. Fang, S.-C. Zhang, Topological insulators in Bi_2Se_3, Bi_2Te_3 and Sb_2Te_3 with a single Dirac cone on the surface, Nat. Phys. 5 (6) (2009) 438–442, http://dx.doi.org/10.1038/nphys1270.

[215] W.G. Zeier, A. Zevalkink, Z.M. Gibbs, G. Hautier, M.G. Kanatzidis, G.J. Snyder, Thinking like a chemist: Intuition in thermoelectric materials, Angew. Chem. Int. Ed. 55 (24) (2016) 6826–6841, http://dx.doi.org/10.1002/anie.201508381.

[216] S. Lee, K. Esfarjani, T. Luo, J. Zhou, Z. Tian, G. Chen, Resonant bonding leads to low lattice thermal conductivity, Nat. Commun. 5 (1) (2014) 3525, http://dx.doi.org/10.1038/ncomms4525.

[217] Z. Ren, A.A. Taskin, S. Sasaki, K. Segawa, Y. Ando, Optimizing $Bi_{2-x}Sb_xTe_{3-y}Se_y$ solid solutions to approach the intrinsic topological insulator regime, Phys. Rev. B 84 (2011) 165311, http://dx.doi.org/10.1103/PhysRevB.84.165311, URL https://link.aps.org/doi/10.1103/PhysRevB.84.165311.

[218] J.P. Heremans, R.J. Cava, N. Samarth, Tetradymites as thermoelectrics and topological insulators, Nat. Rev. Mater. 2 (2017) http://dx.doi.org/10.1038/natrevmats.2017.49.

[219] I.T. Witting, T.C. Chasapis, F. Ricci, M. Peters, N.A. Heinz, G. Hautier, G.J. Snyder, The thermoelectric properties of bismuth telluride, Adv. Electron. Mater. 5 (6) (2019) 1800904, http://dx.doi.org/10.1002/aelm.201800904.

[220] S.K. Mishra, S. Satpathy, O. Jepsen, Electronic structure and thermoelectric properties of bismuth telluride and bismuth selenide, J. Phys.: Condens. Matter. 9 (2014) 461, http://dx.doi.org/10.1088/0953-8984/9/2/014.

[221] D. Greenaway, G. Harbeke, Band structure of bismuth telluride, bismuth selenide and their respective alloys, J. Phys. Chem. Solids 26 (1965) 1585–1604, http://dx.doi.org/10.1016/0022-3697(65)90092-2.

[222] R. Venkatasubramanian, E. Siivola, T. Colpitts, B. O'Quinn, Thin-film thermoelectric devices with high room-temperature figures of merit, Nature 413 (2001) 597–602, http://dx.doi.org/10.1038/35098012.

[223] V. Narayanamurti, H.L. Störmer, M.A. Chin, A.C. Gossard, W. Wiegmann, Selective transmission of high-frequency phonons by a superlattice: The "dielectric" phonon filter, Phys. Rev. Lett. 43 (1979) 2012–2016, http://dx.doi.org/10.1103/PhysRevLett.43.2012, URL https://link.aps.org/doi/10.1103/PhysRevLett.43.2012.

[224] H.-S. Kim, N.A. Heinz, Z.M. Gibbs, Y. Tang, S.D. Kang, G.J. Snyder, High thermoelectric performance in $(Bi_{0.25}Sb_{0.75})_2Te_3$ due to band convergence and improved by carrier concentration control, Mater. Today 20 (8) (2017) 452–459.

[225] C.-T. Hsieh, Y. Tachikawa, K. Yonekura, Anomaly inflow and p-form gauge theories, Comm. Math. Phys. 391 (2022) 495–608, http://dx.doi.org/10.1007/s00220-022-04333-w.

[226] S. Deser, R. Jackiw, S. Templeton, Three-dimensional massive gauge theories, Phys. Rev. Lett. 48 (1982) 975–978, http://dx.doi.org/10.1103/PhysRevLett.48.975, URL https://link.aps.org/doi/10.1103/PhysRevLett.48.975.

[227] E.B. Bogomol'nyi, The stability of classical solutions, Sov. J. Nucl. Phys. 24 (4) (1976) 449–454.

[228] S.I. Kruglov, Maxwell–Chern–Simons topologically massive gauge fields in the first-order formalism, Internat. J. Theoret. Phys. 51 (2012) 1–13, http://dx.doi.org/10.1007/s10773-011-0872-1.

[229] N. Yamamoto, R. Yokokura, Topological mass generation in gapless systems, Phys. Rev. D 104 (2) (2021) 025010, http://dx.doi.org/10.1103/PhysRevD.104.025010.

[230] M.L. Bellac, Thermal field theory, in: Cambridge Monographs of Mathematical Physics, Cambridge University Press, 1996.
[231] A. Das, Finite Temperature Field Theory, World Scientific, 1997, http://dx.doi.org/10.1142/3277.
[232] M. Lohse, C. Schweizer, O. Zilberberg, M. Aidelsburger, I. Bloch, A thouless quantum pump with ultracold bosonic atoms in an optical superlattice, Nat. Phys. 12 (4) (2016) 350–354, http://dx.doi.org/10.1038/nphys3584.
[233] S. Nakajima, T. Tomita, S. Taie, T. Ichinose, H. Ozawa, L. Wang, M. Troyer, Y. Takahashi, Topological thouless pumping of ultracold fermions, Nat. Phys. 12 (4) (2016) 296–300, http://dx.doi.org/10.1038/nphys3622.
[234] T. Kitagawa, E. Berg, M. Rudner, E. Demler, Topological characterization of periodically driven quantum systems, Phys. Rev. B 82 (2010) 235114, http://dx.doi.org/10.1103/PhysRevB.82.235114, URL https://link.aps.org/doi/10.1103/PhysRevB.82.235114.
[235] L. Privitera, A. Russomanno, R. Citro, G.E. Santoro, Nonadiabatic breaking of topological pumping, Phys. Rev. Lett. 120 (2018) 106601, http://dx.doi.org/10.1103/PhysRevLett.120.106601, URL https://link.aps.org/doi/10.1103/PhysRevLett.120.106601.
[236] M.M. Wauters, A. Russomanno, R. Citro, G.E. Santoro, L. Privitera, Localization, topology, and quantized transport in disordered floquet systems, Phys. Rev. Lett. 123 (2019) 266601, http://dx.doi.org/10.1103/PhysRevLett.123.266601, URL https://link.aps.org/doi/10.1103/PhysRevLett.123.266601.
[237] A.L.C. Hayward, E. Bertok, U. Schneider, F. Heidrich-Meisner, Effect of disorder on topological charge pumping in the Rice-Mele model, Phys. Rev. A 103 (2021) 043310, http://dx.doi.org/10.1103/PhysRevA.103.043310, URL https://link.aps.org/doi/10.1103/PhysRevA.103.043310.
[238] P. Marra, M. Nitta, Topologically quantized current in quasiperiodic thouless pumps, Phys. Rev. Res. 2 (2020) 042035, http://dx.doi.org/10.1103/PhysRevResearch.2.042035, URL https://link.aps.org/doi/10.1103/PhysRevResearch.2.042035.
[239] R. Wang, Z. Song, Robustness of the pumping charge to dynamic disorder, Phys. Rev. B 100 (2019) 184304, http://dx.doi.org/10.1103/PhysRevB.100.184304, URL https://link.aps.org/doi/10.1103/PhysRevB.100.184304.
[240] E. Abrahams, P.W. Anderson, D.C. Licciardello, T.V. Ramakrishnan, Scaling theory of localization: Absence of quantum diffusion in two dimensions, Phys. Rev. Lett. 42 (1979) 673–676, http://dx.doi.org/10.1103/PhysRevLett.42.673, URL https://link.aps.org/doi/10.1103/PhysRevLett.42.673.
[241] D. Vanderbilt, Berry Phases in Electronic Structure Theory: Electric Polarization, Orbital Magnetization and Topological Insulators, Cambridge University Press, 2018.
[242] J. Zinn-Justin, Quantum Field Theory and Critical Phenomena, Oxford Academic, 2024.
[243] H.-Z. Lu, W.-Y. Shan, W. Yao, Q. Niu, S.-Q. Shen, Massive Dirac fermions and spin physics in an ultrathin film of topological insulator, Phys. Rev. B 81 (2010) 115407, http://dx.doi.org/10.1103/PhysRevB.81.115407, URL https://link.aps.org/doi/10.1103/PhysRevB.81.115407.
[244] L. Zhang, Berry curvature and various thermal Hall effects, New J. Phys. 18 (10) (2016) 103039, http://dx.doi.org/10.1088/1367-2630/18/10/103039.
[245] X. Wan, A.M. Turner, A. Vishwanath, S.Y. Savrasov, Topological semimetal and Fermi-arc surface states in the electronic structure of pyrochlore iridates, Phys. Rev. B 83 (2011) 205101, http://dx.doi.org/10.1103/PhysRevB.83.205101.
[246] A.A. Burkov, L. Balents, Weyl semimetal in a topological insulator multilayer, Phys. Rev. Lett. 107 (2011) 127205, http://dx.doi.org/10.1103/PhysRevLett.107.127205.
[247] S.-M. Huang, S.-Y. Xu, I. Belopolski, C.-C. Lee, G. Chang, B.-K. Wang, N. Alidoust, G. Bian, M. Neupane, A. Bansil, H. Lin, M.Z. Hasan, A Weyl Fermion semimetal with surface Fermi arcs in the transition-metal monopnictide TaAs class, Nat. Commun. 6 (2015) 7373, http://dx.doi.org/10.1038/ncomms8373.
[248] H. Weng, C. Fang, Z. Fang, B.A. Bernevig, X. Dai, Weyl semimetal phase in noncentrosymmetric transition-metal monophosphides, Phys. Rev. X 5 (2015) 011029, http://dx.doi.org/10.1103/PhysRevX.5.011029.
[249] B.Q. Lv, H.M. Weng, B.B. Fu, X.P. Wang, H. Miao, J. Ma, P. Richard, X.C. Huang, L.X. Zhao, G.F. Chen, Z. Fang, X. Dai, T. Qian, H. Ding, Experimental discovery of Weyl semimetal TaAs, Phys. Rev. X 5 (2015) 031013, http://dx.doi.org/10.1103/PhysRevX.5.031013.
[250] P. Park, J. Oh, K. Uhlířová, J. Jackson, A. Deák, L. Szunyogh, K.H. Lee, H. Cho, H.-L. Kim, H.C. Walker, D. Adroja, V. Sechovský, J.-G. Park, Magnetic excitations in non-collinear antiferromagnetic Weyl semimetal Mn3Sn, Npj Quantum Mater. 3 (1) (2018) 63, http://dx.doi.org/10.1038/s41535-018-0137-9.
[251] M. Kanagaraj, J. Ning, L. He, Topological Co3Sn2S2 magnetic Weyl semimetal: From fundamental understanding to diverse fields of study, Rev. Phys. 8 (2022) 100072, http://dx.doi.org/10.1016/j.revip.2022.100072, URL https://www.sciencedirect.com/science/article/pii/S2405428322000041.
[252] S. Borisenko, D. Evtushinsky, Q. Gibson, A. Yaresko, K. Koepernik, T. Kim, M. Ali, J. van den Brink, M. Hoesch, A. Fedorov, E. Haubold, Y. Kushnirenko, I. Soldatov, R. Schäfer, R.J. Cava, Time-reversal symmetry breaking type-II Weyl state in YbMnBi2, Nat. Commun. 10 (1) (2019) 3424, http://dx.doi.org/10.1038/s41467-019-11393-5.
[253] S. Kumar, Y.-H. Tu, S. Luo, N.A. Lanzillo, T.-R. Chang, G. Liang, R. Sundararaman, H. Lin, C.-T. Chen, Surface-dominated conductance scaling in Weyl semimetal NbAs, Npj Comput. Mater. 10 (1) (2024) 84, http://dx.doi.org/10.1038/s41524-024-01263-0.
[254] K. Behnia, Fundamentals of thermoelectricity in metals and semimetals, C. R. Phys. 17 (3) (2016) 302–316, http://dx.doi.org/10.1016/j.crhy.2015.09.005.
[255] V. Kozii, B. Skinner, L. Fu, Thermoelectric Hall conductivity and figure of merit in Dirac/Weyl materials, Phys. Rev. B 99 (2019) 155123, http://dx.doi.org/10.1103/PhysRevB.99.155123, URL https://link.aps.org/doi/10.1103/PhysRevB.99.155123.
[256] F.R. Pratama, R. Saito, N.T. Hung, Magneto-seebeck coefficient of the Fermi liquid in three-dimensional Dirac and Weyl semimetals, Phys. Rev. B 106 (2022) L081304, http://dx.doi.org/10.1103/PhysRevB.106.L081304, URL https://link.aps.org/doi/10.1103/PhysRevB.106.L081304.
[257] C. Fu, Z. Wang, H. Pan, W. Zhang, et al., Large Nernst power factor over a broad temperature range in polycrystalline Weyl semimetal NbP, Energy Environ. Sci. 11 (2018) http://dx.doi.org/10.1039/C8EE02077A.
[258] H. Sakai, S. Nakatsuji, et al., Critical enhancement of thermopower in a chemically tuned polar semimetal, Sci. Adv. 2 (11) (2016) e1601378, http://dx.doi.org/10.1126/sciadv.1601378.
[259] Y. Pan, Y. Liang, et al., Ultrahigh transverse thermoelectric power factor in flexible WTe_2 single crystals, Nat. Commun. 13 (2022) XXXX, http://dx.doi.org/10.1038/s41467-022-31372-7.
[260] S.N. Guin, P. Vir, Y. Zhang, N. Kumar, S.J. Watzman, C. Fu, E. Liu, K. Manna, W. Schnelle, J. Gooth, C. Shekhar, Y. Sun, C. Felser, Zero-field nernst effect in a ferromagnetic kagome-lattice weyl-semimetal co3sn2s2, Adv. Mater. 31 (25) (2019) e1806622, https://doi.org/10.1002/adma.201806622.
[261] H. Weng, X. Dai, Z. Fang, Weyl semimetal phase in non-centrosymmetric transition-metal monopnictides, Phys. Rev. X 5 (1) (2015) 011029, http://dx.doi.org/10.1103/PhysRevX.5.011029.
[262] S.-Y. Xu, I. Belopolski, N. Alidoust, M. Neupane, G. Bian, C. Zhang, R. Sankar, G. Chang, Z. Yuan, C.-C. Lee, S.-M. Huang, H. Zheng, J. Ma, D.S. Sanchez, B. Wang, A. Bansil, F. Chou, P.P. Shibayev, H. Lin, S. Jia, M.Z. Hasan, Discovery of a Weyl Fermion semimetal and topological Fermi arcs, Science 349 (6248) (2015) 613–617, http://dx.doi.org/10.1126/science.aaa9297.
[263] Z. Wang, D. Gresch, A.A. Soluyanov, W. Xie, S. Kushwaha, X. Dai, M. Troyer, R.J. Cava, B.A. Bernevig, $MoTe_{(2)}$: A type-II Weyl topological metal, Phys. Rev. Lett. 117 (5) (2016) 056805, http://dx.doi.org/10.1103/PhysRevLett.117.056805.
[264] A. Rossi, V. Ivanov, S. Sreedhar, A.L. Gross, Z. Shen, E. Rotenberg, S.Y. Savrasov, I.M. Vishik, Electronic structure and topology across (T_C) in magnetic Weyl semimetal $Co_{(3)}Sn_{(2)}S_{(2)}$, 2021, ArXiv:2107.**.

[265] B. Jiang, J. Zhao, J. Qian, S. Zhang, X. Qiang, L. Wang, R. Bi, J. Fan, H.-Z. Lu, E. Liu, X. Wu, Antisymmetric seebeck effect in a tilted Weyl semimetal, Phys. Rev. Lett. 129 (2022) 056601, http://dx.doi.org/10.1103/PhysRevLett.129.056601, URL https://link.aps.org/doi/10.1103/PhysRevLett.129.056601.
[266] V.L. Ginzburg, Nobel lecture: On superconductivity and superfluidity (what I have and have not managed to do) as well as on the "physical minimum" at the beginning of the XXI century, Rev. Modern Phys. 76 (2004) 981–998, http://dx.doi.org/10.1103/RevModPhys.76.981, URL https://link.aps.org/doi/10.1103/RevModPhys.76.981.
[267] C.D. Shelly, E.A. Matrozova, V.T. Petrashov, Resolving thermoelectric "paradox" in superconductors, Sci. Adv. 2 (2016) e1501250, http://dx.doi.org/10.1126/sciadv.1501250.
[268] C.X. Trang, N. Shimamura, K. Nakayama, S. Souma, K. Sugawara, I. Watanabe, K. Yamauchi, T. Oguchi, K. Segawa, T. Takahashi, Y. Ando, T. Sato, Conversion of a conventional superconductor into a topological superconductor by topological proximity effect, Nat. Commun. 11 (1) (2020) 159, http://dx.doi.org/10.1038/s41467-019-13946-0.
[269] B. Hamdou, et al., Thermoelectric properties of band structure engineered topological insulator $(Bi_{1-x}Sb_x)_2Te_3$ nanowires, Adv. Energy Mater. 5 (2015) http://dx.doi.org/10.1002/aenm.201500280.
[270] L. Schneider, K.T. Ton, I. Ioannidis, J. Neuhaus-Steinmetz, T. Posske, R. Wiesendanger, J. Wiebe, Proximity superconductivity in atom-by-atom crafted quantum dots, Nature (2023) http://dx.doi.org/10.1038/s41586-023-06312-0.
[271] L. Fu, C.L. Kane, Superconducting proximity effect and Majorana Fermions at the surface of a topological insulator, Phys. Rev. Lett. 100 (2008) 096407, http://dx.doi.org/10.1103/PhysRevLett.100.096407, URL https://link.aps.org/doi/10.1103/PhysRevLett.100.096407.
[272] J.D. Sau, R.M. Lutchyn, S. Tewari, S. Das Sarma, Generic new platform for topological quantum computation using semiconductor heterostructures, Phys. Rev. Lett. 104 (2010) 040502, http://dx.doi.org/10.1103/PhysRevLett.104.040502, URL https://link.aps.org/doi/10.1103/PhysRevLett.104.040502.
[273] Y.S. Hor, A.J. Williams, J.G. Checkelsky, P. Roushan, J. Seo, Q. Xu, H.W. Zandbergen, A. Yazdani, N.P. Ong, R.J. Cava, Superconductivity in $Cu_xBi_2Se_3$ and its implications for pairing in the undoped topological insulator, Phys. Rev. Lett. 104 (2010) 057001, http://dx.doi.org/10.1103/PhysRevLett.104.057001, URL https://link.aps.org/doi/10.1103/PhysRevLett.104.057001.
[274] M. Kriener, K. Segawa, Z. Ren, S. Sasaki, S. Wada, S. Kuwabata, Y. Ando, Electrochemical synthesis and superconducting phase diagram of $Cu_xBi_2Se_3$, Phys. Rev. B 84 (2011) 054513, http://dx.doi.org/10.1103/PhysRevB.84.054513, URL https://link.aps.org/doi/10.1103/PhysRevB.84.054513.
[275] L.A. Wray, S.-Y. Xu, Y. Xia, Y.S. Hor, D. Qian, A.V. Fedorov, H. Lin, A. Bansil, R.J. Cava, M.Z. Hasan, Observation of topological order in a superconducting doped topological insulator, Nat. Phys. 6 (11) (2010) 855–859, http://dx.doi.org/10.1038/nphys1762.
[276] J.A. Schneeloch, R.D. Zhong, Z.J. Xu, G.D. Gu, J.M. Tranquada, Dependence of superconductivity in $Cu_xBi_2Se_3$ on quenching conditions, Phys. Rev. B 91 (2015) 144506, http://dx.doi.org/10.1103/PhysRevB.91.144506, URL https://link.aps.org/doi/10.1103/PhysRevB.91.144506.
[277] P.P. Kong, J.L. Zhang, S.J. Zhang, J. Zhu, Q.Q. Liu, R.C. Yu, Z. Fang, C.Q. Jin, W.G. Yang, X.H. Yu, J.L. Zhu, Y.S. Zhao, Superconductivity of the topological insulator Bi_2Se_3 at high pressure, J. Phys.: Condens. Matter. 25 (36) (2013) 362204, http://dx.doi.org/10.1088/0953-8984/25/36/362204.
[278] R. Vilaplana, D. Santamaría-Pérez, O. Gomis, F.J. Manjón, J. González, A. Segura, A. Muñoz, P. Rodríguez-Hernández, E. Pérez-González, V. Marín-Borrás, V. Muñoz-Sanjose, C. Drasar, V. Kucek, Structural and vibrational study of Bi_2Se_3 under high pressure, Phys. Rev. B 84 (2011) 184110, http://dx.doi.org/10.1103/PhysRevB.84.184110, URL https://link.aps.org/doi/10.1103/PhysRevB.84.184110.
[279] J. Zhu, J.L. Zhang, P.P. Kong, S.J. Zhang, X.H. Yu, J.L. Zhu, Q.Q. Liu, X. Li, R.C. Yu, R. Ahuja, W.G. Yang, G.Y. Shen, H.K. Mao, H.M. Weng, X. Dai, Z. Fang, Y.S. Zhao, C.Q. Jin, Superconductivity in topological insulator Sb_2Te_3 induced by pressure, Sci. Rep. 3 (1) (2013) 2016, http://dx.doi.org/10.1038/srep02016.
[280] S.B. Chung, S.-C. Zhang, Detecting the Majorana Fermion surface state of ^3He−B through spin relaxation, Phys. Rev. Lett. 103 (2009) 235301, http://dx.doi.org/10.1103/PhysRevLett.103.235301, URL https://link.aps.org/doi/10.1103/PhysRevLett.103.235301.
[281] J.R. Schrieffer, Theory of Superconductivity, AbeBooks, 2009.
[282] P.-G. de Gennes, Superconductivity of Metals and Alloys, W.A. Benjamin, 1966.
[283] J. Bardeen, L.N. Cooper, J.R. Schrieffer, Theory of superconductivity, Phys. Rev. 108 (1957) 1175–1204, http://dx.doi.org/10.1103/PhysRev.108.1175, URL https://link.aps.org/doi/10.1103/PhysRev.108.1175.
[284] A.Y. Kitaev, Unpaired Majorana fermions in quantum wires, Phys.-Usp. 44 (2001) 131, http://dx.doi.org/10.1070/1063-7869/44/10S/S29.
[285] A.Y. Kitaev, Fault-tolerant quantum computation by anyons, Ann. Physics 303 (2003) 2–30, http://dx.doi.org/10.1016/S0003-4916(02)00018-0.
[286] A. Kitaev, Anyons in an exactly solved model and beyond, Ann. Physics 321 (2006) 2–111, http://dx.doi.org/10.1016/j.aop.2005.10.005.
[287] X. Chen, Z.-C. Gu, X.-G. Wen, Classification of gapped symmetric phases in one-dimensional spin systems, Phys. Rev. B 83 (2011) 035107, http://dx.doi.org/10.1103/PhysRevB.83.035107, URL https://link.aps.org/doi/10.1103/PhysRevB.83.035107.
[288] O. Andersson, I. Bengtsson, M. Ericsson, E. Sjöqvist, Geometric phases for mixed states of the Kitaev chain, Philos. Trans. R. Soc. A: Math., Phys. Eng. Sci. 374 (2068) (2016) 20150231, http://dx.doi.org/10.1098/rsta.2015.0231.
[289] J.D. Lutchyn, S. Das Sarma, Majorana Fermions and a topological phase transition in semiconductor-superconductor heterostructures, Phys. Rev. Lett. 105 (2010) 077001, http://dx.doi.org/10.1103/PhysRevLett.105.077001, URL https://link.aps.org/doi/10.1103/PhysRevLett.105.077001.
[290] S. Tewari, J.D. Sau, Topological invariants for spin-orbit coupled superconductor nanowires, Phys. Rev. Lett. 109 (2012) 150408, http://dx.doi.org/10.1103/PhysRevLett.109.150408, URL https://link.aps.org/doi/10.1103/PhysRevLett.109.150408.
[291] C.W.J. Beenakker, Random-matrix theory of Majorana fermions and topological superconductors, Rev. Modern Phys. 87 (2015) 1037–1066, http://dx.doi.org/10.1103/RevModPhys.87.1037, URL https://link.aps.org/doi/10.1103/RevModPhys.87.1037.
[292] L. Ahlfors, Complex Analysis: An Introduction to the Theory of Analytic Functions of One Complex Variable, McGraw-Hill Education, 1979.
[293] H. Yi, Y.-F. Zhao, Y.-T. Chan, J. Cai, R. Mei, X. Wu, Z.-J. Yan, L.-J. Zhou, R. Zhang, Z. Wang, S. Paolini, R. Xiao, K. Wang, A.R. Richardella, J. Singleton, L.E. Winter, T. Prokscha, Z. Salman, A. Suter, P.P. Balakrishnan, A.J. Grutter, M.H.W. Chan, N. Samarth, X. Xu, W. Wu, C.-X. Liu, C.-Z. Chang, Interface-induced superconductivity in magnetic topological insulators, Science 383 (6683) (2024) 634–639, http://dx.doi.org/10.1126/science.adk1270.
[294] M. Mandal, N.C. Drucker, P. Siriviboon, T. Nguyen, A. Boonkird, T.N. Lamichhane, R. Okabe, A. Chotrattanapituk, M. Li, Topological superconductors from a materials perspective, Chem. Mater. 35 (16) (2023) 6184–6200, http://dx.doi.org/10.1021/acs.chemmater.3c00713.
[295] K. Fan, Z. Hua, S. Gu, P. Zhu, G. Liu, H. Ren, R. Shao, Z. Wang, L. Lu, F. Yang, Superconductivity at Pd/Bi2Se3 interfaces due to self-formed PdBiSe interlayers, Materials 17 (22) (2024) http://dx.doi.org/10.3390/ma17225460, URL https://www.mdpi.com/1996-1944/17/22/5460.
[296] Z. Zhang, Z. Wu, C. Fang, F.-c. Zhang, J. Hu, Y. Wang, S. Qin, Topological superconductivity from unconventional band degeneracy with conventional pairing, Nat. Commun. 15 (1) (2024) 7971, http://dx.doi.org/10.1038/s41467-024-52156-1.
[297] X.-K. Wei, A.R. Jalil, P. Rüßmann, Y. Ando, D. Grützmacher, S. Blügel, J. Mayer, Atomic diffusion-induced polarization and superconductivity in topological insulator-based heterostructures, ACS Nano 18 (1) (2024) 571–580, http://dx.doi.org/10.1021/acsnano.3c08601.
[298] E. Mascot, S. Cocklin, M. Graham, M. Mashkoori, S. Rachel, D.K. Morr, Topological surface superconductivity in FeSe0.45Te0.55, Commun. Phys. 5 (1) (2022) 188, http://dx.doi.org/10.1038/s42005-022-00943-x.
[299] J. Lee, S. Lee, A. Kreisel, J. Paaske, B.M. Andersen, K.M. Bastiaans, D. Chatzopoulos, G. Gu, D. Cho, M.P. Allan, Signatures of amorphous shiba state in FeTe0.55Se0.45, Nano Lett. 25 (11) (2025) 4227–4233, http://dx.doi.org/10.1021/acs.nanolett.4c05650.

[300] L. Kaufhold, A. Rosch, Stability of Majorana modes in Coulomb-disordered topological insulator nanowires, Phys. Rev. B 112 (2025) 045310, http://dx.doi.org/10.1103/bsxt-n9ls.
[301] A.Y. Kitaev, Unpaired Majorana fermions in quantum wires, Phys.-Usp. 44 (10S) (2001) 131–136, http://dx.doi.org/10.1070/1063-7869/44/10S/S29.
[302] J. Alicea, New directions in the pursuit of Majorana fermions in solid state systems, Rep. Progr. Phys. 75 (7) (2012) 076501, http://dx.doi.org/10.1088/0034-4885/75/7/076501.
[303] R.M. Lutchyn, E.P.A.M. Bakkers, L.P. Kouwenhoven, P. Krogstrup, C.M. Marcus, Y. Oreg, Majorana zero modes in superconductor–semiconductor heterostructures, Nat. Rev. Mater. 3 (5) (2018) 52–68, http://dx.doi.org/10.1038/s41578-018-0003-1.
[304] T.D. Stanescu, S. Tewari, Majorana fermions in semiconductor nanowires: fundamentals, modeling, and experiment, J. Phys.: Condens. Matter. 25 (23) (2013) 233201, http://dx.doi.org/10.1088/0953-8984/25/23/233201.
[305] C.W.J. Beenakker, Search for Majorana fermions in superconductors, Annu. Rev. Condens. Matter Phys. 4 (2013) 113–136, http://dx.doi.org/10.1146/annurev-conmatphys-030212-184337.
[306] W.P. Su, J.R. Schrieffer, A.J. Heeger, Solitons in polyacetylene, Phys. Rev. Lett. 42 (1979) 1698–1701, http://dx.doi.org/10.1103/PhysRevLett.42.1698, URL https://link.aps.org/doi/10.1103/PhysRevLett.42.1698.
[307] L. Li, Z. Xu, S. Chen, Topological phases of generalized Su-Schrieffer-Heeger models, Phys. Rev. B 89 (2014) 085111, http://dx.doi.org/10.1103/PhysRevB.89.085111, URL https://link.aps.org/doi/10.1103/PhysRevB.89.085111.
[308] D. Xie, W. Gou, T. Xiao, B. Gadway, B. Yan, Topological characterizations of an extended Su–Schrieffer–Heeger model, Npj Quantum Inf. 5 (1) (2019) 55, http://dx.doi.org/10.1038/s41534-019-0159-6.
[309] M.-C. Liang, Y.-D. Wei, L. Zhang, X.-J. Wang, H. Zhang, W.-W. Wang, W. Qi, X.-J. Liu, X. Zhang, Realization of Qi-Wu-Zhang model in spin-orbit-coupled ultracold fermions, Phys. Rev. Res. 5 (2023) L012006, http://dx.doi.org/10.1103/PhysRevResearch.5.L012006, URL https://link.aps.org/doi/10.1103/PhysRevResearch.5.L012006.
[310] G. Jotzu, M. Messer, R. Desbuquois, M. Lebrat, T. Uehlinger, D. Greif, T. Esslinger, Experimental realization of the topological Haldane model with ultracold fermions, Nature 515 (2014) 237–240, http://dx.doi.org/10.1038/nature13915.
[311] C.L. Kane, E.J. Mele, Quantum spin Hall effect in graphene, Phys. Rev. Lett. 95 (2005) 226801, http://dx.doi.org/10.1103/PhysRevLett.95.226801, URL https://link.aps.org/doi/10.1103/PhysRevLett.95.226801.
[312] C.-K. Chiu, J.C.Y. Teo, A.P. Schnyder, S. Ryu, Classification of topological quantum matter with symmetries, Phys. Rep. 950 (2016) 1–104, http://dx.doi.org/10.1016/j.physrep.2016.02.001.
[313] B.A. Bernevig, T.L. Hughes, S.-C. Zhang, Quantum spin Hall effect and topological phase transition in HgTe quantum wells, Science 314 (2006) 1757–1761, http://dx.doi.org/10.1126/science.1133734.
[314] Y. Tanaka, M. Sato, N. Nagaosa, Symmetry and topology in superconductors –odd-frequency pairing and edge states–, J. Phys. Soc. Japan 81 (1) (2012) http://dx.doi.org/10.1143/JPSJ.81.011013.
[315] N. Read, D. Green, Paired states of fermions in two dimensions with breaking of parity and time-reversal symmetries and the fractional quantum Hall effect, Phys. Rev. B 61 (2000) 10267–10297, http://dx.doi.org/10.1103/PhysRevB.61.10267, URL https://link.aps.org/doi/10.1103/PhysRevB.61.10267.
[316] E.M. Nica, Q. Si, Multiorbital singlet pairing and d + d superconductivity, Npj Quantum Mater. 6 (1) (2021) 3, http://dx.doi.org/10.1038/s41535-020-00304-3.
[317] X. Gong, M. Kargarian, A. Stern, D. Yue, H. Zhou, X. Jin, V.M. Galitski, V.M. Yakovenko, J. Xia, Time-reversal symmetry-breaking superconductivity in epitaxial bismuth/nickel bilayers, Sci. Adv. 3 (2017) e1602579, http://dx.doi.org/10.1126/sciadv.1602579.
[318] A.P. Schnyder, S. Ryu, A. Furusaki, A.W.W. Ludwig, Classification of topological quantum matter with symmetries: topology of superconductors and insulators, Phys. Rep. 658 (2016) 1–190, http://dx.doi.org/10.1016/j.physrep.2016.09.003.